

8-2014

Predictive Model Development for Adsorption of Organic Contaminants by Carbon Nanotubes

Onur Apul

Clemson University, oapul@clemson.edu

Follow this and additional works at: https://tigerprints.clemson.edu/all_dissertations



Part of the [Environmental Engineering Commons](#)

Recommended Citation

Apul, Onur, "Predictive Model Development for Adsorption of Organic Contaminants by Carbon Nanotubes" (2014). *All Dissertations*. 1290.

https://tigerprints.clemson.edu/all_dissertations/1290

This Dissertation is brought to you for free and open access by the Dissertations at TigerPrints. It has been accepted for inclusion in All Dissertations by an authorized administrator of TigerPrints. For more information, please contact kokeefe@clemson.edu.

PREDICTIVE MODEL DEVELOPMENT FOR ADSORPTION OF ORGANIC
CONTAMINANTS BY CARBON NANOTUBES

A Dissertation
Presented to
the Graduate School of
Clemson University

In Partial Fulfillment
of the Requirements for the Degree
Doctor of Philosophy
Environmental Engineering and Earth Sciences.

by
Onur Guven Apul
August 2014

Accepted by:
Dr. Tanju Karanfil, Committee Chair
Dr. Brian Powell
Dr. Cindy Lee
Dr. Steve Klaine

ABSTRACT

The main objective of the study was to investigate mechanisms and statistical modeling of synthetic organic contaminant (SOC) adsorption by carbon nanotubes (CNTs). First, predictive models were developed for adsorption of low molecular weight aromatic compounds by multi-walled carbon nanotubes (MWCNTs) using experimental data for 59 compounds. Quantitative structure-activity relationship (QSAR) and linear solvation energy relationship (LSER) approaches were employed and developed models were externally validated using an independent dataset obtained from the literature. Up to date, no QSAR model has been reported for predicting adsorption of organics by CNTs. No LSER model is available which comprehensively investigates the adsorption of organics on CNTs. Only recently, one study reported an LSER equation for the modeling of their experimental adsorption data on one MWCNT. Then, adsorption of ten environmentally relevant halogenated aliphatic SOC's by a single walled (SWCNT) and MWCNT was tested experimentally for the first time in the literature. Several LSER models were developed to further examine the adsorption mechanisms. The LSER equations constitute the first predictive models generated for adsorption of aliphatic SOC's by CNTs. In addition, the poly-parameter LSER model was compared to those previously generated for adsorption of aromatic SOC's by CNTs. The LSER model generated in this research is currently the most comprehensive models available in the literature. Finally, the role of carbon nanotube morphology (i.e. surface area, diameter, and length) on the adsorption of phenanthrene (PNT) was investigated by analyzing the

adsorption isotherms obtained with several SWCNTs and MCWNTs in the laboratory and the literature.

The QSAR ($r^2 = 0.88$), and LSER ($r^2 = 0.83$) equations and their external validation accuracies indicated the success of parameter selection, data fitting ability, and the prediction strength of the developed models. These models were developed for adsorption of low-molecular weight (<200 g/mol) aromatic SOC by MWCNTs (with less than 5% oxygen content) in distilled and deionized water. For aromatic SOC adsorption models, the molecular volume term (V) of the LSER model was the most influential descriptor controlling adsorption at all concentrations. At higher equilibrium concentrations, hydrogen bond donating (A) and hydrogen bond accepting (B) terms became significant in the models. For halogenated aliphatic SOC adsorption models, at higher concentrations, the B parameter, capturing hydrogen bond accepting ability, was the most influential descriptor both for SWCNT and MWCNT. The negative dependence on B indicates that as the hydrogen bond accepting ability of an aliphatic compound increases, it becomes less likely to be adsorbed by CNTs. The other important LSER parameters were V (size) followed by P (polarizability), and they were positively correlated with adsorption, indicating that size and polarizability favors adsorption. The contribution of these parameters was 2 - 3 times less than the B parameter. However, there was no single parameter predominant in the aliphatic SOC models. The number of data points for aliphatic SOC were much smaller than aromatic models. These results indicated that adsorption of aromatic SOC by CNTs strongly depend on adsorbate

hydrophobicity; while for aliphatic SOCs, in addition to hydrophobic driving force, other interactions (i.e., hydrogen bond accepting ability) also play a role.

Additional investigation of CNT properties on adsorption of PNT showed that at low (e.g., 1 $\mu\text{g/L}$) equilibrium concentrations, MWCNTs with the larger outer diameters exhibit higher adsorption capacity on a specific surface area basis than those with smaller diameters. With increasing equilibrium concentration, adsorption on a specific surface area basis becomes independent of MWCNT diameter, and maximum adsorption capacity was controlled by the total surface area. A similar analysis for the adsorption of naphthalene (NPT), a planar molecule with one less benzene ring but twenty times higher solubility than PNT, showed no correlation with respect to MWCNT outer diameter at both low and high equilibrium concentrations. The results indicated that the surface curvature of MWCNT was more important on the adsorption of PNT than on the adsorption of NPT due to its smaller molecular size and lower adsorption capacity than PNT. Specific surface area normalized isotherms did not show a correlation between PNT adsorption and lengths of SWCNTs and MWCNTs. Carbon nanotube characterization results showed that the morphology of CNTs impacts their aggregation and plays an important role on the available surface area and pore volume for adsorption. Manufacturer's data may not always represent the characteristics of CNTs in a particular batch. Therefore, accurate characterization of CNTs is essential to systematically examine the behavior of CNTs (e.g., adsorption, transport) in environmental systems.

A fundamental understanding of CNT-SOC adsorption interactions is important to (i) assess the environmental implications of CNT releases and spills to natural waters, and

their roles as the contaminant carriers in the environment and, (ii) evaluate the potentials of CNTs as adsorbents in water and wastewater treatment applications. Predictive LSER modeling can be used to gain insight to the adsorption mechanisms by examining the individual contribution of intermolecular interactions to overall adsorption. This study examined and showed adsorption mechanisms and CNT properties (such as surface area, pore volume, outer diameter, and surface oxygen content) on the adsorption behavior of different classes of SOCs by CNTs.

DEDICATION

to my parents...

ACKNOWLEDGMENTS

I would like to express my sincere appreciation to my advisor Dr. Tanju Karanfil and committee members, Drs. Cindy Lee, Brian Powell and Steve Klaine for providing me their valuable guidance, continuous support and inspiration. I am also thankful to EEES family including all faculty, staff and students for their endless support.

Special thanks go to the members of Karanfil research group for their help inside and outside the lab. The financial support was provided by National Science Foundation (CBET 0967425) research grant.

TABLE OF CONTENTS

	Page
TITLE PAGE	i
ABSTRACT.....	ii
DEDICATION	vi
ACKNOWLEDGMENTS	vii
LIST OF TABLES	x
LIST OF FIGURES	xii
CHAPTER	
I. PROSPECTUS.....	1
Introduction and Motivation	1
Research Objectives.....	3
Organization.....	5
II. LITERATURE SURVEY.....	6
General Features of SOC Adsorption by CNTs.....	6
Characterization of CNTs	9
Adsorption of SOCs by CNTs	20
Predictive Models for Adsorption of SOCs by CNTs	39
Conclusions.....	44
III. PREDICTIVE MODEL DEVELOPMENT FOR ADSORPTION OF AROMATIC CONTAMINANTS BY MULTI-WALLED CARBON NANOTUBE	47
Introduction.....	47
Materials and Methods.....	49
Results and Discussion	55
Conclusions.....	68

Table of Contents (Continued)

	Page
IV. ADSORPTION OF HALOGENATED ALIPHATIC SOC _s BY CARBON NANOTUBES	69
Introduction.....	69
Materials and Methods.....	70
Results and Discussion	77
Conclusions.....	92
V. THE IMPACT OF CARBON NANOTUBE MORPHOLOGY ON PHENANTHRENE AND NAPHTHALENE ADSORPTION	95
Introduction.....	95
Materials and Methods.....	97
Results and Discussion	99
Conclusions.....	110
VI. CONCLUSIONS AND RECOMMENDATIONS	112
APPENDICES	118
A: Supplementary information for Chapter I.....	119
B: Supplementary information for Chapter II	128
C: Supplementary information for Chapter III	129
D: Supplementary information for Chapter IV	148
E: Supplementary information for Chapter V	182
REFERENCES	185

LIST OF TABLES

Table		Page
2.1.	Summary of CNTs employed for SOC adsorption in the literature, their characteristics and characterization methods	10
2.2.	Summary of correlative equations between CNT adsorption descriptors and independent variables	43
3.1.	List of compounds for training dataset, data sources and adsorption descriptors	51
3.2.	List compounds for external validation dataset and adsorption descriptors	52
4.1.	Physical characteristics of CNTs	72
4.2.	Selected properties of aliphatic SOCs.....	73
4.3.	Freundlich model parameters of adsorption isotherms for aliphatic SOCs.....	81
4.4.	Single parameter linear correlation between hydrophobicity and adsorption descriptors	84
4.5.	Poly-parameter linear solvation energy relationship coefficients for SWCNTs and MWCNTs.....	89
5.1.	Physical characteristics of carbon nanotubes.....	101
5.2.	Freundlich isotherm parameters (mass and specific surface area (SSA) basis) for phenanthrene (PNT) adsorption by carbon nanotubes (CNTs)	105
5.3.	Comparison of phenanthrene (PNT) adsorption capacities of carbon nanotubes (CNTs) with different diameters	108
A.1.	List of SOCs that were used as adsorbate in aqueous phase CNT adsorption studies.....	119

LIST OF TABLES (Cont'd)

Table		Page
B.1.	Manufacturer and supplier full names and countries provided by the articles compiled for CNT adsorption studies tabulated in Table 2.1.....	128
C.1.	The percentage of solubility at infinite dilution conditions concentrations	131
C.2.	Surface area normalized adsorption descriptors (K_{SA} values)	132
C.3.	The solvatochromic descriptors of training dataset	133
C.4.	The solvatochromic descriptors of validation dataset.....	134
C.5.	Comparison of residual values (actual- predicted) and RMSE values for three models (i) the model developed by Xia et al. ¹⁷ , (ii) the model developed for 29 compounds (eq. 3) and (iii) the combined model (eq. 5)	139
D.1.	Molecular structures of aliphatic SOCs	153
D.2.	Adsorption descriptors for aliphatic SOCs	154
D.3.	Solvatochromic parameters of aliphatic SOCs	155
D.4.	LSER model parameters for adsorption of aliphatic SOCs by SWCNTs and MWCNTs without R	156
D.5.	model parameters for adsorption of aromatic SOCs by MWCNTs with and without R	157

LIST OF FIGURES

Figure	Page
2.1 Schematic representation of a typical CNT bundle and its adsorption sites (1) inner cavities, (2) interstitial channels, (3) external grooves, (4) outermost surface	8
2.2 Adsorption sites of SWCNTs and MWCNTs.....	27
3.1 Box and whisker plots for the QSAR descriptors.....	57
3.2 Experimentally measured adsorption descriptors reported by Xia et al. (2010a) vs. the predicted adsorption descriptors by QSAR model (eq. 3) for training and external validation datasets.....	58
3.3 Box and whisker plots for the LSER descriptors.....	61
3.4 Experimentally measured adsorption descriptors reported by Xia et al. (2010a) vs. the predicted adsorption descriptors by LSER model (eq. 4) for training and external validation datasets.....	62
3.5 Box and whisker plots for the LSER descriptors for combination of training and validation datasets.	64
3.6 Experimentally measured adsorption descriptors vs. the predicted adsorption descriptors obtained by the LSER equations for (a) 1% and (b) 10% of adsorbate aqueous solubility for training dataset	67
4.1 Adsorption isotherms of aliphatic SOCs by (a) SWCNT and (b) MWCNT.....	79
4.2 Comparison of adsorption affinities of SWCNT vs. MWCNTs depicted by (a) $\log K_{Fm}$ (b) $\log K_{Fm,SSA}$ – specific surface area normalized (c) $\log K_{Fm,microPV}$ – micro pore volume normalized	80
4.3 PCE, TCE and 1,1-DCE adsorption isotherms (top) and after solubility normalization (bottom).....	86

LIST OF FIGURES (Cont'd)

Figure	Page
4.4 Comparison of 1,1,1-TCA and 1,1,2-TCA adsorption isotherms on CNTs	87
5.1 Average outer diameter and specific surface area relationship for multi-walled carbon nanotubes	101
5.2 Specific surface area (SSA) normalized Phenanthrene (PNT) adsorption capacities of multi-walled carbon nanotubes (MWCNTs) at the equilibrium concentration of 1, 10, 100 and 1000 ppb (A, B, C and D, respectively).....	107
C.1 Residual analyses of QSAR model independent variables for (a) $\theta\chi$, (b) $\theta\chi_V$, and (c) $3\chi_p$	135
C.2 Residual analyses of LSER model independent variables for (a) A (b) B (c) V, and (d) P. The circled points are for phenolic compounds in the dataset following a trend represented by the regression line and coefficient of determination (r^2).....	136
C.3 Examination of p -values for each LSER parameter by one by one elimination of highest descriptor values from the independent parameter list	137
C.4 Experimentally measured adsorption descriptors vs. the predicted adsorption descriptors by LSER model generated by combination of training and validation datasets.....	138
D.1 Comparison of SWCNT vs. MWCNT adsorption isotherms (top) and after surface area normalized within 0.5 – 0.8 nm pore size range (below) For comparison SWCNT and MWCNT adsorption isotherms were plotted on the same graph with the surface area normalized isotherms.....	148
D.2 Solubility normalized adsorption isotherms of aliphatic SOC by (a) SWCNT and (b) MWCNT	149

LIST OF FIGURES (Cont'd)

Figure	Page
D.3 Correlation of molar volume (top) and polarizability (bottom) with solubility normalized adsorption descriptors ($K_{F,ms}$) for PCE, TCE and 1,1-DCE	150
D.4 Solubility normalized adsorption isotherms of TCE and 1,1,2-TCA	151
D.5 Solubility normalized adsorption isotherms of PCE and 1,1,1,2-TeCA	151
D.6 Change of LSER model parameter coefficients with aqueous equilibrium concentration	152
D.7 Change of LSER model coefficient of determination with increasing aqueous equilibrium concentration for adsorption of aliphatic SOCs by SWCNTs with and without R parameter	152
E.1 Sample transmission electron microscopy (TEM) images of multiwalled carbon nanotubes (MWCNTs). Small-diameter MWCNTs (left), medium-diameter MWCNTs (middle) and large-diameter MWCNTs (right)	182
E.2 Diameter distribution of small-diameter multiwalled carbon nanotubes (MWCNTs), medium-diameter MWCNTs and large-diameter MWCNTs.....	183
E.3 Specific surface area (SSA) normalized naphthalene adsorption capacities of multiwalled carbon nanotubes (MWCNTs) at the equilibrium concentrations of 10, 200, and 12,000 ppb, respectively	184

CHAPTER I

PROSPECTUS

1.1. Introduction and Motivation

Graphitic carbon is sp^2 hybridized solid phase of pure carbon where three of the four valence electrons are covalently shared in a two-dimensional plane and the fourth valence electron is delocalized among all atoms present as a weak π bond in the third dimension [Ajayan 1999; Terrones 2003; 2004]. Carbon nanotubes (CNTs) can be visualized as graphitic carbon sheets rolled into hollow cylinders with nanometer scale diameters and micrometer scale lengths [Terrones 2003; 2004, Iijima 1991]. There are two types of CNTs: single-walled (SWCNT) and multi-walled (MWCNT) [Ajayan 1999]. Owing to their unique structures, the production and use of CNTs has been growing rapidly [Lam et al. 2006]. The CNT market estimates were approximately 90.5 million dollars in 2010, and global revenues are projected to exceed 1 billion dollars by 2015 [Nanoposts 2010]. CNTs are now synthesized at larger scales, and used in many electronic, medical, space and military applications [Klaine et al. 2008; Mauter and Elimelech 2008]. In addition, superior hydrophobicity, high specific surface area, and hollow and layered structures of CNTs make them also particularly promising adsorbents [Upadhyayula et al. 2009; Zhang et al. 2011]. CNT adsorption of many compounds in water such as various classes of synthetic organic contaminants (SOCs) [Apul et al. 2013; Gotovac et al. 2006;. 2007a; 2007b; Yang et al. 2006a; 2006b; Cho et al. 2008; Wang et al. 2008; Chen et al. 2007; Lin and Xing 2008a; Oleszczuk et al. 2009; Ji et al. 2009a;

Gupta et al. 2013; Pyrznska et al. 2007] (see Table A1 in Appendix A), natural organic matter (NOM) [Su et al. 2007; Yang et al. 2009], and metallic ions [Li et al. 2003; 2005; Rao et al. 2007] have been widely reported.

The remarkable increase in production and use of CNTs raises health and environmental concerns, particularly upon release into the environment [Lam et al. 2006; Powell and Kanarek 2006; Johnston et al. 2010; Petosa et al. 2010]. CNTs may enter the environment through either intentional or unintentional releases (e.g. atmospheric emissions and solid or liquid waste streams) from production facilities, causing damage to plant and animal life at the cellular level [Lam et al. 2006; Klaine et al. 2008; Petosa et al. 2010]. The toxicity of CNTs may also be enhanced by the adsorbed organic contaminants in the environment [Ferguson et al. 2008; Xia et al. 2010b; Yang et al. 2007]. Therefore, it is of critical importance to understand adsorption of SOC by CNTs to adequately assess the environmental impact of CNTs.

Adsorption of SOC by CNTs may also be important for the operations of engineered water and wastewater treatment systems. The fundamentals of SOC adsorption by CNTs and activated carbons are similar in terms of intermolecular physical, chemical, electrical interactions [Chen et al. 2007]. Therefore, the use of CNTs as an alternative adsorbent to activated carbon may be a feasible option in the future.

Despite the voluminous research in the literature, the available data for adsorption of SOC by CNTs still covers only a small portion of approximately 70,000 anthropogenic pollutants. Obtaining experimental adsorption data for pollutants is laborious, costly and time consuming. Therefore, predictive models for the adsorption of

organic chemicals by CNTs are of great significance to scientists, engineers and practitioners. These models may also provide insights to the adsorption mechanisms of SOCs by CNTs, and they can be useful to assess the fate and transport of adsorbed toxic contaminants with CNTs in environment.

1.2. Research Objectives

Given the (i) adsorption affinity of SOCs to CNTs (ii) potential uses of CNTs as an alternative adsorbent to activated carbon, (iii) potential hazards of CNTs to the environment and; the main objectives of this study were:

- to examine the adsorption mechanism(s) of SOCs by CNTs.
- to develop predictive statistical models for the adsorption of SOCs by CNTs.

To fulfill the main objectives, the study was divided into three phases.

Phases (1)

The objective of the first phase was to develop statistical predictive models for adsorption of aromatic SOCs by MWCNTs and gain insight for the adsorption mechanisms. Aromatic SOCs and MWCNTs were selected because they constituted the largest data set available after a comprehensive literature survey. The data compiled from literature were combined with the data produced in our laboratory to generate a comprehensive SOC adsorption database. Then, statistical quantitative structure-activity

relationship approaches were employed for modeling the adsorption of aromatics by MWCNTs. Two common techniques were adopted: quantitative structure-activity relationship (QSAR) and linear solvation energy relationship (LSER). Finally, an independent verification dataset was employed to validate the accuracy and reliability of the models.

Phase (2)

The objective of Phase 2 was to investigate the adsorption of environmentally relevant halogenated aliphatic SOC_s by CNT_s and extend the LSER modeling work to the aliphatic SOC class. First, adsorption isotherms of a suite of halogenated aliphatic SOC_s by CNT_s (one SWCNT and one MWCNT) were generated in our laboratory. Then, adsorption of aliphatic SOC_s by SWCNT_s and MWCNT_s were compared and the molecular-level intermolecular interactions governing adsorption were examined. Lastly, statistical predictive models were developed and LSER model parameters and their coefficients were compared with the LSER model parameters generated for adsorption of aromatic SOC_s by MWCNT_s in Phase 1.

Phase (3)

In the third phase, the objective was to examine the role(s) of CNT properties such as surface area, diameter, and length on the adsorption of phenanthrene (PNT) by analyzing the adsorption isotherms obtained with several CNT_s in our laboratory and

available in the literature. Firstly, adsorption isotherms of PNT by eight CNTs were generated in our laboratory. Then, several PNT isotherms with different CNTs were obtained from literature and overall a dataset of 16 isotherms for PNT were employed to examine and analyze the role of CNT properties on the adsorption of PNT. Lastly, to further examine the impact of MWCNT diameter on SOC adsorption, the adsorption data for naphthalene (NPT) on MWCNTs in literature was also examined.

1.3. Organization

Chapter I provides a general introduction including: research motivation and significance, main and specific objectives for each phase and the organization of the dissertation.

Chapter II is a critical review of the SOC adsorption by CNT and a summary of related modeling efforts in the literature.

Chapter III presents the predictive model development for adsorption of aromatic contaminants by multi-walled carbon nanotubes.

Chapter IV portrays adsorption of halogenated aliphatic contaminants by carbon nanotubes.

Chapter V discusses the impact of carbon nanotube morphology on phenanthrene and naphthalene adsorption.

Chapter VI summarizes conclusions and future research recommendations.

Appendix A-E contains supplementary material for Chapters I-V.

CHAPTER II

LITERATURE SURVEY

2.1. General Features of SOC Adsorption by CNTs

Adsorption of SOCs from water by activated carbon and other porous carbon materials has been studied for several decades [US EPA 1980; Giusti et al. 1974; Moreno-Castilla 2004; Kutics and Suzuki 1993]. Studies in the literature regarding the adsorption of SOCs by CNTs has been rapidly increasing [Iijima 1991; Yang et al. 2006b]. More than 70 articles have been published in peer-reviewed journals on SOC adsorption by CNTs over the last ten years (2003 - 2013). These studies included the adsorption of a multitude of organic contaminants by CNTs: polycyclic aromatic hydrocarbons (PAHs) [Yang et al. 2006a; 2006b; Yang and Xing 2007; Zhang et al. 2010b], benzene derivatives [Wang et al. 2008; Chen et al. 2007; Peng et al. 2003; Chen et al. 2008a], phenolic compounds [Lin and Xing 2008a; Shen et al. 2009; Yang et al. 2008; Salam and Burk 2008; Chen et al. 2009], pharmaceuticals [Oleszczuk et al. 2009; Ji et al. 2009a; Chen et al. 2011; Ji et al. 2010a; 2010b; Peng et al. 2012; Yang et al. 2012; Zhang et al. 2010c; Fu et al. 2011], insecticides [Peng et al. 2009], herbicides [Pyrznska et al. 2007; Chen et al. 2009], organic dyes [Gupta et al. 2013], aliphatics [Lu et al. 2006; Wang et al. 2010] and dioxin [Long and Yang 2001].

Multiple mechanisms, of varying relative importance, have been proposed to control the adsorption of SOCs by CNTs. The quantification of these individual contributions is a challenging task, and it has yet to be addressed in any significant

fashion in the current CNT adsorption literature. However, some previous studies indicated that certain parameters are more predominant in controlling adsorption than others. According to Yang et al. (2006), K_{ow} of SOC_s were strongly correlated with adsorption capacity of CNTs. Evidently, hydrophobic driving forces play important roles; however, they cannot completely explain adsorption. Electrostatic interactions, π - π interactions and hydrogen bonding also influence adsorption interactions considerably [Lin and Xing 2008a; Chen et al. 2008b]. According to the mechanism proposed by Chen et al. (2007), π -electron donor and acceptor interactions influence adsorption of aromatic SOC_s by CNTs. Similarly, among CNT parameters, specific surface area was reported to be a controlling parameter of adsorption capacity, though not the only controlling factor [Zhang et al. 2010b]. Pore volume, pore size distribution and functional groups of CNTs were also influential on adsorption [Yang et al. 2006b; Cho et al. 2008; Lin and Xing 2008a]. As a result, describing SOC adsorption by CNTs may require considering multiple adsorption mechanisms and factors [Chen et al. 2007; Pan and Xing 2008].

In addition to the already complicated nature of SOC adsorption, CNTs are prone to aggregation. Aggregation (homo- and hetero-) is a characteristic that differentiates CNTs from other carbonaceous adsorbents, further complicating the adsorption properties. According to Saleh et al. (2008), CNTs exhibited Derjaguin-Landau-Verwey-Overbeek (DLVO) interactions that are predominantly similar to most other aqueous colloidal particles. Aggregation may reduce the surface area during the formation of interstitial channels between nanotubes and grooves on the periphery of the bundles. The

outermost surface, interstitial channels, inner cavities and grooves are the four proposed adsorption sites for CNT bundles (Figure 2.1) [Agnihotri et al. 2006; 2008].

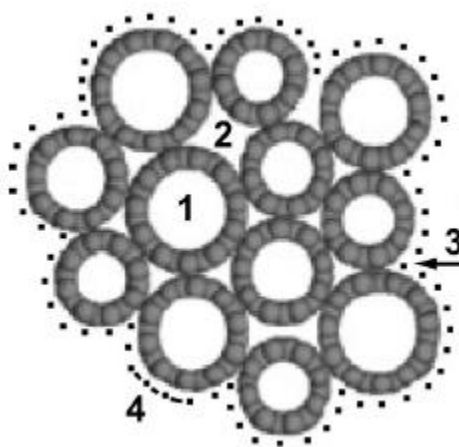


Figure 2.1. Schematic representation of a typical CNT bundle and its adsorption sites (1) inner cavities, (2) interstitial channels, (3) external grooves, (4) outermost surface [Agnihotri et al. 2008]

In natural waters, the behavior of CNTs and the interactions between organic compounds and CNTs are further complicated by the presence of natural organic matter (NOM) [Zhang et al. 2011]. The suspension stability of CNTs in aqueous solutions may be improved by the presence of NOM due to the increased electrostatic and steric repulsion among NOM-coated nanotubes, while NOM molecules compete with SOC molecules for adsorption sites [Hyung et al. 2007].

The aqueous phase adsorption of SOCs by CNTs depends on the physicochemical properties of the adsorbate and CNTs as well as the background water chemistry [Ma et al. 2011]. To simplify the complicated nature of intermolecular adsorption interactions, to

gain a more comprehensive insight into the adsorption mechanism, understand the interactions of CNTs and SOCs and systemize the available literature, the influence of adsorbent (CNT), adsorbate (SOC) and background solution were investigated separately, as detailed in the following sections. A literature review of the characteristics of CNTs is also provided below prior to the review of adsorption mechanisms.

2.2. Characterization of CNTs

Adsorption of organic contaminants is influenced by both CNT morphology and surface chemistry. To examine the CNT properties, a rigorous literature survey was conducted and tabulated in Table 2.1. The compiled information indicated that the properties of two types of CNTs (i.e. SWCNT and MWCNT) varied significantly in literature. In the 57 journal articles reviewed, adsorption of SOCs was investigated using 18 SWCNTs and 81 MWCNTs as adsorbents. Five studies, however, did not report the type of CNT used. The abundance of MWCNT in these adsorption studies was likely due to the higher market prices of SWCNTs than MWCNTs. A compilation of prices in 2013 from 44 commercially available lab grade CNT products revealed that the average market price for MWCNTs was approximately 10 \$/g, and the average price for SWCNTs was higher than 100 \$/g. However, it should be noted that obtaining cheaper SWCNTs and MWCNTs (e.g., 45 \$/g and 1.5 \$/g, respectively) is possible depending on the purity sought. In 2008, Cho et al., (2008) reported the average price of MWCNT as 140 \$/g, which shows the remarkable decrease of its price recently.

Table 2.1. Summary of CNTs employed for SOC adsorption in the literature, their characteristics and characterization methods

Source	Adsorbent Name	Supplier	Pretreat.	Surface Area		Pore Volume		Inner Diameter		Outer Diameter		Length		Purity	
				Value (m ² /g)	Mthd	Value (cm ³ /g)	Mthd	Value (nm)	Mthd	Value (nm)	Mthd	Value (μm)	Mthd	Value (%)	Mthd
[Yang et al. 2006b]	MWCNT 8	Chengdu, China	HNO ₃ , H ₂ SO ₄	348	BET	0.816	BET	2-3	TEM	<8	TEM	10-50	TEM	95+	TGA
[Yang et al. 2006b]	MWCNT 15	Chengdu, China	HNO ₃ , H ₂ SO ₄	174	BET	0.665	BET	3-5	TEM	8-15	TEM	10-50	TEM	95+	TGA
[Yang et al. 2006b]	MWCNT 30	Chengdu, China	HNO ₃ , H ₂ SO ₄	107	BET	0.317	BET	5-15	TEM	15-30	TEM	10-50	TEM	95+	TGA
[Yang et al. 2006b]	MWCNT 50	Chengdu, China	HNO ₃ , H ₂ SO ₄	95	BET	0.253	BET	5-15	TEM	30-50	TEM	10-50	TEM	95+	TGA
[Oleszczuk et al. 2009]	MWCNT 10	Shenzen, China	HNO ₃ , H ₂ SO ₄	357	BET	1.093	BET	NR	-	9.4 (10)	TEM (MC)	1-2	TEM	95+	MC
[Oleszczuk et al. 2009]	MWCNT 20	Shenzen, China	HNO ₃ , H ₂ SO ₄	126	BET	0.415	BET	NR	-	21 (20)	TEM (MC)	1-2	TEM	95+	MC
[Oleszczuk et al. 2009]	MWCNT 40	Shenzen, China	HNO ₃ , H ₂ SO ₄	86	BET	0.319	BET	NR	-	28 (40)	TEM (MC)	1-2	TEM	95+	MC
[Oleszczuk et al. 2009]	MWCNT 60	Shenzen, China	HNO ₃ , H ₂ SO ₄	73	BET	0.191	BET	NR	-	43 (60)	TEM (MC)	1-2	TEM	95+	MC
[Oleszczuk et al. 2009]	MWCNT 100	Shenzen, China	HNO ₃ , H ₂ SO ₄	58	BET	0.137	BET	NR	-	70 (100)	TEM (MC)	1-2	TEM	95+	MC
[Zhang et al. 2009]	MWCNT-P	NAM, USA	-	164	BET	0.664	BET	3-5	MC	8-15	MC	10-50	MC	89.9	TGA
[This study]	MWCNT-SD	NAM, USA	-	178	BET	0.848	BET	5-10	MC	10-20	MC	10-30	MC	99.1	TGA
[This study]	MWCNT-MD	NAM, USA	-	127	BET	0.722	BET	5-10	MC	20-30	MC	10-30	MC	97.1	TGA
[This study]	MWCNT-LD	NAM, USA	-	157	BET	0.702	BET	5-15	MC	30-50	MC	10-20	MC	98.6	TGA
[This study]	MWCNT-SL	Nanoshel, USA	-	163	BET	0.728	BET	NR	-	4-12	MC	3-10	MC	95.0	TGA
[This study]	MWCNT-ML	Nanoshel, USA	-	80	BET	0.367	BET	NR	-	4-12	MC	5-15	MC	99.2	TGA
[This study]	MWCNT-LL	Nanoshel, USA	-	301	BET	0.978	BET	NR	-	4-12	MC	15-30	MC	95.3	TGA
[Zhang et al. 2009]	MWCNT-OH	NAM, USA	-	192	BET	0.765	BET	3-5	MC	8-15	MC	10-50	MC	95+	MC
[Zhang et al. 2009]	MWCNT-COOH	NAM, USA	-	134	BET	0.589	BET	3-5	MC	8-15	MC	10-50	MC	95+	MC

[Zhang et al. 2009]	MWCNT-S	Cheap Tube, USA	-	192	BET	0.925	BET	3-5	MC	8-15	MC	0.5-2	MC	97.8	TGA
[Lu et al. 2006]	MWCNT	Shenzen, China	HNO ₃ , H ₂ SO ₄ , Ultrasound	295	BET	NR	-	5-10	MC	10-30	MC	0.5-500	MC	98.9	TGA
[Chen et al. 2007]	MWCNT 1030	Shenzen, China	Heat, NaClO ₄ , Ultrasound	148	BET	0.240	BET	NR	-	10-30	MC	5-15	MC	95	MC
[Chen et al. 2007]	MWCNT 4060	Shenzen, China	Heat, NaClO ₄ , Ultrasound	74	BET	0.104	BET	NR	-	40-60	MC	5-15	MC	95	MC
[Yan et al. 2008]	r-MWCNT	Shenzen, China	-	300	BET	0.793	BJH	NR	-	20-40	MC	<10	MC	97.9	MC
[Cho et al. 2008]	MWCNT 3.3	Nanolab, USA	-	283	BET	NR	-	7	MC	15	MC	1-5	AFM	95+	MC
[Cho et al. 2008]	MWCNT Ox.	Lab	-	287	BET	NR	-	7	MC	15	MC	1-5	AFM	95	MC
[Pyrzynska et al. 2007]	MWCNT	Modified Aldrich	-	40-600	MC	NR	-	NR	-	10-30	MC	NR	-	95+	MC
[Chen et al. 2009a]	MWCNT 8	Chengdu, China	HNO ₃	559	BET	1.775	BET	2-5	TEM	<8	TEM	10-30	TEM	95+	NR
[Chen et al. 2009a]	MWCNT 15	Chengdu, China	HNO ₃	181	BET	0.426	BET	5-8	TEM	10-15	TEM	10-30	TEM	90+	NR
[Chen et al. 2009a]	MWCNT 20	Chengdu, China	HNO ₃	167	BET	0.566	BET	5-10	TEM	10-20	TEM	10-30	TEM	95+	NR
[Chen et al. 2009a]	MWCNT 30	Chengdu, China	HNO ₃	91	BET	0.300	BET	5-15	TEM	30-50	TEM	10-20	TEM	95+	NR
[Chen et al. 2009a]	MWCNT 50	Chengdu, China	HNO ₃	68	BET	0.160	BET	5-10	TEM	>50	TEM	10-20	TEM	95+	NR
[Chen et al. 2009b]	MWCNT 0.85	Chengdu, China	-	167	BET	NR	-	NR	-	10-20	MC	NR	-	NR	-
[Chen et al. 2009b]	MWCNT 2.16	Chengdu, China	-	185	BET	NR	-	NR	-	10-20	MC	NR	-	NR	-
[Chen et al. 2009b]	MWCNT 7.07	Chengdu, China	-	178	BET	NR	-	NR	-	10-20	MC	NR	-	NR	-
[Shen et al. 2009]	MWCNT	Lab Synthesized	-	160	BET	0.652	BJH	NR	-	NR	-	NR	-	93	EA
[Shen et al. 2009]	MWCNT Ox.	Lab Synthesized	-	274	BET	0.382	BJH	NR	-	NR	-	NR	-	93	EA
[Salam and Burk 2008]	MWCNT	Sun Nanotech, China	-	148	BET	NR	-	NR	-	100-200	SEM	NR	-	NR	-
[Salam and Burk 2008]	MWCNT H ₂ O ₂	Lab Synthesized	-	144	BET	NR	-	NR	-	NR	-	NR	-	NR	-
[Salam and Burk 2008]	MWCNT HNO ₃	Lab	-	140	BET	NR	-	NR	-	NR	-	NR	-	NR	-

and Burk 2008]		Synthesized													
[Brooks et al. 2012]	MWCNT PD15L1-5	Nanolab, USA	-	200	MC	NR	-	NR	-	15	MC	1-5	MC	95	TGA
[Brooks et al. 2012]	MWCNT PD30L1-5	Nanolab, USA	-	200	MC	NR	-	NR	-	30	MC	1-5	MC	95	TGA
[Brooks et al. 2012]	MWCNT PD30L5-20	Nanolab, USA	-	200	MC	NR	-	NR	-	30	MC	5-20	MC	95	TGA
[Toth et al. 2012]	MWCNT	Chengdu, China	HCl	167	BET	1.08	BET	5-10	MC	10-20	MC	10-30	MC	95+	
[Toth et al. 2012]	MWCNT-COOH	Chengdu, China	HCl	187	BET	1.08	BET	5-10	MC	10-20	MC	10-30	MC	95+	
[Li et al. 2011]	MWCNT 3.84	Chengdu, China	HCl	563	BET	0.780	BET	<5	MC	<8	MC	10-30	TEM	NR	-
[Li et al. 2011]	MWCNT 10.08	Lab Modified	-	520	BET	0.568	BET	NR	-	NR	-	<3	TEM	NR	-
[Li et al. 2011]	MWCNT 18.01	Lab Modified	-	384	BET	0.333	BET	NR	-	NR	-	<0.5	TEM	NR	-
[Li et al. 2011]	MWCNT 22.8	Lab Modified	-	143	BET	0.131	BET	RN	-	NR	-	<0.3	TEM	NR	-
[Hou et al. 2013]	O-MWCNT	Shenzen, China	HCl	114	BET	NR	-	NR	-	10-30	MC	5-15	MC	95+	MC
[Wang et al. 2010]	MWCNT 10	Chengdu, China	-	176	BET	1.748	BJH	NR	-	10-20	MC	NR	-	95+	MC
[Wang et al. 2010]	MWCNT 20	Chengdu, China	-	130	BET	1.169	BJH	NR	-	20-30	MC	NR	-	95+	MC
[Wang et al. 2010]	MWCNT 50	Chengdu, China	-	77	BET	0.696	BJH	NR	-	>50	MC	NR	-	95+	MC
[Wang et al. 2010]	F-MWCNT 10	Chengdu, China	-	174	BET	1.366	BJH	NR	-	10-20	MC	NR	-	95+	MC
[Wang et al. 2010]	F-MWCNT 20	Chengdu, China	-	123	BET	1.060	BJH	NR	-	20-30	MC	NR	-	95+	MC
[Wang et al. 2010]	F-MWCNT 50	Chengdu, China	-	77	BET	0.587	BJH	NR	-	>50	MC	NR	-	95+	MC
[Shi et al. 2010]	MWCNT	Shenzen, China	-	52	BET	0.16	BET	NR	-	20-40	MC	NR	-	NR	-
[Yu et al. 2012]	MWCNT 2.0	Lab Synthesized	Heat, Air, HNO ₃	471	BET	0.64	BET	NR	-	NR	-	NR	-	NR	-
[Yu et al. 2012]	MWCNT 3.2	Lab Synthesized	Heat, Air, HNO ₃	381	BET	0.58	BET	NR	-	NR	-	NR	-	NR	-
[Yu et al. 2012]	MWCNT 4.7	Lab Synthesized	Heat, Air, HNO ₃	382	BET	0.58	BET	NR	-	NR	-	NR	-	NR	-
[Yu et al. 2012]	MWCNT 5.9	Lab Synthesized	Heat, Air, HNO ₃	327	BET	0.49	BET	NR	-	NR	-	NR	-	NR	-
[Ji et al. 2009b]	MWCNT in	Nanothinx, Greece	Ultrasound, HNO ₃	525	BET	NR	-	NR	-	12-31	MC	>10	MC	97	MC
[Ji et al. 2009b]	MWCNT 500	Lab Modified	-	320	BET	NR	-	NR	-	NR	-	NR	-	NR	-
[Pan et al. 2013]	MWCNT MH	Chengdu, China	Hydoxylized	228	BET	NR	-	NR	-	NR	-	NR	-	94	EA

[Pan et al. 2013]	MWCNT MC	Chengdu, China	Carboxylized	164	BET	NR	-	NR	-	NR	-	NR	-	97	EA
[Pan et al. 2013]	MWCNT MG	Chengdu, China	Graphitized	117	BET	NR	-	NR	-	NR	-	NR	-	98	EA
[Kotel et al. 2009]	MWCNT 800	Lab Modified	-	263	BET	NR	-	NR	-	NR	-	NR	-	NR	-
[Kotel et al. 2009]	MWCNT 1200	Lab Modified	-	245	BET	NR	-	NR	-	NR	-	NR	-	NR	-
[Liu et al. 2008]	MWCNT	Shenzen, China	HCl	NR	-	NR	-	NR	-	20-30	MC	NR	-	NR	-
[Shahryari et al. 2010]	MWCNT	R.I.P.I., Iran	-	280	NR	NR	-	NR	-	<10	MC	5-15	MC	95+	MC
[Wu 2007a]	MWCNT	Lab Synthesized	-	82	BET	1.07	BET	5-10	TEM	20-80	TEM	5-15	-	98+	-
[Ghaedi et al. 2011]	MWCNT	Merck, Germany	HCl	NR	-	NR	-	NR	-	NR	-	NR	-	NR	-
[Ghaedi et al. 2012b]	MWCNT-COOH	Lab Modified	HCl	97	NR	NR	-	NR	-	NR	-	NR	-	NR	-
Machado et al. 2012]	MWCNT	Lab Synthesized	HCl	181	BET	0.345	BET	NR	-	3-40	TEM	NR	-	95+	FTIR
[Mishra et al. 2010]	f-MWCNT	Lab Synthesized	Air, Acid	92	BET	0.22	BET	5-10	TEM, SEM	40-50	TEM, SEM	NR	-	NR	-
[Rodríguez et al. 2010]	MWCNT	Sun Nanotech, China	HCl, HNO ₃	162	BET	NR	-	NR	-	20-50	SEM	20-50	SEM	NR	-
[Li et al. 2013]	MWCNT	Lab Synthesized	-	NR	-	NR	-	NR	-	20	NR	NR	-	NR	-
[Li et al. 2013]	O-MWCNT	Lab Synthesized	-	NR	-	NR	-	NR	-	20	NR	NR	-	NR	-
[Ji et al. 2010b]	P-SWCNT	Shenzen, China	-	411	BET	NR	-	NR	-	<2	MC	5-15	MC	90+	MC
[Ji et al. 2010b]	P-MWCNT	Shenzen, China	-	157	BET	NR	-	NR	-	10-30	MC	5-15	MC	95+	MC
[Ji et al. 2010b]	K-SWCNT	Shenzen, China	-	653	BET	NR	-	NR	-	NR	-	NR	-	NR	-
[Ji et al. 2010b]	K-MWCNT	Shenzen, China	-	423	BET	NR	-	NR	-	NR	-	NR	-	NR	-
[Liao et al. 2008]	MWCNT	NR	-	157	BET	NR	-	NR	-	NR	-	NR	-	NR	-
[Liao et al. 2008]	NH ₃ -MWCNT	Lab Modified	-	195	BET	NR	-	NR	-	NR	-	NR	-	NR	-
[Liao et al. 2008]	HNO ₃ -MWCNT	Lab Modified	-	152	BET	NR	-	NR	-	NR	-	NR	-	NR	-
[Yang et al. 2006b]	SWCNT	Chengdu, China	HNO ₃ , H ₂ SO ₄	541	BET	1.021	BET	0.8-1.6	TEM	1-2	TEM	10-50	TEM	90+	TGA
[Zhang	SWCNT-P	Cheap Tube,	-	486	BET	0.722	BET	0.8-	MC	1-2	MC	5-30	MC	88.6	TGA

et al. 2009]		USA						1.6							
[This study]	SWCNT-L	Cheap Tube, USA	-	442	BET	0.917	BET	0.8-1.6	MC	1-2	MC	5-30	MC	96.0	TGA
[This study]	SWCNT-S	Chengdu, China	-	413	BET	0.613	BET	0.8-1.6	MC	1-2	MC	0.5-2	MC	97.3	TGA
[Zhang et al. 2009]	SWCNT-OH	Chengdu, China	-	420	BET	0.739	BET	0.8-1.6	MC	1-2	MC	5-30	MC	91.1	TGA
[Zhang et al. 2009]	SWCNT-COOH	Chengdu, China	-	386	BET	0.680	BET	0.8-1.6	MC	1-2	MC	5-30	MC	95.9	TGA
[Chen et al. 2007]	SWCNT	Shenzen, China	Heat, NaClO, Ultrasound	370	BET	0.425	BET	NR	-	<2	MC	5-15	MC	90	MC
[Yan et al. 2008]	SWCNT 20	Shenzen, China	-	167	BET	0.417	BJH	NR	-	10-20	MC	1-2	MC	95+	MC
[Lin and Xing 2008b]	SWCNT	Shenzen, China	HNO ₃ , H ₂ SO ₄	541	BET	1.021	BET	NR	-	1.4 (1-2)	TEM (MC)	5-15	TEM	90+ 50+	MC
[Chen et al. 2008b]	SWCNT	Shenzen, China	-	447	BET	0.974	BET	NR	-	NR	-	NR	-	87	EA
[Chin et al. 2007]	SWCNT	Aldrich, USA	-	248	BET	NR	-	NR	-	1.2-1.5	SEM	2-5	SEM	50-70	NR
[Chin et al. 2007]	SWCNT Ox.	Lab Synthesized	HNO ₃	284	BET	NR	-	NR	-	1.2-1.5	SEM	2-5	SEM	50-70	NR
[Brooks et al. 2012]	SWCNT 1	Cheap Tube, USA	-	407	MC	NR	-	NR	-	1-2	MC	5-30	MC	90	Raman, XRD
[Brooks et al. 2012]	SWCNT 2	Carbon Solutions, USA	-	355	Calculated	NR	-	NR	-	1.55	MC	1-5	MC	40-60	NIR
[Brooks et al. 2012]	SWCNT Carbolex AP	Aldrich, USA	-	240	Calculated	NR	-	NR	-	1.4	MC	3-5	MC	66	TGA
[Brooks et al. 2012]	SWCNT HipCo	Carbon Nanotechnologies, USA	-	633	BET	NR	-	NR	-	1-2	Source	0.4-0.7	MC	85	TGA
[Shi et al. 2010]	SWCNT	Shenzen, China	-	406	BET	1.11	BET	NR	-	<2	MC	NR	-	NR	-
[Machado et al. 2012]	SWCNT	Lab Synthesized	HCl	388	BET	0.662	BET	NR	-	1-2	TEM	NR	-	99+	FTIR
[Peng et al. 2003]	As grown CNT	Lab Synthesized	-	134	NR	NR	-	NR	-	NR	-	NR	-	NR	-
[Peng et al. 2003]	Graphitized CNT	Lab Synthesized	Heat, N ₂	126	NR	NR	-	NR	-	NR	-	NR	-	NR	-
[Su and Lu 2007]	CNT	Shenzen, China	-	550	BET	1.150	BET	4.5	TEM	<10	MC	5-15	MC	95+	MC
[Wang et al. 2007]	CNT	Lab Synthesized	Heat	145	BET	0.398	BET	NR	-	30	TEM	NR	-	NR	-

[Rambabu et al. 2012]	CNT	Shenzen, China	-	189	BET	NR	-	NR	-	20-40	MC	5-10	MC	97	NR
[Yao et al. 2010]	CNT	Lab Synthesized	Acid Wash, Air	NR	-	NR	-	NR	-	NR	-	NR-	-	NR	-

Adsorbent Name: Adsorbent names were assigned by their associated authors in the original articles; Supplier: The short names for manufacturer companies and their countries (full names of companies can be found in Table B1 in Appendix B); Pretreat: The pretreatment techniques that were applied to CNTs after purchase if reported by the authors

Acronyms used in the table: MC: Manufacturer claimed, NR: Not reported, Mthd: Analytical method employed for obtaining the morphological information, BET: Brunauer-Emmett-Teller, BJH: Barrett-Joyner-Halenda, FTIR: Fourier transform infrared spectroscopy, TEM: Transmission electron microscopy, SEM: Scanning electron microscopy, TGA: Thermogravimetric analysis, EA: Elemental Analysis, AFM: Atomic force microscopy, XRD: x-ray diffraction, NIR: near-infrared spectroscopy

In the articles reviewed, approximately 30 different CNTs were synthesized in the lab, whereas the remaining 75 CNTs were obtained from manufacturers, indicating the widespread use of commercially available CNTs.

The most common CNT characteristics reported in the adsorption literature were specific surface area (SSA), pore volume (PV), pore size distribution (PSD), purity, elemental analysis (EA) and morphological information such as length, the inner and outer diameter and the number of walls. The mean SSA of SWCNTs and MWCNTs were $373 \pm 146 \text{ m}^2/\text{g}$ and $216 \pm 159 \text{ m}^2/\text{g}$, respectively. Considering various manufacturing, purification, and surface modification techniques, high standard deviations of SSA are reasonable. The theoretical SSA of SWCNTs with open ends was calculated as $2630 \text{ m}^2/\text{g}$ [Peigney et al. 2001]. The theoretical SSA calculations assumed that CNTs were composed of perfect sheets of carbons that covalently form hexagonal arrays. If the ends were closed, the inner cavity of the tube would be unavailable and the theoretical SSA would decrease to $1315 \text{ m}^2/\text{g}$. The reported SSAs of SWCNTs were significantly lower than the calculated theoretical surface areas, a decrease attributed to the tight aggregation of SWCNTs [Peigney et al. 2001]. Zhang et al. (2009) reported 19 - 37 individual tubes were forming bundles with a diameter 5 – 7 times larger than an individual SWCNTs. MWCNTs were assumed to be concentric tubular sheets with a distance of 0.45 nm between walls; therefore, the theoretical SSA is a function of number of walls. The measured and theoretical SSA of MWCNTs were reported to be in better agreement, which was attributed to the looser aggregation state of MWCNTs allowing the tubes to behave like isolated ones [Zhang et al. 2009].

The PV of SWCNTs was similar to the PV of MWCNTs. The mean total PVs were $0.78 \pm 0.23 \text{ cm}^3/\text{g}$ and $0.64 \pm 0.39 \text{ cm}^3/\text{g}$ for SWCNT and MWCNT, respectively. Theoretically, the pore volume occupied by the inner pores of SWCNTs is considerably higher when compared to MWCNT inner pore volume because the inner walls of MWCNTs occupy space whereas the SWCNTs have open inner channels. Zhang et al. (2009) reported that the availability of inner pores significantly affected the pore volume especially for SWCNTs.

SSA and PV are similar parameters that are expected to show an association with each other. However, the data compiled for all CNTs from the literature showed no correlation between SSA and the total PV ($r^2 = 0.18$). Investigating the CNT types separately yielded higher correlations ($r^2 = 0.50$ for SWCNT; $r^2 = 0.27$ for MWCNT) supporting that SWCNTs and MWCNTs have different aggregation states. It should be also noted that the SSA and PV of CNTs are determined with N_2 gas adsorption in their bulk phases. Given the aggregating nature of CNTs in water, to better interpret adsorption experiments performed in aqueous systems, it is important to develop techniques to characterize the SSA and PV distribution of CNT aggregates in water.

The inner and outer diameter ranges of MWCNTs were 2 – 15 nm and 4 – 200 nm, respectively. The wide range of the outer diameter was attributed to variations in the number of concentric tubular layers (walls) of CNTs. The diameters of SWCNTs were in the range of 0.8 – 2 nm with one exception, in which the SWCNT diameter range was reported as 10 – 20 nm as claimed by the manufacturer [Yan et al. 2008]. The length of MWCNT and SWCNT were in the ranges of 0.3 – 500 μm and 0.4 – 50 μm , respectively.

Almost all reported morphological properties (i.e. inner and outer diameter, length) were either claimed by the manufacturer and/or measured by electron microscopy (transmission, scanning electron microscopy) [e.g., Oleszczuk et al. 2009; Lin and Xing 2008b].

Approximately 50% of the CNTs reported were subject to pretreatment for purification or targeted functionalization prior to use (Table 2.1). The characterization of CNTs after pretreatment, and not relying only on the information provided by the manufacturers for virgin CNTs, is critical to avoid misinterpretation of the adsorption results. The most common pretreatment techniques used have been acid wash (HNO_3 , HCl , H_2SO_4), heat treatment and ultrasonication. Several studies oxidized the CNTs to increase the surface polarity [Salam and Burk 2008; Chen et al. 2009; Zhang et al. 2010a]. Functionalization of the CNTs has occurred at the sidewalls, and either at ends of the tubes or the defect sites through the covalent and non-covalent attachment of functional groups. Non-covalent functionalization may be beneficial since it has been shown to not change the CNT pore texture [Upadhyayula et al. 2009; Ma et al. 2011]. Adding oxygen containing functional groups on the CNT surface is the most commonly used functionalization approach. The amount and form of oxygen-containing functional groups ($-\text{OH}$, $-\text{COOH}$, $>\text{C}=\text{O}$) depend upon the type of oxidation technique and the acid utilized for purification [Ma et al. 2011]. Oxidation gives CNTs hydrophilic moieties and removes impurities, amorphous carbon and hemispherical caps and also adds acid/base reactivity through the production of carboxylic and phenolic groups.

The chemical modification of CNTs may also alter their physical properties. There are different reports regarding the impact of surface oxidation on the CNT morphology. Cho et al. (2008) oxidized MWCNTs by refluxing varying strengths (10 – 70% w/w) of HNO₃, KMnO₄ and H₂O₂ solutions at elevated temperatures (80 – 140⁰C). The controlled oxidation produced an array (1 pristine and 8 oxidized) of CNTs with surface oxygen ranging from 3.3 to 14%. The authors reported no change in SSAs after oxidation. Salam and Burk (2008) examined CNT surface oxidation by 18% H₂O₂ and 8M HNO₃ at elevated temperatures (80 - 140⁰C). Attachment of ~1 mmol/g acidic functional groups was detected; however, there was no change in SSA. Wang et al. (2010) also reported no SSA difference between the raw (0.2 - 1.0%) and oxidized (2.2 - 4.3%) CNTs. In their studies, raw and oxidized CNTs were purchased from a supplier and the oxidation techniques were not reported. On the other hand, Ji et al. (2010b) reported a “remarkable” increase in SSA from 410 to 650 m²/g and 160 to 420 m²/g for SWCNTs and MWCNTs, respectively, while using dry KOH etching to functionalize SWCNTs and MWCNTs. The dry KOH etching was described as contacting CNTs with KOH powder and heating to 800⁰C under N₂ stream. CNT surfaces yielding ~10% oxygen containing functional groups. The increase in SSA after oxidation was attributed to the removal of amorphous carbon during functionalization [Shen et al. 2009; Chen et al. 2009]. In contrast, Yu et al. (2012) reported a notable decrease in SSA (from 471 m²/g to 327 m²/g) when the total surface oxygen content was increased from 2% to 5.9%. The researchers used NaClO solution at ambient temperature for 12 hours to oxidize the pristine MWCNTs. Salam and Burk (2008) also reported a 26% decrease (from 144 to

106 m²/g) in SSA when 1M KMnO₄ was applied to CNTs at 80⁰C for 4 hours followed by a H₂SO₄ treatment. This decrease was attributed to the strength of the oxidizing agent that damaged the MWCNTs. These different findings indicate the importance of CNT type as well as the oxidizing agent and its strength on alteration of CNT surface chemistry. In addition to SSA, Cho et al., (2008) reported no change in structure or length distribution of CNTs after oxidation. However, Wu (2007b) reported a decrease in the diameter of MWCNTs after oxidation and attributed the modification of this diameter to the removal of the amorphous carbon from the surface. These results clearly demonstrate the necessity of extensive characterization of CNTs after pretreatment and/or functionalization for more accurate interpretation of their adsorption behaviors.

2.3. Adsorption of SOCs by CNTs

2.3.1. Influence of CNT Properties

The physical and chemical properties of CNTs play an important role in the adsorption of organic contaminants. Of all the known properties reported in the literature, none was found to solely control the adsorption of SOCs. Yang et al. (2006b) experimentally estimated that adsorption capacity of hydrophobic SOCs (i.e. PAHs with log K_{ow} ranging between 3.36 - 5.18) on CNTs increased with SSA and PV. Similarly Oleszczuk et al. (2009) showed a positive correlation of SSA, and micro- and mesopore volumes with the adsorption capacity of MWCNTs for two rather hydrophilic pharmaceuticals (i.e. carbamazepine, log K_{ow} -1.22 and oxytetracycline, log K_{ow} 2.45). Both studies presented strong linear relationships ($r^2 \geq 0.97$) between the adsorption

capacity of SOCs on MWCNTs and their SSAs. Zhang et al. (2009) also reported that SSA and PV were influential for the adsorption of hydrophobic SOCs, but they were not the exclusive factors determining adsorption capacities. On the other hand, Wang et al. (2009) observed SSA dependency for adsorption of macromolecular humic acids by MWCNTs only at higher concentrations because the site availability was not a limiting factor at the low concentration range.

Sorption sites such as inner pores and interstitial channels can impede the penetration of especially large organic macromolecules. Known as the size exclusion phenomenon, this remarkably decreases the adsorption of organics by CNTs [Wang et al. 2009]; a similar observation has also been reported on activated carbons [e.g. Kilduff et al. 1996]. The access of SOCs to the inner regions of CNTs or CNTs bundles may also be hindered due to amorphous carbon or metal catalysts that were introduced during synthesis [Gotovac et al. 2007c], and water cluster formation around the oxygen containing functional groups [Zhang et al. 2009].

The nanocurvature and diameter of CNTs also influence SOC adsorption. In their study, Gotovac et al. (2007a) reported that the alignment between PAH molecules and CNT surface affected adsorption. Tetracene molecules have four benzene rings aligning with the SWCNT surface whereas; phenanthrene had only 2.5 rings in alignment. Better alignment of tetracene resulting in a six-fold greater adsorption over phenanthrene. Also the increasing strength of π - π interaction caused more benzene rings to align on the surface. To the best of our knowledge, the effect of CNT length, and chirality (a

parameter related to the angle between graphene plane and the tube axis) on SOC adsorption has yet to be reported in the literature.

In addition to physical characteristics, CNT surface chemistry can also influence the SOC adsorption. The unintended oxidation of the surface during manufacturing and/or in the environment, and the intentional oxidation with treatment are some possible causes of CNT surface oxidation. Surface oxidation of CNTs may result in hindering or promoting SOC adsorption, while the former has been more frequently reported than the latter. Several studies have reported an overall decrease in the SOC adsorption with an increase in surface oxygen content [Cho et al. 2008; Shen et al. 2009; Salam and Burk 2008; Chen et al. 2009b; Zhang et al. 2010a; Li et al. 2011]. Two mechanisms have been proposed to explain the hindrance of adsorption: (i) the presence of oxygen on the CNT surface making adsorption of water molecules energetically more favorable relative to SOC adsorption, which results in water clusters that deplete the available surface area for SOCs; and (ii) the presence of oxygen on CNT surface localizes the π electrons, which reduces the π - π interactions between the CNT graphitic surface and benzene rings of aromatic SOCs. On the other hand, in their investigation of the adsorption of hydroxyl- and amino- substituted aromatics on oxidized CNTs, Chen et al. (2008b) reported stronger nonhydrophobic adsorption of 2,4-dichlorophenol and 2-naphthol than 1,3-dichlorobenzene and naphthalene by oxidized CNTs, which was attributed to the hydrogen bonding and π -hydrogen bonding interactions between -OH containing adsorbates and oxidized CNT surface. Yu et al. (2012) reported a remarkable increase (~100%) in adsorption capacities of toluene, ethylbenzene and *m*-xylene with increasing

surface oxygen content per SSA, up to ~8%, for MWCNTs. The increase was attributed to the increase in the dispersion of CNTs, also increasing the available adsorption sites. However, a further increase in the oxygen content per SSA (up to 18%) showed a decreasing trend in the adsorption capacity. The authors attribute this opposing behavior to the water cluster formation effect dominating over the CNT dispersion for SOC adsorption.

The surface charge of the CNTs will influence adsorption affinities of SOCs depending on their molecular structure, presence of ionizable groups and background pH. All these factors will be discussed in the following sections, SOC properties and background solution effects.

2.3.2. Influence of SOC Properties

Adsorbate properties such as solubility, molecular size, molecular configuration and polarizability play a role in adsorption of organic contaminants by CNTs. To understand the influence of SOC properties on adsorption, intermolecular interactions that govern the SOC adsorption should be examined. From the adsorbate point of view, the driving forces of adsorption are attraction to the CNT surface and repulsion from the background solution (i.e. water). The predominant repulsive force that repels SOCs from water onto the CNT surface are hydrophobic forces that are either associated with the size and polarity of the molecule or with the protonation state of ionizable compounds. There are also physical and chemical attractive forces between the SOCs and CNT surface. Nonspecific interactions are major contributors of overall attractive forces, which result

from the affinity of electron-deficient and electron-rich regions of uncharged molecules. These nonspecific attractions are generally referred as *van der Waals* interactions. The time-varying uneven electron distribution between the adjacent molecules generates London dispersive energy, and an increase in polarizability of the molecule increases the intensity of these forces. The differences of atomic electronegativities in the chemical structure of a molecule can cause a permanent dipole moment. This permanent dipole moment, in turn, causes a temporary dipole moment by inducing the even time-averaged electron distribution of the second molecule. The interaction between the permanent dipole moment and the induced dipole moment is referred as Debye energies. The last component of *van der Waals* interactions is the dipole-dipole interactions caused by the orientation of two molecules with dipole moments. These attractive forces are referred as Keesom energies [Schwarzenbach et al. 2003]. Though nonspecific attractive forces contribute to the overall intermolecular attraction regardless of the SOC properties, the intensity of these forces depends upon the molecular size, electric charge and polarizability. Other conditional attractive forces may contribute to adsorption depending on the SOC properties, such as π - π interactions between the resonating π electrons of the graphitic structure of the CNT surface and the π electron density of aromatic SOCs. Hydrogen bonding is a polarity dependent electrostatic attraction between certain SOCs with functional groups (such as OH) and functionalized surfaces of CNTs. Electrostatic interactions also occur between the charges of ionizable SOCs and charged surfaces of CNTs.

Hydrophobicity, represented mostly by octanol-water partitioning coefficient (K_{ow}) or aqueous solubility (C_w), was reported as the most predominant adsorbate property controlling adsorption of several SOCs by MWCNTs [Yang et al. 2006a; 2006b; Wang et al. 2008; 2009] and by SWCNTs [Brooks et al. 2012]. After hydrophobicity normalization, MWCNT and SWCNT adsorption capacities were relatively comparable for two SOCs (phenanthrene and biphenyl) [Zhang et al. 2009]. On the other hand, Wang et al. (2009) reported hydrophobicity normalized adsorption capacities following the order of molecular sizes for tested SOCs (phenanthrene > naphthalene > 1-naphthol) indicated that larger molecules have more affinities provided that SOCs had no other hydrophobic differences. Their study using MWCNTs, however, indicates that a micropore-filling mechanism may not be a major contributor to overall adsorption. On the other hand, Yang et al. (2006b) reported a negative correlation between the adsorption of naphthalene, phenanthrene and pyrene to molecular size, which they attributed to the poor access of large molecules to the micropores of SWCNTs and MWCNTs. The molecular size directly influences adsorption because the hydrophobic affinity cannot overcome the steric hindrances, a finding that was confirmed by Chen et al. (2007) in which, they determined that the molecular sieving effect prevented bulky 1,2,4,5-tetrachlorobenzene molecules from accessing the innermost surfaces [Chen et al. 2007; Wang et al. 2010a]. These findings show the importance of the bundle structure of CNTs and the availability of adsorption sites to SOCs. Gotovac et al. (2007c) tested the adsorption of naphthalene onto SWCNTs and investigated the adsorbed state of naphthalene on dry SWCNT using X-ray photoelectron spectroscopy and Raman

spectroscopy. In Gotovac et al. (2007c)'s study, the primary adsorption sites of SOCs were found to be the external curved surfaces of CNTs since the probe molecules (naphthalene) failed to penetrate into the hollow spaces within the nanotubes. Toth et al. (2012) also concluded that CNT adsorption occurred on the external surfaces exclusively. Chen et al. (2007) supported the concept that sorption sites of MWCNT were located on the innermost and outermost surfaces because the interlayer spacing between coaxial tubes are impenetrable to SOCs. Kinetic experiments conducted by Shen et al. (2009) suggest that the MWCNT pore-filling mechanism of nitroaromatic organics has a relatively low contribution to overall adsorption, indicating sorption to external surfaces rather than interstitial channel spaces. Zhang et al. (2009) reported that rigid and planar phenanthrene molecules can attach to the external surface area of interstitial channels of SWCNTs. Unlike phenanthrene, nonplanar and flexible biphenyl and 2-phenylphenol molecules have adjustable molecular configurations for better packing in the tubular spaces of MWCNTs (see Figure 2.2). Similarly, Pan et al. (2008) reported that the easily rotating structure of bisphenol-A allowed the molecule to wedge into the groove regions of CNTs unlike rigid 17α -ethinyl estradiol molecules. In both studies, flexible SOC molecules were less site-selective. Oleszczuk et al. (2009) applied ultrasonication to disperse CNT bundles and quantified the desorption of carbamazepine and oxytetracycline from CNTs. After ultrasonic pretreatment (i.e. disintegration of CNT bundles) oxytetracycline molecules were released more from CNTs than non-sonicated CNTs, indicating the presence of molecules trapped in the interstitial areas of CNTs. However, the dispersion state of CNTs did not influence carbamazepine adsorption, due

to the attraction of adsorbed carbamazepine molecules to free carbamazepine molecules that cause stacking of carbamazepine regardless of the aggregation state. Overall, these reports indicate that the hydrophobicity itself may not explain the adsorption affinity of SOC molecules on CNTs, and the accessibility of SOC molecules to different regions of CNT bundles and pores can be important for the adsorption of SOC molecules.

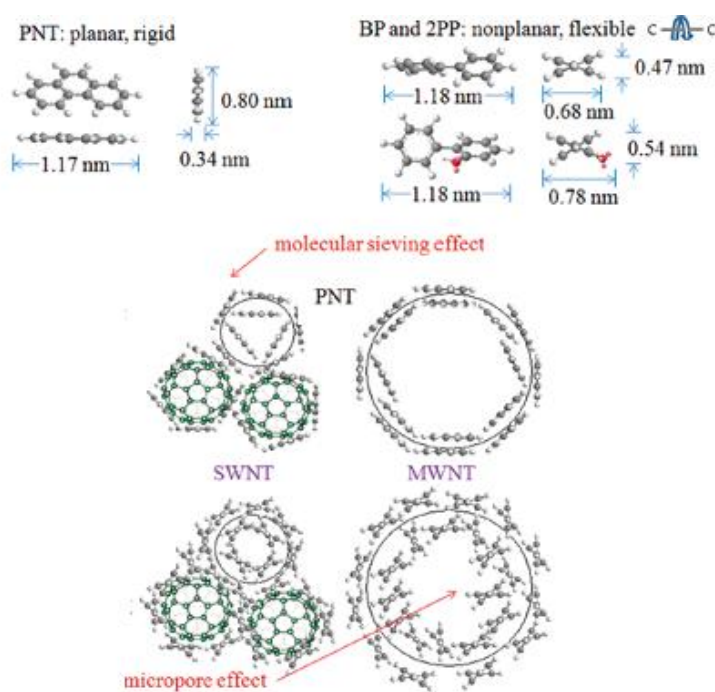


Figure 2.2. Adsorption sites of SWCNTs and MWCNTs [Yang et al. 2008]

Another principle SOC property influencing adsorption by CNTs is the π electron density of the compounds resonating in aromatic rings (also possibly for some aliphatic chains with double bonds). In that the graphitic surfaces of CNTs have regions with rich and poor π electrons, the interaction of π electrons influence adsorption [Gotovac et al.

2006; Oleszczuk et al. 2009; Chen et al. 2009b; Long and Yang 2001; Zhang et al. 2009; Wang et al. 2010a]. In their comparison of hydrophobicity normalized adsorption affinities of lindane (i.e. a cyclic chlorinated aliphatic molecule) with atrazine and phenanthrene (i.e. two aromatic SOCs), Wang et al. (2010a) concluded that $\pi - \pi$ interactions influence adsorption positively. Chin et al. (2007) reported a 60% increase in the adsorption of *o*-xylene after purification of SWCNTs at pH 3. This increase was attributed to $\pi - \pi$ attraction of xylene molecules and CNT surface. At pH 5 and 7, no notable increase was observed because at pH 3, the methyl groups on *o*-xylene were protonated and pushing electrons towards the benzene ring increasing the electron density of resonating π electrons. According to Lin and Xing (2008a), the sorption affinity of cyclohexanol was lower than phenol, and this difference was attributed to the $\pi - \pi$ interaction because cyclohexanol is missing π electrons and has comparable hydrophobicity with even a lower solubility than phenol. According to Chen et al. (2007), the adsorption affinity of the two-ring 2-naphthol was stronger than one ring 2,4-dichlorophenol. The higher adsorption of 2-naphthol was attributed to stronger conjugation potential of two rings resulting with stronger $\pi - \pi$ interactions. This study is supported by a comparison of two aromatic compounds: phenanthrene is adsorbed more than naphthalene because it has one more benzene ring that allows more polarization and higher dispersive forces with highly polarizable CNT surfaces (Wang et al. 2009). Additionally, the electron induction effect of chlorine atoms reduces the electron density of 2,4-dichlorophenol in the benzene ring, which suppresses its adsorption affinity. The $\pi - \pi$ stacking is obtained when the benzene rings of SOCs align with the CNT surface as

demonstrated by Gotovac et al. (2007a); therefore, the contribution of $\pi - \pi$ interaction between CNTs and the π electrons in aliphatic compounds depends on the molecular arrangement of molecules. Pan et al. (2008) supported the importance of molecular configuration by demonstrating the attachment of bisphenol-A with two benzene rings on CNTs along the circumference, suggesting that the $\pi - \pi$ electron donor acceptor complexes were stronger than $\pi - \pi$ donor or acceptor pairs. The thermodynamic calculations indicated that adsorption of bisphenol-A along the outer circumference of CNTs was very unlikely due to the high energy requirement for the steric conformation. Therefore, the presence of $\pi - \pi$ bonds may not always promote adsorption, and molecular configuration or surface conformation may also play an important role. Chen et al. (2007) proposed $\pi - \pi$ electron donor acceptor interactions between the π electron rich aromatic rings of adsorbates and π electron depleted regions of CNT surface. The ground-state hybrid structure of the $\pi - \pi$ electron donor acceptor system consisted of electrostatic forces between $\sigma - \pi$ quadrupoles of opposing benzene rings. This mechanism involved one-electron transfer from the highest occupied molecular orbital to the lowest unoccupied molecular orbital. The resulting bond was a weak covalent bond formed by unpaired electrons [Lin and Xing 2008a]. Chen et al. (2007) also reported an “extremely strong adsorption of 1-naphthylamine on CNTs”. This finding was attributed to the presence of the unshared pair of electrons of nitrogen on the amino group ($-\text{NH}_2$) making the benzene ring electron rich, which strongly (stronger than $-\text{OH}$) interacts with electron poor groups of the CNT surface. Since electron depleted regions are likely to be limited, strong adsorption affinity is expected to be more notable at low concentrations.

Similarly, Chin et al. (2007) concluded that adsorption of xylenes depended upon the position of the methyl group on the benzene ring resulting from the repulsive impact of the methyl group on the π electron density of the xylene molecule. Wang et al. (2010b) tested the adsorption of dialkyl phthalate esters and proposed $\pi - \pi$ electron donor acceptor interactions after hydrophobicity normalization because of the π electron-accepting ester functional group. Lin and Xing (2008a) investigated the adsorption of chlorophenols onto pristine and functionalized MWCNTs and reported a reduced capacity on oxidized CNT surfaces, because the $\pi - \pi$ dispersion was weakened by the oxygen containing functional groups on the surface. The substituent on the benzene ring was found to influence the resonance and time-dependent electron density of the aromatic SOCs, thus influencing the $\pi - \pi$ interactions.

Hydrogen bonding is another principal dipole-dipole attraction between a hydrogen atom and an electronegative atom such as nitrogen or oxygen. Hydrogen is also a possible contributor to adsorption, even though it cannot be evaluated completely independent from $\pi - \pi$ interactions [Chen et al. 2008b]. Several CNT adsorption studies emphasized the contribution of hydrogen bonding on overall adsorption [Lin and Xing 2008a; Yang and Xing 2009; Wang et al. 2010b; Li et al. 2011]. Lin and Xing (2008a) reported increasing order of adsorption affinities with decreasing hydrophobicities i.e. pyrogallol (3 -OH) > catechol (2 -OH) > phenol (1 -OH), which was attributed to the presence of hydrogen bonding. According to Wang et al. (2009) 1-naphthol molecules may form hydrogen bonds with the oxygen containing functional groups of CNT surface or benzene rings of 1-naphthol can be aligned to the CNT surface, which leaves the -OH

functional group facing the aqueous phase that forms new hydrogen bonding sites for free 1-naphthol molecules in water. Li et al. (2011) proposed hydrogen bonding between 4-nitrophenol and oxygen containing groups of MWCNTs. Though, Yang et al. (2010) also proposed hydrophobic attraction between 2,4-dichlorophenol, 4-chloroaniline and oxygen containing groups of MWCNTs, they emphasized the dependency of pH, because once the molecules are dissociated, the hydrogen bonding ability disappears.

Yang et al. (2008) found that nitro-, chloride- and methyl- functional groups attached to phenols or anilines enhance the affinity to MWCNTs. The order of their influence followed nitro group > chloride group > methyl group. They also reported the dependency of the phenol substitution pattern by observing higher adsorption when the hydroxyl group was attached in the *meta*- position rather than the *ortho*- and *para*- position. However, the authors avoided conclusive statements about the influence of group positions because different functional groups had different influences on adsorption affinity [Yang et al. 2008].

On the other hand, Chen et al. (2007) found that the contribution of hydrogen bonding on overall CNT adsorption of nitroaromatics was not significant. After testing the adsorption of 2,4-dinitrotoluene onto oxidized SWCNTs (17% oxygen) at a pH range of 2.8 – 7.3, they observed a slight decrease in adsorption capacity with decreasing pH. On the contrary, an increase in adsorption capacity was expected as the pH decreases if the hydrogen bonding was the controlling adsorption mechanism. In such a case, the COO^- functional groups on the CNT surface would be protonated and -COOH groups would act as H-bond donor and form hydrogen bonds with H-bond accepting nitro

groups. Lin and Xing (2008a) and Oleszczuk et al. (2009) also reported that hydrogen bonding might not be significant in that there was no proportional increase with the number of –OH groups of their adsorbates; the CNTs they used for adsorption, however, had a very low hydrogen and oxygen content. Yang et al. (2009) also determined that fulvic acid can act as a hydrogen bond donor due to carboxylic and phenolic moieties, while the CNT surface may act as hydrogen bond acceptors. They also reported electrostatic interactions between the surface charges of fulvic acid and CNTs, indicating that these interactions would strongly depend on the pH. In demonstrating the adsorption of 2,4,6-trichlorophenol at different pH values Chen et al. (2009a) found that increasing the pH values increased the dissociated (i.e. negatively charged) fraction of the compound, which decreased the adsorption due to repulsion between the negatively charged surface of CNT and anionic 2,4,6-trichlorophenol. In addition, the increased solubility of the ionized form of the adsorbate reduced the adsorption. Shen et al. (2009) presented stronger adsorption affinities of aromatic compounds with more nitro groups because these groups are strong electron acceptors interacting with highly polarizable electron-donating graphitic surfaces of MWCNTs. At lower pH values, adsorption was favored because of less ionization of contaminants such as acidic herbicides [Pyrzyska et al. 2007], direct dyes [Kuo et al. 2008] or sulfonamide antibiotics [Ji et al. 2009b]. At pH levels around pK_a , both electrostatic and hydrophobic sorption mechanisms were anticipated; however, it was not possible to distinguish between those two mechanisms [Pyrzyska et al. 2007].

2.3.3. Influence of Background Solution Properties

An array of background water chemistry conditions such as pH, ionic strength and NOM can influence the adsorption of SOCs by CNTs [Pan and Xing 2008; Zhang et al. 2010a]. NOM is ubiquitous in natural waters and adsorbs on CNT surfaces influencing its SOC adsorption [Su and Lu 2007; Yang and Xing 2009; Wang et al. 2007]. The net influence of NOM on SOC adsorption by CNTs is a tradeoff between two opposite effects [Zhang et al. 2010a]: (i) the competition by NOM depleting the sorption sites for SOC adsorption [Hou et al. 2013], and (ii) coating of NOM dispersing CNTs, thus exposing more adsorption sites for SOC [Pan et al. 2013]. According to Hou et al. (2013), though humic acid coated MWCNTs were better dispersed in water forming a loosely coiled network of tubes, the coverage of MWCNT adsorption sites reduced the adsorption affinity of phenanthrene, 2-naphthol and 1-naphthylamine noticeably. The reduction was attributed to the decrease in surface area due to effective humic acid coating of individual tubes. Chen et al. (2008a) reported a moderate reduction of naphthalene, 1,3-dinitrobenzene and 1,3,5-trinitrobenzene adsorption from humic acid competition. In addition to the direct competition for sorption sites, molecular sieving in micropores due to steric hindrance was proposed because the suppression of SOC adsorption was proportional to molecular sizes of tested SOCs. Wang et al. (2008) explored the adsorption of phenanthrene, naphthalene and 1-naphthol by MWCNTs coated with humic acid, α -phenylalanine and peptone. Peptone coating substantially reduced the surface area (from 87 to 35 m²/g) and shifted the pore size distribution from micro- to meso- and macro- ranges, indicating that the peptone coating was depleting

adsorption sites and blocking micropores. The authors also reported the introduction of polar moieties to CNT surfaces through peptone adsorption further repelled hydrophobic contaminants. On the other hand, the humic acid coating showed a much lower suppression of adsorption, which was attributed to the negatively charged polar functionalities of humic-acid dispersing MWCNTs that increased the effective surface area. According to Pan et al. (2013), humic acid suspended CNTs exhibited up to two orders of magnitude greater adsorption capacity for sulfamethoxazole than aggregated CNTs. The formation of a stable CNT suspension in tannic acid solution was also previously demonstrated by Lin and Xing (2008b). The increasing dispersion in water leading to higher surface area is likely to counterbalance the depletion of surface area due to humic acid coating. The authors suggested that the influence of NOM on SOC adsorption by CNTs depended upon the NOM properties. Another study by the same group [Wang et al. 2009] entailed an investigation of the influence of humic acid concentrations in competition with SOCs. At higher NOM concentrations, the competition was less pronounced because CNTs have limited number of high-energy adsorption sites and once these high-energy sorption sites are depleted, the competition for low-energy sorption sites was lower. Zhang et al. (2010a) also reported competition for high-energy sorption sites that was indicated by increasing surface heterogeneity represented by Freundlich n values. The study also showed a greater NOM-to-SOC ratio and a longer contact-time that reduced the SOC adsorption capacity. The comparison of simultaneous SOC and NOM adsorption with the preloading of CNTs with NOM

indicated that NOM preloading further decreased the adsorption capacities, suggesting a slower adsorption rate of NOM than SOCs.

The pH of the background solution is another major factor controlling adsorption. For organic acids, if $\text{pH} < \text{pK}_a$, the non-dissociated species for organic bases dominate the solution and vice versa. Therefore, the influence of background solution pH and ionic strength depends upon the ionizability and the electron donor acceptor ability of SOCs. The pH change also influences the protonation/deprotonation state of the functional groups on CNT surfaces. Deprotonation of acidic functional groups may increase the density of negatively charged functional groups that may create repulsive forces between negatively charged SOCs or may promote π -electron donor ability of CNT surface and enhance $\pi - \pi$ electron donor interactions between CNTs and SOCs. The formation of water clusters decreasing hydrophobicity and reduction of hydrogen bond formation decreasing adsorption affinity are other possible mechanisms for this increase in either repulsive forces or the promotion of electron donor ability [Pan and Xing 2008; Zhang et al. 2010a]. In their comparison of the adsorption of nonionic phenanthrene and ionizable 2-phenylphenol by CNTs under varying pH values, Zhang et al. (2010a) found that if the background solution had pH values ranging from 4 – 10, phenanthrene adsorption remained unaffected. However, there was an observable decrease in adsorption of ionizable 2-phenylphenol when the pH of the solution was over the pK_a of 2-phenylphenol. This decrease was attributed to the increased ionization and decreased hydrophobicity. Lin and Xing (2008a) tested adsorption of three phenolic adsorbates (phenol, pyrogallol and 1-naphthol) and one apolar adsorbate (naphthalene) over a pH

range of 2.2 -11. The decrease of adsorption affinities for phenolic compounds over their pK_a values were attributed to the increased electrostatic repulsion between dissociated adsorbates and negatively charged MWCNTs and the increase in hydrophilicities. In addition, the authors also noted that the dissociation of $-OH$ groups on phenolic compounds might be inhibiting the formation of hydrogen bonding. The adsorption affinities of phenolic compounds increased up to their pK_a values (from pH 2 to 6), indicating the π -electron donating properties of these compounds were altered. The change in adsorption affinity with increasing pH was not attributed to changing CNT properties because the adsorption affinity of nonionic naphthalene to the same CNTs remained constant in the same pH range. Similar results were demonstrated by Chen et al. (2008b) in the pH range of 3 – 11. For two nonionic aromatics (1,3-dichlorobenzene and naphthalene) adsorption was minimally affected. However, 2,4-dichlorophenol showed a significant decrease above the compound's pK_a value. The authors also reported an increase in the adsorption capacity of 2-naphthol above its pK_a value due to adsorption enhancing interactions counterbalancing the decrease in hydrophobicity. It should be noted that single point adsorption data were presented at pH 11 and the increase of adsorption was relatively small. In another study, Chen et al. (2007) tested adsorption of nonionic 1,2,4-trichlorobenzene and ionic 2,4-dinitrotoluene by varying the pH from 2.8 to 7.4. Nonionic adsorbate was independent of pH. Ionic 2,4-dichlorotoluene showed a very slight increase as the pH increased. Li et al. (2011) reported a decrease in adsorption of perfluorooctanic acid ($pK_a = -0.5$) onto MWCNTs with increasing pH from 2 to 10. This was attributed to the increase of electrostatic repulsion between deprotonated

perfluorooctanic acid and negatively charged functional groups of MWCNT at elevated pH values. In the same study, Li et al. (2011) reported an increase in adsorption of 4-nitrophenol ($pK_a = 10.7$) with increasing pH. In the pH range tested (2 - 10) 4-nitrophenol was protonated hence the increase was attributed to the increase in hydrogen bonding between the $-OH$ group of 4-nitrophenol and oxygen containing functional groups of MWCNTs inducing stronger attraction. Yao and Strauss (1992) observed an increasing attraction between cationic dyes and negatively charged CNT surfaces as the pH of the solution was increased. Among all tested ionizable compounds, the adsorption of dissociated compounds was remarkably lower than their non-dissociated forms.

The variance of the ionic strength of natural waters can be another factor that may influence adsorption of SOCs. Only a limited number of studies have been undertaken to determine the influence of ionic strength on SOC adsorption by CNTs. Further research is needed to examine the influence of ionic strength on CNT adsorption. Generally, ions have a salting out effect on hydrophobic compounds that decreases the solubility which may in turn enhance the CNT adsorption affinity [Chen et al. 2008c]. Kuo et al. (2008) reported the aggregation of dye molecules at higher salt ion concentrations and the promotion of adsorption. Ions may penetrate into the diffuse double layer and eliminate the repulsive energy between CNTs, however, which in turn forms a more compact aggregation structure that is unfavorable for SOC adsorption [Zhang et al. 2010a]. According to Zhang et al. (2010a), the ionic strength (in the range of 0.001 – 0.1 M) had negligible impact on adsorption of SOCs on CNTs because of these two counterbalancing effects. Chen et al. (2008a) also observed negligible influence of ionic strength on SOC

adsorption, which they attributed to a relatively narrow range of ionic strength (0.02 – 0.1 M). Clearly, tested ionic strengths exhibited no significant difference on nonionic SOCs, which have low electronic coordination abilities. Kuo et al. (2008) reported the aggregation of dye molecules at higher salt ion concentrations that promoted adsorption. In addition to ionic strength, the presence of metal ions has also been the subject of separate investigations. Wang et al. (2007) reported a significant increase in fulvic acid adsorption on CNTs with increasing $\text{Ca}^{2+}/\text{Mg}^{2+}$ ions. They attributed this increase to (i) the compression of the diffuse double layer and/or charge neutralization that decreases the repulsive forces between NOM and CNTs; (ii) bridging of cations with negatively charged functional groups of NOM molecules; and (iii) bridging of cations between the NOM and functional groups of the CNT surface. Chen et al. (2008a) found that the presence of 50 mg/L of Cu^{+2} reduced adsorption of SOCs up to 20%. This reduction was attributed to the complexation of metal ions with surface oxygen functionalities and formation of hydration shells of dense water that competed with SOCs. Chen et al. (2009a) observed the suppression of 2,4,6-trichlorophenol adsorption by MWCNTs in the presence of 6.5 - 65 mg/L Cu^{+2} especially for oxidized MWCNTs. In a separate study, Chen et al. (2008c) reported a reduction in adsorption capacities in the presence of copper, lead and cadmium, which they attributed to the large hydration spheres around the copper complexes. Additionally, the cross-bridging effect of cations between the anionic functional groups of CNT surfaces was suggested to form tighter CNT bundles, which in turn shielded the sorption sites.

Adsorption is predominantly a temperature-dependent process in which physical sorption occurs mostly as an exothermic process releasing energy. Thermodynamic investigations for the adsorption of nitroaromatics [Shen et al. 2009], trihalomethane [Lu et al. 2006], atrazine [Chen et al. 2009b; Yan et al. 2008; Rambabu et al. 2012], NOM [Su and Lu 2007; Wang et al. 2007], and TEX (toluene, ethylbenzene and m-xylene) [Yu et al. 2012] revealed that the CNT adsorption capacity decreases as the temperature increases. Su and Lu (2007) observed faster NOM adsorption kinetics when they increased the temperature, which in turn increased the diffusion rate. On the other hand, the adsorption of 1,2-dichlorobenzene [Peng et al. 2003] and pentachlorophenol [Salam and Burk 2008], dyes [Kuo et al. 2008; Wu 2007a; Ghaedi et al. 2012a; Rodriguez et al. 2010], and methylene blue [Shahryari et al. 2010] exhibited product-favored (endothermic) reactions, which again resulted in an increase in adsorption capacity with an increase in temperature. The commonality of all reported endothermic sorption behavior was the potential electrostatic attraction between the surface and the adsorbates, indicating that the adsorption thermodynamics depends upon the nature of the predominant sorption mechanism.

2.4. Predictive Models for Adsorption of SOCs by CNTs

Although many adsorption studies have been undertaken, they cover only a small portion of the approximately 40,000 anthropogenic pollutants that are known to us [Nirmalakhandan and Speece 1990]. While it is possible to expand conventional adsorption studies on CNTs to amass data, these adsorption isotherm experiments are

time consuming, costly and laborious. Therefore, predictive models are useful in rapidly gathering adsorption data and more thoroughly elucidating the mechanism of SOC adsorption on CNTs.

Several studies involved the use of physical properties (e.g. molecular refraction, aromaticity, parachor and the number of hydrophilic functional groups) to predict the adsorption of chemicals on activated carbon [Abe et al. 1981a; 1981b; 1983]. Fundamental thermodynamic concepts have also been used to explain the adsorption phenomena, the most ubiquitous of these being the Polanyi Theory, proposed by Manes (1978), the Net Adsorption Energy Concept, proposed by Suffet and McGuire (1978) and the Solvophobic Approach by Belfort (1979). The input parameters for these theoretical models are complicated and difficult to obtain

Similar to those methods, the quantitative structure-activity relationship (QSAR) is a statistical model development tool that has been employed to predict the adsorption of organic chemicals by activated carbon with computational input parameters that are relatively easier to obtain [Blum et al. 1994]. In QSAR modeling, chemical properties are related to molecular structures through molecular connectivity indices (MCI or χ index). MCIs are computational descriptors that are calculated via the hydrogen-suppressed molecular structure based on the sigma electrons. Simple MCIs encode topological information and the branching of a molecule is also encoded. Another common predictive model development approach, known as the Linear Solvation Energy Relationship (LSER), involves the use of solvatochromic parameters predicting the adsorption by activated carbon. In the LSER model, these parameters are used to relate chemical

properties to solvation energies such as cavity formation, dipolar interactions and the hydrogen-bonding energies [Hickey and Passionreader 1991]. First introduced by Kamlet et al. (1985), LSER has also been used to predict the activated adsorption of carbon [Luehrs et al. 1996; Shih and Gschwend 2009; Dickenson and Drewes 2010]. Solvatochromic descriptors contain chemical/physical information about the organic molecules used to explain the interactions between the adsorbate, the adsorbent and the solvent by five independent descriptors. The LSER model is expressed as follows (see eq. 1).

$$\text{Log } K = aA + bB + vV + pP + rR + c \quad [\text{eq. 1}]$$

where A is the hydrogen bond donating ability, B is the hydrogen bond accepting ability, V is the molecular volume or McGowan's volume, P is the polarizability/dipolarity, R is the excess molar refraction, c is the regression constant and the a , b , v , p and r are the regression coefficients.

There are several statistical predictive CNT models with dependent and independent variables, all of which are listed in Table 2.2. Yang et al. (2006b) presented single parameter linear relationships between the adsorbed volume capacity and the specific surface area, which is the monolayer N_2 adsorption volume capacity, also known as the micropore volume of CNTs. In all of their generated equations for five CNTs, all coefficients of determination (r^2) were above 0.99. Similarly in their correlations between

adsorption coefficients with specific surface areas, mesopore volume, and micropore volume of five CNTs, Oleszczuk et al. (2009) obtained an $r^2 > 0.96$.

Yang et al. (2008) reported a single parameter linear relationship between the Dubinin-Ashtakhov correlating divisor (E) parameter with hydrogen bond donor (A) properties of anilines and phenols, the individual correlation of the rest of solvatochromic parameters (B , V , and P) were statistically insignificant at $\alpha = 0.95$. In addition, the effort of a stepwise variable selection technique provided the P term to the LSER equation, indicating that like hydrogen bonding, π -electron polarizability is necessary for adsorption.

Xia et al. (2010a) developed an LSER equation to depict relative contributions of molecular interactions on CNT adsorption, which [eq. 2] expressed as follows:

$$\begin{aligned} \text{Log } K &= -0.37A - 2.78B + 4.18V + 1.75P + 0.043R - 1.33 \\ & \quad (n = 28, r^2 = 0.93) \qquad \qquad \qquad \text{[eq. 2]} \end{aligned}$$

The authors employed a mixture of 28 aromatic SOC's assuming that the SOC concentrations are low enough to prevent compound-compound interactions. According to their LSER derivative [eq. 2] the strongest contributor to adsorption is hydrophobicity, which is represented by the V term. The second most predominant factor is the hydrogen-bond donating ability with a negative correlation, which indicates an increase in the adsorbate-water interactions with an increase in B values.

Table 2.2. Summary of correlative equations between CNT adsorption descriptors and independent variables

Source	Dependent variable	Independent Variables	Number of cmpds-n	Coefficient of determination - r^2	Notes
Yang et al. (2006)	PMM adsorption capacity descriptor- (Q_0)	Specific surface area (SSA)	5	0.99	Phenanthrene on 5 different MWCNTs
Yang et al. (2006)	PMM adsorption capacity descriptor- (Q_0)	Micropore volume (PV_{micro})	5	0.99	Phenanthrene on 5 different MWCNTs
Oleszczuk et al. (2009)	Adsorption coefficient ($\log K$ at $C_e = 0.01 C_s$)	Specific surface area (SSA)	5	0.97	Two aromatic pharmaceuticals on 5 different MWCNTs
Oleszczuk et al. (2009)	Adsorption coefficient ($\log K$ at $C_e = 0.01 C_s$)	Micropore volume (PV_{micro})	5	0.97	Two aromatic pharmaceuticals on 5 different MWCNTs
Oleszczuk et al. (2009)	Adsorption coefficient ($\log K$ at $C_e = 0.01 C_s$)	Mesopore volume (PV_{meso})	5	0.99	Two aromatic pharmaceuticals on 5 different MWCNTs
Yang et al. (2008)	Dubinin-Ashtakhov “correlating divisor” (E)	Acidity (hydrogen bond donating ability - α)	13	0.68	13 anilines/phenolic compounds on MWNCT; single parameter correlation
Yang et al. (2008)	Dubinin-Ashtakhov “correlating divisor” (E)	Acidity and polarizability (hydrogen bond donating ability - α and polarizability - π)	13	0.68	13 aniline and phenolic compounds on MWNCT; poly parameter correlation using stepwise parameter selection indicated two significant parameters at 95% level of significance
Xia et al. (2010a)	Adsorption constant ($k = C_{ad}/C_e$)	LSER solvatochromic parameters (α , β , V and π)	28	0.93	Mixture of 28 aromatic compounds on MWCNT, poly parameter correlation indicated V and B as the most predominant contributors

Our survey of predictive modeling efforts indicated that both CNT (SSA, PV) and SOC properties (solvatochromic parameters) can be used to correlate CNT adsorption of SOCs. Both single parameter and poly-parameter linear regression studies were reported. Poly-parameter linear regression studies were either conducted by employing a predefined set of independent variables (solvatochromic parameters) or through the use of a parameter selection technique (e.g. stepwise parameter selection) [Yang et al. 2008]. The increasing number of data points decreased the linearity of correlations (smaller r^2) which reflected the ease fitting a straight line to a fewer number of data points. As such, a higher coefficient of determination (r^2) need not necessarily indicate a successful predictive model. An external validation may be required to enhance the reliability and accuracy of the model, however. In that modeling studies have only been undertaken to elucidate the adsorption of aromatic organics by MWCNTs, further research is required to model various classes of organics and other CNT types, most particularly SWCNTs.

2.5. Conclusions

Adsorption of several classes of SOCs (PAHs, benzene derivatives, phenolic compounds, pharmaceuticals, insecticides, herbicides, organic dyes, aliphatics etc.) by CNTs in water has been reported in the literature. Adsorption depends on the physicochemical properties of the adsorbates and CNTs as well as the background water chemistry. Multiple mechanisms, of varying relative importance, have been proposed to control the adsorption. However, the quantification of the individual contributions to overall adsorption remains as a challenging task.

Extensive characterization of CNTs, especially after pre-treatment and/or functionalization, should be included in the research articles. Overall, the SSA and PV have been influential for the adsorption of hydrophobic SOC_s, but they were not the exclusive factors determining the adsorption capacities. The SSA and PV of CNTs are determined with N₂ gas adsorption in their bulk phases. Given the aggregating nature of CNTs in water, it is important to develop methods to quantify the CNT aggregation in water. The particle size detection techniques may present indirect evidences of CNT aggregate sizes in water.

Surface oxidation of CNTs may result in hindering or promoting SOC adsorption, while the former has been more frequently reported than the latter. Two mechanisms have been proposed: (i) the presence of oxygen on the CNT surface making adsorption of water molecules energetically more favorable relative to SOC adsorption, reducing the available surface area for SOC_s; and (ii) the presence of oxygen on CNT surface localizes the π electrons, which reduces the π - π interactions between the CNT graphitic surface and benzene rings of aromatic SOC_s. On the other hand, the increase in adsorption capacities as a result of surface oxidation was attributed to better dispersion of CNTs, exposing more adsorption sites, and the increase in the ability to form hydrogen bonds with some SOC_s.

A large number of adsorption studies have been conducted for adsorption of aromatics. Research is also needed to examine the CNT adsorption of aliphatic compounds.

Natural organic matter is ubiquitous in natural waters. The competition between NOM and SOC may deplete sorption sites and hinder adsorption, while NOM coatings may also disperse CNTs, resulting in more sites for adsorption. More systematic studies are needed to examine the influence of NOM properties (source water type, hydrophobicity, molecular size, functional groups etc.) on CNT adsorption is recommended. This information will be critical to better assess the fate and transport of CNTs with SOC and NOM in environment.

Some statistical SOC adsorption models have emerged in recent years, but more research is needed to develop comprehensive SOC adsorption models on CNTs. Because there is a very large number of SOC and obtaining experimental adsorption data is laborious, costly and time consuming, predictive models for the adsorption of organic chemicals by CNTs will be of great significance to scientists, engineers and practitioners.

CHAPTER III

PREDICTIVE MODEL DEVELOPMENT FOR ADSORPTION OF AROMATIC CONTAMINANTS BY MULTI-WALLED CARBON NANOTUBES*

3.1. Introduction

Carbon nanotubes are nanomaterials exhibiting strong adsorption affinities to a wide range of SOCs. Despite the voluminous research reported in the literature, the available adsorption data for CNTs still covers only a small portion of approximately 70,000 anthropogenic pollutants [Luehrs et al. 1996]. Obtaining experimental adsorption data for pollutants can be laborious, costly and time consuming. Therefore, predictive models for the adsorption of organic chemicals by CNTs are of great significance to researchers and practitioners. These models may also provide some insights to the adsorption mechanisms of organic chemicals by CNTs, and they can be useful to assess the fate and transport of toxic chemicals with CNTs in the environment.

Quantitative structure-activity relationship (QSAR) and linear solvation energy relationship (LSER) have been used for the development of predictive models. Both approaches have input parameters that are much easier to obtain than the input parameters of thermodynamic models.

*Apul, O.G., Wang, Q., Shao, T., Rieck J. and Karanfil, T. 2013. Predictive model development for adsorption of aromatic contaminants by multi walled carbon nanotubes. *Environmental Science and Technology*, 47(5):2295-230.

In previous studies, QSAR and LSER methods have been successfully applied for the modeling of organic contaminant adsorption by activated carbons [Luehrs et al. 1996; Kamlet et al. 1985; Blum et al. 1994; Brasquet and Le Cloirec 1999; Dickenson and Drewes 2010; Shih and Gschwend 2009]. In the QSAR approach, adsorption of an adsorbate is related to molecular descriptors known as molecular connectivity indices (χ index). For the LSER approach, solvatochromic descriptors are employed as independent variables. Solvation energies including cavity formation, dipolar interactions, and the hydrogen-bonding energies [Hickey and Passino 1991] are used for modeling adsorption. To date, no QSAR model has been reported for predicting adsorption of organics by CNTs. In addition, no LSER model is available which comprehensively investigates the adsorption of organics on CNTs. Only recently, Xia et al. (2010a) developed an LSER equation to characterize the intermolecular interactions for adsorption of organic compounds on a multi-walled carbon nanotube (MWCNT).

In this chapter, QSAR and LSER techniques were used to develop predictive models for adsorption of organic contaminants by CNTs. Adsorption data for 29 aromatic compounds from literature including some of the experimental data obtained in our laboratory were used to develop predictive models with multiple linear regression analysis. LSER models at different concentrations were generated, and LSER parameter coefficients were examined to gain insights to the predominant adsorption interactions of low molecular weight aromatics on MWCNTs. The validity of the developed QSAR and LSER equations were evaluated using the dataset of 30 aromatics reported by Xia et al. (2010a). Finally, the data for all 59 compounds were used to obtain a combined LSER equation that would be used for predicting adsorption of aromatics by MWCNTs.

3.2. Materials and Methods

3.2.1. Selection of Adsorbates and Adsorbents for Modeling

A rigorous literature review was conducted to compile all the adsorption data for SOCs by CNTs. A database was created for adsorption of 46 organic compounds from 24 different studies including some of the data collected in our laboratory. Since the majority of the available data was for aromatics (39 compounds), modeling effort was focused on these compounds in the present study. Ten aromatic compounds had molecular weights larger than 200 g/mol, and they were rather complex and branched molecules. Preliminary modeling showed that these larger compounds did not follow the modeling trends of the remaining 29 compounds. This was attributed to their more complex physical and chemical interactions with CNTs as compared to the low molecular weight aromatic compounds. Therefore, the final dataset used for model development included 29 compounds (Table 3.1).

Type and surface chemistry of the activated carbons and CNTs have been shown to impact the adsorption of organic compounds [Zhang et al. 2009; 2010b; Karanfil and Kilduff 1999]. Therefore, the data for the adsorption on MWCNTs with less than 5% of oxygen content were used in the modeling. Since the available dataset for single-walled carbon nanotubes (SWCNTs) was much smaller than that of MWCNTs, model development in the present study focused on the MWCNTs.

3.2.2. Training Dataset

Single point adsorption descriptors ($K = q_e/C_e$, where q_e : solid phase equilibrium concentration and C_e : liquid phase equilibrium concentration) at three different C_e values, infinite dilution conditions (K_∞ , at an average of 0.2% of sorbate aqueous solubility, Table C1), 1%, and

10% of the aqueous solubility of each adsorbate represented by $K_{0.01}$ and $K_{0.1}$, respectively, were obtained from the isotherm data, and used as dependent variables in the model development. The details of K_{∞} , $K_{0.01}$, and $K_{0.1}$ determination are provided in Appendix C. To account for the differences in the surface areas of different MWCNTs, ranging from 60 to 560 m^2/g used in different studies, adsorption descriptors were also normalized with the specific surface areas of MWCNTs. Both mass (Table 3.1) and surface area (Table C2, Appendix C) basis K values were used for model generation. These constituted the training datasets for modeling.

3.2.3. Validation Dataset

Independent of the training dataset, the data reported by Xia et al. (2010a) was used as an independent validation dataset to verify the developed model equations. The validation and the training datasets had nine common compounds (chlorobenzene, phenol, naphthalene, biphenyl, 2-chlorophenol, nitrobenzene, 2,4-dichlorophenol, 1,2,4-trichlorobenzene, 2,4-dinitrotoluene). They were excluded from the validation dataset to prevent repetition. In addition, one aliphatic compound (hexachloroethane) was also excluded since the models were developed for aromatic compounds. Overall, 30 aromatics constituted the validation dataset. The $\log K_{\infty}$, and $\log K_{SA,\infty}$ values are listed in Table 3.2. The data for higher C_e values were not available to use for validation.

3.2.4. Molecular Connectivity Indices for QSAR Model

Molecular connectivity index is represented with ${}_n X_c$ where 'n' represents the order of the index, while 'c' represents the fragment configuration (p for path, c for cluster, ch for chain, pc for path-cluster). The index of a molecule is calculated via its hydrogen-suppressed structure based on the sigma electrons, and it encodes topological information for the compound. The

index order increases with branching structure of a molecule. The second superscript ‘v’ is enabled (χ_v) when the descriptors are calculated based on their valance electrons, which represents electronic information of a compound [Kier and Hall 1986]. In the present study, 33 χ indices were computed by MolconnZ 3.24 software, and used as independent variable for QSAR model development.

Table 3.1. List of compounds for training dataset, data sources and adsorption descriptors

	Compound	Reference	Log K_∞*	Log K_{0.01}	Log K_{0.1}
1	Phenanthrene	Yang et al. (2006a)	3.29	3.04	2.37
2	Pyrene	Yang et al. (2006a)	4.01	3.80	3.30
3	Naphthalene	Yang et al. (2006a)	1.63	1.33	0.76
4	1-naphthol	Lin and Xing (2008a)	0.76	0.91	0.20
5	Biphenyl	Zhang et al. (2010a)	2.05	1.91	1.47
6	2-phenylphenol	Zhang et al. (2010a)	1.63	0.82	-0.18
7	Benzene	Chen et al. (2007)	-0.45	N.A	N.A
8	Chlorobenzene	Chen et al. (2007)	-0.33	0.64	-0.36
9	1,2,4-trichlorobenzene	Chen et al. (2007)	1.17	1.23	0.87
10	Nitrobenzene	Chen et al. (2007)	0.33	N.A	N.A
11	2,4-dinitrotoluene	Chen et al. (2007)	2.38	0.57	-0.18
12	Phenol	Lin and Xing (2008a)	-0.54	-1.58	-2.27
13	Catechol	Lin and Xing (2008a)	0.21	N.A	N.A
14	Pyrogallol	Lin and Xing (2008a)	1.18	N.A	N.A
15	2,4,6-trichlorophenol	Chen et al. (2009a)	1.43	-0.56	-0.12
16	3-nitrotoluene	Shen et al. (2009)	1.03	N.A	N.A
17	4-nitrophenol	Yang et al. (2008)	0.77	N.A	N.A
18	Aniline	Yang et al. (2008)	-0.77	-1.43	-1.87
19	4-chloroaniline	Yang et al. (2008)	-0.66	-0.30	-0.84
20	2-nitroaniline	Yang et al. (2008)	1.60	0.21	-0.56
21	3-nitroaniline	Yang et al. (2008)	0.72	0.19	-0.50
22	4-nitroaniline	Yang et al. (2008)	0.95	0.43	-0.26
23	4-methylphenol	Yang et al. (2008)	0.06	-0.81	-1.56
24	2-chlorophenol	Yang et al. (2008)	0.08	N.A	N.A
25	4-chlorophenol	Yang et al. (2008)	0.74	N.A	N.A
26	2,4-dichlorophenol	Yang et al. (2008)	0.96	0.01	-0.75
27	2-nitrophenol	Yang et al. (2008)	0.56	0.14	-0.46
28	3-nitrophenol	Yang et al. (2008)	0.92	0.22	-0.47
29	1,3-dinitrobenzene	Shen et al. (2009)	1.46	N.A	N.A

N.A: Data was not available within the experimental isotherm range. *: K is in mg/g

Table 3.2. List compounds for external validation dataset and adsorption descriptors (Xia et al. 2010a)

	Compound	Log K_{∞}	Log $K_{\infty,SA}$
1	Ethylbenzene	0.19	-2.18
2	4-xylene	0.26	-2.11
3	Bromobenzene	0.50	-1.87
4	Propylbenzene	0.76	-1.61
5	4-chlorotoluene	0.82	-1.55
6	Benzonitrile	0.04	-2.33
7	4-fluorophenol	-0.32	-2.69
8	Benzyl alcohol	-0.90	-3.27
9	Iodobenzene	0.88	-1.49
10	Acetophenone	0.26	-2.11
11	3-methylphenol	0.08	-2.29
12	Methyl benzoate	0.70	-1.67
13	4-chloroanisole	1.07	-1.30
14	Phenethyl alcohol	-0.46	-2.83
15	3-methylbenzyl alcohol	-0.15	-2.52
16	4-ethylphenol	0.62	-1.75
17	3,5-dimethylphenol	0.49	-1.88
18	Ethyl benzoate	1.14	-1.23
19	Methyl 2-methylbenzoate	1.12	-1.25
20	3-chlorophenol	0.62	-1.75
21	4-nitrotoluene	1.44	-0.93
22	4-chloroacetophenone	1.28	-1.09
23	3-bromophenol	0.79	-1.58
24	1-methylnaphthalene	1.89	-0.48
25	2-dichlorobenzene	0.56	-1.81
26	3-dichlorobenzene	0.65	-1.72
27	4-dichlorobenzene	0.51	-1.86
28	Isophorone	0.01	-2.36
29	2-chloronaphthalene	2.73	0.36
30	Azobenzene	2.72	0.35

*: K is in mg/g, $K_{\infty,SA}$ in mg/m²

3.2.5. Solvatochromic Descriptors for LSER Model

Adsorption of organic compounds by CNTs is controlled by a number of physicochemical interactions, some of which are described with solvatochromic descriptors (Abraham descriptors) as independent variables in the LSER model. Solvatochromic theory

explains the adsorption interactions between adsorbate, adsorbent and solvent with solute specific descriptors capturing the cavity formation, dipolar interactions and hydrogen bonding interactions. In the LSER equation A is hydrogen bond donating ability (acidity), B is hydrogen bond accepting ability (basicity), which, are related to the hydrogen bonding interactions. However, LSER model cannot distinguish the H-bonding from π -H bonding, for which the interaction intensity is expected to be proportional to the H-donating ability of the adsorbate. V is molecular volume or McGowan's volume, associated with the size of the molecule; and it represents hydrophobically driven adsorption as well as non-specific interactions between adsorbate and adsorbent. P is the polarizability/dipolarity term; and it represents the dipolar interactions. It should be noted that the V term may not be completely independent of the P term. For example, for aromatic molecules, the P term does not explicitly quantify π - π interactions, but polarizability may be influenced by electron withdrawing or donating functional groups, which may influence π electron density. A higher π electron density may cause more interactions with the π electrons at the CNT surface. The c is the regression constant and a , b , v and p are the regression coefficients. All solvatochromic descriptors were obtained from Absolv module of ADME Suite 5.0 software (Tables C3 and C4, Appendix C).

3.2.6. Multiple Linear Regression

Multiple linear regression was employed to develop correlations between adsorption descriptors and independent variables. Fitting equations were obtained using SAS v.9.2 software. The generalized linear model (GLM) procedure of SAS was applied for parameter selection. The least absolute shrinkage and selection operator (LASSO) method was used for variable selection and determination of coefficients in QSAR model. LASSO is an operator that simultaneously

selects the independent variable and determines the coefficient which is superior to ordinary least square estimates providing interpretable coefficients and avoids multicollinearity and inflated correlation coefficients [Tibshirani 1996]. The GLM procedure of SAS was applied to estimate the coefficients of LSER model. Since the independent variables were already set, no variable selection method was necessary for LSER.

The regression models were evaluated by the p -values presented in analysis of variance (ANOVA). At 95% level of significance the p -value less than 0.05 indicated that at least one of the independent variables of the developed equation is useful in predicting the dependent variable. The significance of selected individual variables was quantified by individual p -values that are testing the coefficients of variables being different from zero. The individual parameters' p -values less than 0.05 indicate that at 95% level of significance the coefficient is different from zero. The goodness of the fit was examined by coefficient of determination (r^2). Multicollinearity or the correlation of independent variables with each other was tested by the variation inflation factor (VIF). Multicollinearity occurs when an independent variable is highly correlated with one or more other independent variables. Thus, if the value of one independent variable is changed, the values for other independent variables will also change since the independent variables are highly correlated. The potential harm due to multicollinearity is that it is difficult to infer the separate influence of the independent variables on the dependent variable [Belsley et al. 1980]. Higher VIF values indicate higher correlations with one or more of the remaining independent variables. The independent variables were accepted as correlated, if the VIF values were larger than 10. The predictive precision of the models were quantified by the prediction error sum of squares (PRESS). A smaller PRESS value indicates a stronger prediction tendency of a model. PRESS values were used to quantify the internal validation strength. The predictive precision of

the models for external validation data were checked by root mean squared error (RMSE). RMSE is calculated by taking the square root of the squared sum of residuals. Residuals are the differences between predicted values and actual values. Partial residual plots were generated by plotting each independent variable against the residuals. RMSE values were used to quantify the external validation strength of the predictions. Both PRESS and RMSE were used to compare the models.

3.3. Results and Discussion

3.3.1. Development of Quantitative Structure-Activity Relationship (QSAR)

The significant independent variables for QSAR model were determined, and the coefficients were estimated using the training dataset and the LASSO procedure. The fitting equation obtained is presented in eq. 3.

$$\text{Log } K_{\infty} = - (2.98 \pm 0.52) + (0.18 \pm 0.12) {}^0\chi + (0.17 \pm 0.15) {}^0\chi^v + (0.55 \pm 0.20) {}^3\chi_p \quad [\text{eq. 3}]$$

$$(n = 29, r^2 = 0.88)$$

LASSO procedure revealed three independent variables (${}^0\chi$, ${}^0\chi^v$, ${}^3\chi_p$) as the model parameters from 33 χ indices. This procedure prevents over fitting of the data by selecting fewer independent variables when compared to other parameter selection procedures such as forward addition and backward elimination. Fitting equation (eq. 3) had an r^2 of 0.88, and multicollinearity (VIF < 10) was not observed. The r^2 of the model indicated the data fitting ability of the equation. Surface area normalization of K_{∞} did not further improve the QSAR model (eq. 4). No significant impact on the regression model was observed, indicating that

surface area of adsorbent was not a limiting factor at infinite dilution conditions. This was attributed to the much larger surface areas of the MWCNTs than the required area by the amount of each adsorbate on the surface.

$$\text{Log } K_{SA,\infty} = - (4.85 \pm 0.59) + (0.12 \pm 0.14) \chi^0 + (0.14 \pm 0.17) \chi^v + (0.62 \pm 0.23) \chi^p \quad [\text{eq. 4}]$$
$$(n = 29, r^2 = 0.84)$$

The detailed SAS outputs of regression models including *p*-values, VIF numbers, and ANOVA tables were presented in Appendix C.

3.3.2. Validation of the QSAR Model

The range of indices for the compounds in the training dataset was comparable with the range of indices for the compounds in the validation dataset (Figure 3.1), which indicated that the developed QSAR equation (eq. 3) should be able to predict the adsorption of compounds in the validation dataset. The predicted values were compared with the experimentally obtained values, as presented in Figure 3.2. The PRESS value of the training dataset was 5.6. The RMSE value for the validation set was calculated as 0.48, and the compounds were evenly distributed around the perfect prediction line indicating prediction accuracy of the QSAR model.

The adsorption of isophorone was the poorest predicted one within the validation dataset. Similarly, it was the poorest predicted compound in the model developed by Xia et al. (2010a) that measured isophorone adsorption by MWCNT. Although, no reason was stated for this poor prediction in our previous publication (Apul et al. 2013), it should be noted that isophorone is a cyclic ketone; however, QSAR and LSER models were trained by aromatic compounds. The

poor prediction can be attributed to the lack of aromaticity in the molecular structure of isophorone. Therefore, isophorone was excluded from partial residual analysis. Partial residual plots (Figure C1, Appendix C) showed that the independent variables of the QSAR model were not correlated with the residuals.

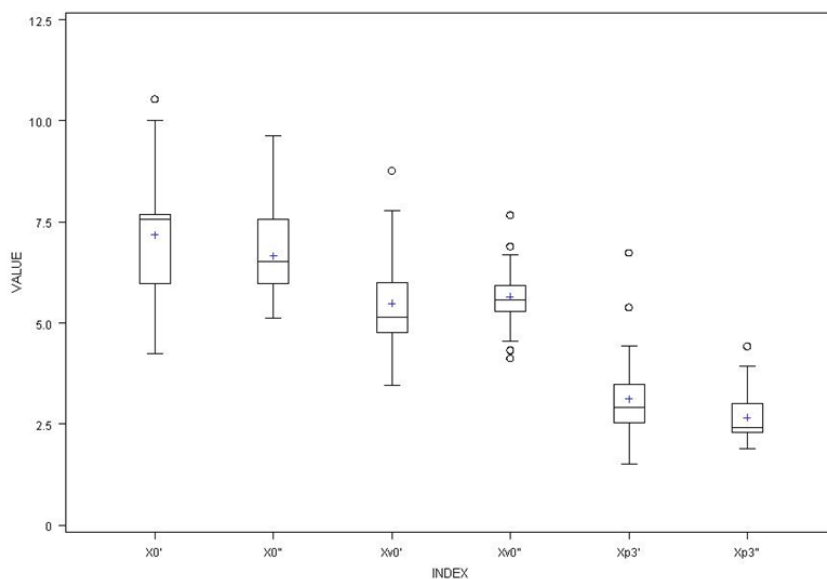


Figure 3.1. Box and whisker plots for the QSAR descriptors. (Xv0, X0, Xp3 and Xp6 represent, χ^0_v , χ^0 , χ^3_p and χ^6_p , respectively. The descriptors representing the training dataset of 29 aromatic compounds are labeled with ('), and the descriptors representing the validation dataset of 30 compounds are shown with (''). The empty circles (o) represent the mild outliers of datasets.)

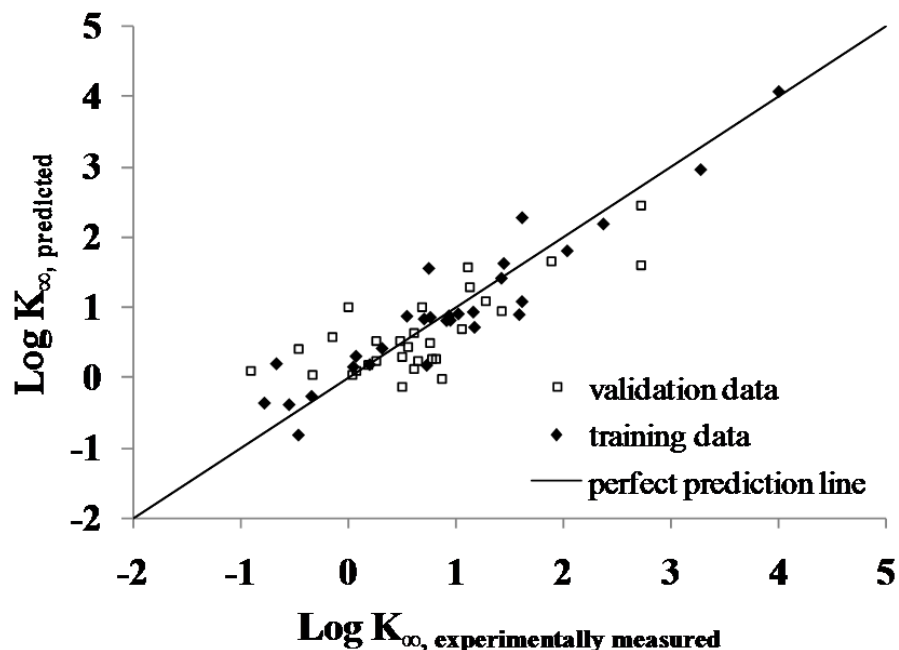


Figure 3.2. Experimentally measured adsorption descriptors reported by Xia et al. (2010a) vs. the predicted adsorption descriptors by QSAR model (eq. 3) for training and external validation datasets.

3.3.3. Development of Linear Solvation Energy Relationship (LSER)

The range of the solvatochromic descriptors (A , B , V and P) for the adsorbates in the training dataset is shown in Figure 3.3, and their numerical values are also provided in Table C3 (Appendix C). Multiple linear regression of LSER descriptors against $\log K_{\infty}$ values determined the coefficients of solvatochromic descriptors. The fitting equation to the training dataset is presented in eq. 5.

$$\text{Log } K_{\infty} = - (4.34 \pm 0.56) + (0.05 \pm 0.32) A - (0.48 \pm 0.86) B + (4.55 \pm 0.56) V + (0.61 \pm 0.34) P$$

[eq, 5]

$$(n = 29, r^2 = 0.83)$$

The V term was the most influential descriptor in the LSER equation. It represents the adsorbate molar volume, capturing the *van der Waals* interactions that are non-specific intermolecular attractions and hydrophobically driven adsorption that is related to the energy requirement for cavity formation in water [Schwarzenbach et al. 2003]. Positive correlation of the V term with the adsorption descriptor indicated the importance of non-specific attractions and hydrophobicity on CNT adsorption. The contribution of these forces represented by the V term was reported as the most influential term ($V = 4.18$) by Xia et al. (2010a) for modeling of their adsorption data on a single MWCNT. In addition, strong positive correlations have been reported between the V term and adsorption for activated carbons [Luehrs et al. 1996; Kamlet et al. 1985; Shih and Gschwend 2009; Schwarzenbach et al. 2003].

The hydrogen bond forming ability captured by A and B terms was statistically insignificant in the LSER equation at 95% level of significance. The lack of significance was attributed to two factors: (i) the low oxygen contents of MWCNTs, for which the hydrogen bonding interactions with the adsorbates may not be important, and (ii) a small range of hydrogen accepting ability of the compounds in the training dataset indicated by their B values, and the absence of hydrogen donating ability (i.e., $A = 0$) of many of the compounds (Table C3, Appendix C). Earlier LSER studies conducted for activated carbon adsorption [Luehrs et al. 1996; Shih, and Gschwend 2009] reported very little or no contribution of the A term to adsorption. On the other hand, the B term was previously reported as a negatively correlated descriptor for activated carbon adsorption. Wang et al. (2009) and Xia et al. (2010a) reported the B as the second most influential descriptor (after V term) that was negatively correlated with adsorption on a MWCNT. However, in eq. 5, the hydrogen bond accepting ability captured by the B term was statistically not different from zero, at the 95% level of significance. More data

are needed with a wider range of B values to further evaluate the role and significance of this parameter. Finally, the polarizability (P) term was also found to be a statistically insignificant parameter in the developed LSER equation at the 95% level of significance. For activated carbon adsorption, the coefficient of the P term was not found to be influential [Luehrs et al. 1996, Kamlet et al. 1985, Xia et al. 2010a]. The P parameter was not significant because both solubility and adsorption affinity of a compound may increase with polarizability [Kamlet et al. 1985]

Surface area normalization of K_{∞} did not have a significant impact on the regression of the LSER model (eq. 6), indicating that surface area was not a limiting factor for adsorption of aromatic compounds at very low concentrations.

$$\text{Log } K_{SA,\infty} = - (6.19 \pm 0.63) - (0.03 \pm 0.37) A - (0.65 \pm 0.97) B + (4.31 \pm 0.63) V + (0.58 \pm 0.39) P$$

[eq. 6]

$$(n = 29, r^2 = 0.77)$$

When compared to the QSAR equation (eq. 3), the coefficient of determination for the LSER model (eq. 5) was slightly lower ($r^2 = 0.83$ vs. $r^2 = 0.88$). The better data fitting with QSAR was attributed to the availability of the larger number of independent variables (i.e., 33 χ indices) to include in the model. The χ indices contain topological information for the adsorbates without describing the adsorption interactions. On the other hand, LSER model has a small number of predetermined independent variables (A , B , V and P), which can be related to some intermolecular interactions of adsorption.

3.3.4. Validation of the LSER Model

The validation dataset descriptor ranges were within the training dataset descriptor ranges as shown in Figure 3.3. The predicted $\log K_{\infty}$ values obtained from eq. 5 were plotted against the experimental $\log K_{\infty}$ values obtained from Xia et al. (2010a) in Figure 3.4. The PRESS value of the LSER model was 9.2. It was higher than the PRESS value of QSAR model (5.6); indicating the QSAR approach has stronger prediction ability than the LSER approach. Since the QSAR has many more independent variables to select from, it is not surprising to have a smaller PRESS value. The RMSE value for the validation set was calculated as 0.45. The predicted values were compared with the experimentally obtained values, as presented in Figure 3.4. The compounds were evenly distributed around the perfect prediction line indicating the prediction accuracy of the LSER model.

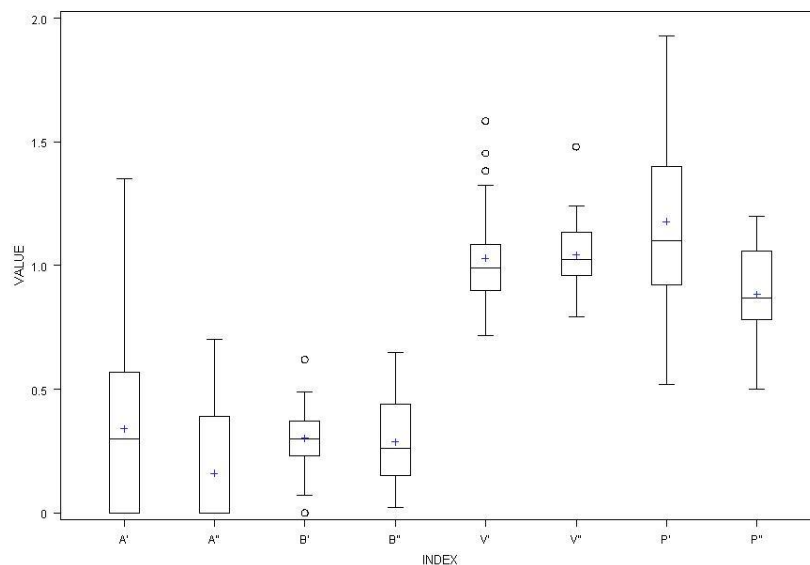


Figure 3.3. Box and whisker plots for the LSER descriptors. (*A*, *B*, *V* and *P* are the solvatochromic descriptors. The descriptors representing the training dataset of 29 aromatic compounds are labeled with (´), and the descriptors representing the validation dataset of 30 compounds are shown with (ˆ). The empty circles (o) represent the mild outliers of datasets.)

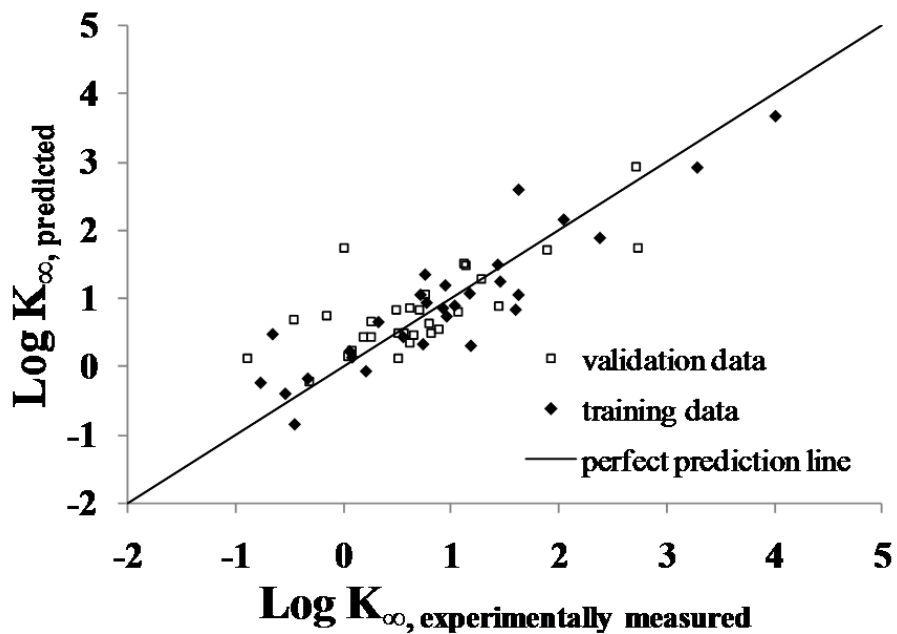


Figure 3.4. Experimentally measured adsorption descriptors reported by Xia et al. (2010a) vs. the predicted adsorption descriptors by LSER model (eq. 4) for training and external validation datasets.

Isophorone was excluded from the partial residual analysis to be consistent with the QSAR residual analysis. The partial residual plots (Figure C2, Appendix C) of the LSER model showed that residuals were scattering around the zero line as expected. The independent parameters were not correlated with the residuals, except for phenolic aromatics. The values of the *A* and *B* terms for the phenols were correlated with the residuals. The increasing hydrogen bond accepting ability (or decreasing hydrogen bond donating ability) increased the residual values, and resulted in overprediction of adsorption because of hydrogen bonding between the compounds and water.

The LSER model developed in the present study (eq. 5) was also compared with the model of Xia et al. (2010a). While *A*, *B*, *V* and *P* terms were significant in the model by Xia et al. (2010a); only the *V* term was statistically significant in eq. 5 of the present study. A close

examination of the datasets suggested that this difference might result from the different ranges of descriptors. To investigate the impact of descriptor ranges on the significance of model parameters, compounds with highest descriptor values in the training dataset were eliminated one by one and LSER models were developed after removing each compound. This analysis indicated that the significance of each descriptor was increasing when the descriptor ranges became narrower. The results are presented in Figure C3 in Appendix C.

Using the data for all 58 compounds in the training and validation datasets, a combined model was also developed (eq. 7). The predicted values were compared with the experimentally obtained values, as presented in Figure C4 in Appendix C. The parameter ranges for the combined model are shown in Figure 3.5. The detailed SAS outputs of regression model including *p*-values, VIF numbers, and ANOVA tables are also presented in Appendix C.

$$\text{Log } K_{\infty} = - (4.31 \pm 0.37) - (0.01 \pm 0.21) A - (1.91 \pm 0.39) B + (4.45 \pm 0.38) V + (1.06 \pm 0.21) P$$

[eq. 7]

$$(n = 58, r^2 = 0.83)$$

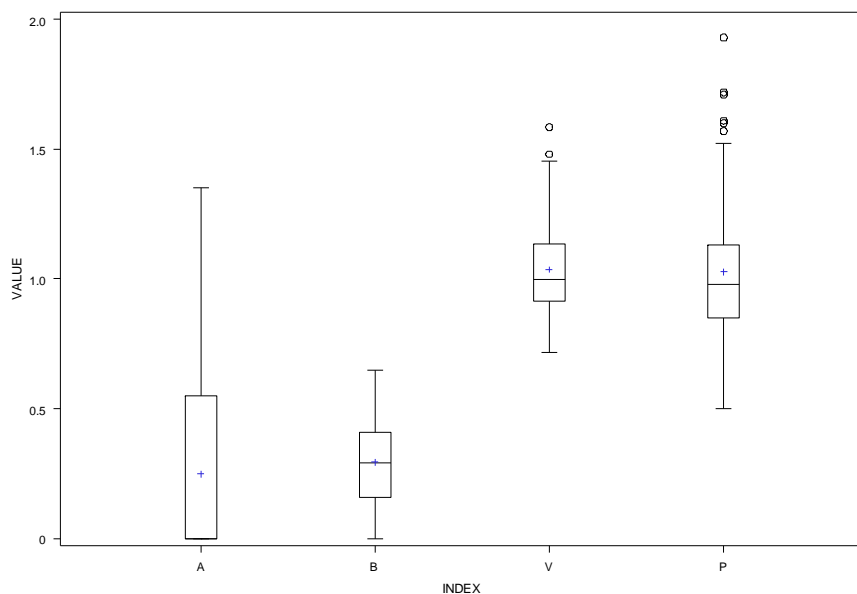


Figure 3.5. Box and whisker plots for the LSER descriptors for combination of training and validation datasets. (*A*, *B*, *V* and *P* are the solvatochromic descriptors. The descriptors represent the training dataset of 59 aromatic compounds of the combined dataset. The empty circles (○) represent the mild outliers of datasets.)

To evaluate these three models [i.e., (i) the model developed by Xia et al.(2010a), (ii) the model developed for 29 compounds (eq. 5) and (iii) the combined model (eq. 7)], their prediction capabilities were compared for 58 compounds by calculating RMSE values (Table C5, Appendix C). The results showed that the combined model (eq. 7) gave the smallest RMSE value (0.40) showing the best prediction capability, while the 29 compound model (eq. 5) and the model by Xia et al. (2010a) had similar RMSE values (0.45) which was 11% higher than the combined model. The use of combined model is recommended for predicting the adsorption of aromatic compounds having *A*, *B*, *V* and *P* values within the ranges used to develop the model on MWCNTs with less than 5% oxygen contents.

3.3.5. LSER Models at Higher Equilibrium Concentrations

To investigate the LSER models across an isotherm, adsorption descriptors of the same compounds at higher equilibrium concentrations were modeled using solvatochromic descriptors. The experimental data were available up to 10% of aqueous solubility for twenty compounds in the training dataset (Table C2, Appendix C). The LSER equations obtained for 1% and 10% of adsorbate aqueous solubility are presented in equations 8 and 9, respectively.

$$\text{Log } K_{0.01} = - (3.81 \pm 0.78) - (1.31 \pm 0.56) A - (2.86 \pm 1.22) B + (4.41 \pm 0.70) V + (0.67 \pm 0.47) P$$

[eq. 8]

$$(n = 20, r^2 = 0.85)$$

$$\text{Log } K_{0.1} = - (4.42 \pm 0.55) - (1.29 \pm 0.40) A - (3.81 \pm 0.85) B + (4.59 \pm 0.49) V + (0.74 \pm 0.33) P$$

[eq. 9]

$$(n = 20, r^2 = 0.93)$$

The predicted and actual adsorption descriptors were plotted to assess the effectiveness of modeling at higher concentrations (Figure 3.6). Two major observations from the higher saturation models are (i) the persistence of the V term as the predominant parameter in the models, and (ii) the increasing influence of A , B and P terms with increasing equilibrium concentration. The coefficients of descriptors were in the order of $V > B > A > P$ for the models indicating non-specific and hydrophobic interactions are the strongest contributor to overall adsorption followed by hydrogen bonding (represented by A and B terms) and dipolar interactions.

In order to examine the change in the LSER parameters as a function of concentration, we developed another infinite dilution concentration model only for the 20 compounds used for modeling at high concentrations. This was necessary because our analysis while comparing our model in the infinite dilution concentration with the model of Xia et al. (2010a) showed that the model parameters can be affected from the descriptor range of the compounds. The results showed that V was the only significant parameter at infinite dilution concentration for the 20 compounds (model not shown). However, at higher concentrations A and B parameters became significant as indicated by eq. 8 and 9. One possible explanation is that the solute – CNT surface interactions become less influential with increasing concentration. This might be due to the possible hindrances from the increasing CNT surface area coverage at high concentrations, and/or increasing solute – solute interactions which decreases the chances of solute molecules interacting with the CNT surface. At the same time, the increasingly negative model coefficients of A and B indicate that adsorption will be less favorable for compounds having high A and B values at higher concentrations. Additionally, this study extended the modeling to higher concentrations (eq. 6 and eq. 7), and the results showed that although the V parameter was still dominant, the A and B parameters also became significant at higher concentrations, as previously discussed.

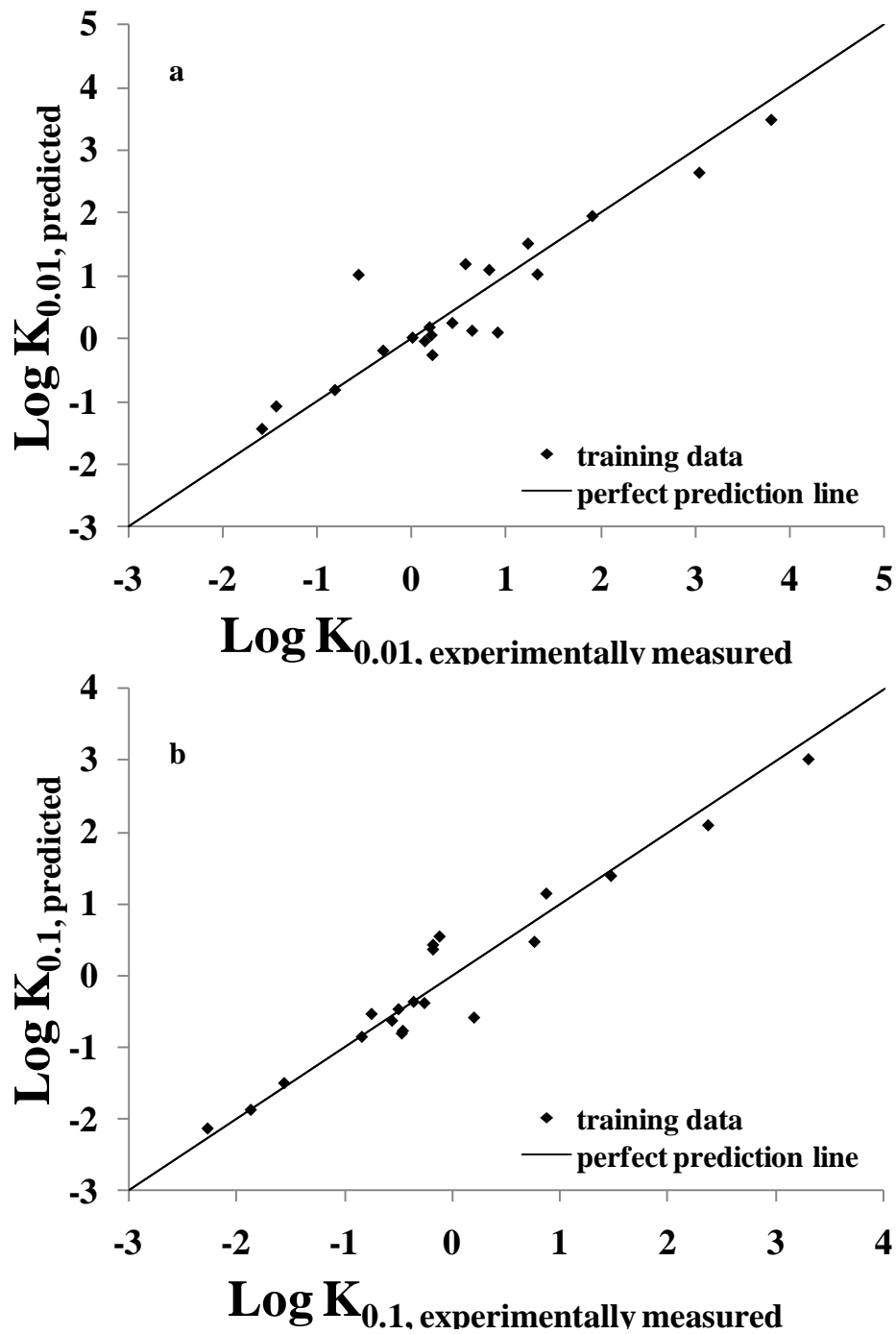


Figure 3.6. Experimentally measured adsorption descriptors vs. the predicted adsorption descriptors obtained by the LSER equations for (a) 1% and (b) 10% of adsorbate aqueous solubility for training dataset ($n = 20$).

3.4. Conclusions

This study demonstrates that successful predictive models can be developed for the adsorption of organic compounds by CNTs using QSAR and LSER techniques. However, the development of models, their statistical validation and applicability in practice will highly depend on the available data, including the number of compounds in the training and external validation datasets, and the ranges of adsorbate descriptors and CNT characteristics. Researchers reporting the detailed characterization of CNTs and the isotherm data/conditions in their publications will be of great value for future data compilation and modeling efforts.

Three models (at infinite concentrations, 1% and 10% of adsorbate aqueous solubility) were developed for adsorption of aromatics by MWCNTs with less than 5% oxygen content. These models will be valuable to assess adsorption of low molecular weight aromatic compounds ($MW < 200$ g/mol) by MWCNTs. Since the dataset used in this study was combined with the dataset obtained by Xia et al. (2010a), the final LSER equation at infinite concentrations was developed for a much wider range of compounds including high solubility phenols (pyrogallol, catechol), and some polyaromatic hydrocarbons (pyrene, phenanthrene). Furthermore, the model by Xia et al. (2010a) was developed only for one MWCNT, whereas the final LSER equations in this study were obtained using the data for a number of MWCNTs with less than 5% oxygen content. The LSER equation demonstrated the significance of hydrophobicity and non-specific attractions for CNT adsorption captured by the V , which was consistent with the results of Xia et al. (2010a).

CHAPTER IV

ADSORPTION OF HALOGENATED ALIPHATIC SOCs BY CARBON NANOTUBES

4.1. Introduction

Carbon nanotubes (CNTs), classified as single walled (SWCNT) and multi-walled CNT (MWCNT), can be visualized as sp^2 hybridized graphitic carbon sheets rolled into hollow cylinders with nanometer scale diameters and micrometer scale lengths. Owing to their unique structures, CNTs have been used in many applications such as electronics, medicine, space industry, and military [Klaine et al. 2008; Mauter and Elimelech 2008]; as a result, their production and use has been rapidly increasing [Lam et al. 2006]. The estimated CNT global market was approximately 90.5 million dollars in 2010, and it was projected to exceed 1 billion dollars by 2015 [Nanoposts 2010]. This rapidly increasing CNT production while raising concerns about their potential harmful impacts in the environment [Ferguson et al. 2008, Xia et al. 2010b] also attracts attention for their potential uses as adsorbents in environmental applications [Klaine et al. 2008; Upadhyayula et al. 2009].

CNTs present strong adsorption affinities to a wide range of organic contaminants [Gotovac et al. 2007b; Yang et al. 2006b; Wang et al. 2008; 2010a; Chen et al. 2007; Lin and Xing 2008a; Brooks et al. 2012; Oleszczuk et al. 2009; Ji et al. 2009a; Gupta et al. 2013]. To date, adsorption of approximately 100 SOCs by CNTs were reported in the literature, and the majority of the tested SOCs has been aromatic compounds. To the best of our knowledge, adsorption of aliphatic compounds by CNTs have been examined only in a small number of

studies, including four cyclic aliphatic [Chen et al. 2007; Lin and Xing 2008a; Brooks et al. 2012; Wang et al. 2010a] and eight acyclic aliphatic compounds [Brooks et al. 2012; Lu et al. 2006; Li et al. 2011]. However, several aliphatic SOCs have been classified by United States Environmental Protection Agency (USEPA) under Priority Pollutants List (e.g., 1,1,1-trichloroethane, 1,1,2,2-tetrachloroethane, carbon tetrachloride) or listed on the Candidate Contaminate List (CCL3) (e.g., 1,1,1,2-tetrachloroethane, 1,1-dichloroethane, 1,2,3-trichloropropane). Therefore, it is also important to understand the adsorption of aliphatic SOCs by CNTs. Furthermore, there has been no attempt to model their adsorption behavior to gain insights to the adsorption mechanisms.

In this study, the main objective was to investigate adsorption affinities of a suite of environmentally significant halogenated aliphatic SOCs by CNTs. We examined intermolecular interactions to gain a mechanistic insight to the adsorption of ten aliphatic SOCs by a SWCNT and a MWCNT. We also developed a quantitative structure-adsorbability relationship for adsorption of aliphatic SOCs by CNTs using linear solvation energy relationship (LSER) modeling. Finally, we compared adsorption of aliphatic and aromatic SOCs by CNTs.

4.2. Materials and Methods

4.2.1. Materials

Pristine SWCNT and MWCNT were obtained from Chengdu Organic Chemicals Co., Ltd. and Nanostructured & Amorphous Materials Inc., respectively, and they were used as received. Selected characteristics of CNTs are summarized in Table 4.1. Nitrogen adsorption at 77 K was performed with a physisorption analyzer (Micromeritics ASAP 2020) to determine the specific surface area (SSA), pore volume (PV) and pore size distributions of CNTs. The

Brunauer-Emmett-Teller (BET) equation was used to calculate surface areas. The total pore volume was calculated from the adsorbed volume of nitrogen near the saturation point ($P/P_0 = 0.99$). Pore size distribution of adsorbents was determined from the nitrogen isotherms using Density Functional Theory (DFT). The distribution of pores were determined by associating pore volumes less than 2 nm as micropores, the range of 2 - 50 nm as mesopores and 50 nm or larger as macropores. The oxygen contents of CNTs were analyzed using a Flash Elemental Analyzer 1112 series (Thermo Electron Corporation). Their purities were determined using a TA Instruments Q5000 IR thermogravimetric analyzer. Morphological characteristics such as length and outer/inner diameter of the CNTs were provided by the manufacturers. The details of CNT characterization methods have been reported in detail elsewhere [Dastgheib et al. 2004].

Ten different aliphatic SOCs were selected as adsorbates. They were obtained in analytic grade from Acros (TeCE, <99%), Fluka (1,2-DCP, >99%; 1,2-DBA, >98%), Matrix Scientific (1,2-DB-3-CP, >98%), Alpha Easer (TCE, >99.5%), TCI (TeCA, >99%), Baker Analytical (1,1,1-TCA, >96.7%), and Sigma Aldrich (1,1,2-TCA, >96%; 1,1-DCE, >99%; CCl₄, >99.9%). The definition of these acronyms and their properties are summarized in Table 4.2. The molecular structures of these SOCs are presented in Table D1.

Table 4.1. Physical characteristics of CNTs

	S_{ABET}	V_T	V_{micro}[†]	V_{meso}[†]	V_{macro}[†]	Oxygen Content	Purity^{**}	O.D.^{**}	I.D.^{**}	Length^{**}	Number of Walls^{**}
	(m ² /g)	(cm ³ /g)	<1 (%) - <2 (%)	2-50 (%)	50> (%)	(%)	(%)	(nm)	(nm)	(μm)	
SWCNT	537	1.240	9.2 – 9.4	46.8	43.8	0.9	98.2	1-2	0.8- 1.6	5-30	1
MWCNT	179	0.752	0.5 - 1.5	31.7	66.8	0.5	99.9	8-16	3-5-	10-50	15

S_{ABET}: Specific surface area, V_T: Total Pore Volume, O.D: Outer Diameter, I.D: Inner Diameter

[†]modeled by DFT ^{**}provided by the manufacturer

Table 4.2. Selected properties of aliphatic SOCs

No.	SOC	Abbreviation	Molecular Weight (g/mol)	Molar Volume (cm ³ /mol)	Log C _w (g/L)	Log K _{OW}
1	1,1-dichloroethylene	1,1-DCE	97	80.2	3.38	1.32
2	1,2-dichloropropane	1,2-DCP	113	97.4	3.45	2.28
3	1,1,1-trichloroethane	1,1,1-TCA	133	100.8	3.13	2.49
4	1,1,2-trichloroethane	1,1,2-TCA	133	92.4	3.65	1.89
5	1,2-dibromoethane	1,2-DBM	188	86.6	3.62	1.96
6	1,1,1,2-tetrachloroethane	1,1,1,2-TeCA	168	108.3	3.04	2.93
7	trichloroethylene	TCE	131	89.7	3.07	2.42
8	1,2-dibromo-3-chloropropane	1,2-DB-3-CP	236	113.5	2.99	2.43
9	tetrachloroethylene	PCE	166	102.5	2.35	3.40
10	carbon tetrachloride	CCL4	154	96.9	2.90	2.83

4.2.2. Adsorption Isotherms

Constant CNT dose liquid phase adsorption isotherms were conducted in distilled and deionized water (DDW) using completely mixed reactors with Teflon-lined screw caps. Concentrated stock solutions of each SOC were prepared in methanol. Isotherm bottles containing predetermined masses of CNTs were first filled with DDW, and then spiked with SOC stock solution. The volume percentage of the methanol spiked per bottle was kept below 0.1% (v/v) to minimize the co-solvent effect. The bottles with no headspace were placed into a rotary tumbler for one week, which was found to be sufficient to reach equilibrium during preliminary kinetic experiments [Zhang et al. 2009]. The supernatants were extracted into hexane by liquid: liquid extraction and analyzed by gas chromatography, micro electron capture detector (GC- μ ECD) equipped with Rxi-624Sil MS Column (Restek, USA). Bottles without any adsorbents served as blank reactors to monitor the loss of adsorbates during equilibration. All experiments were performed at room temperature (20 ± 2 °C) without any buffer addition. The solution pH remained around 6.6.

4.2.3. Isotherm Modeling

Non-linear Freundlich model (FM) was employed to fit the experimental isotherm data (eq.10):

$$q_e = K_F C_e^n \quad [\text{eq. 10}]$$

where K_F [(mg/g)/(Ce) n] is the capacity parameter equal to the amount adsorbed at a value of C_e equal to unity, and n is a dimensionless parameter related to the heterogeneity of the surface [Zhang et al. 2009]. Two K_F parameters ($K_{F,\mu}$ and $K_{F,m}$) were used to represent SOC adsorption capacities at equilibrated concentrations of 1 μ g/L and 1 mg/L, respectively. The $K_{F,\mu}$

was not calculated for MWCNTs because the isotherm ranges did not include 1 $\mu\text{g/L}$. The coefficient of determination (r^2) values indicated that FM exhibited the goodness of fit to the experimental data.

Single point adsorption descriptors at four different aqueous concentrations (500 ppb, 750 ppb and 1000 ppb represented by $K_{D,500}$, $K_{D,750}$ and $K_{D,1000}$, respectively) were also tabulated in Table D2 in Appendix D.

4.2.4. LSER Modeling

The LSER model has the following form (eq. 11):

$$\text{Log } K = aA + bB + vV + pP + rR + c \quad [\text{eq. 11}]$$

where ‘Log K_D ’ is the single point adsorption descriptor (q_e/C_e) at corresponding equilibrium concentration within the empirical isotherm range (i.e. $K_{D,500}$, $K_{D,750}$ and $K_{D,1000}$ at 500, 750 and 1000 $\mu\text{g/L}$, respectively). ‘ A ’ is hydrogen bond donating ability (acidity) describing the ability of the solvent to donate a proton to the solute, ‘ B ’ is hydrogen bond accepting ability (basicity) describing the solvent’s ability to accept a proton from the solute, ‘ V ’ is molecular volume (McGowan’s volume) which is the bulk/cavity term, ‘ P ’ is polarizability (dipolarity) term measures the ability to stabilize a neighboring charge or a dipole by virtue of its non-specific dielectric effect, and ‘ R ’ is excess molar refractivity (permanent dipole) describing non-specific *van der Waals* interactions that a solute can undergo. The ‘ R ’ parameter is inter-correlated with the ‘ V ’ parameter to some extent because the cavity term also captures size dependent non-specific interactions. These two parameters cannot be distinctly separated;

however, the two together cover the cavity formation and non-specific attraction energies. The LSER solvatochromic parameters for SOCs were obtained from the Absolv module of ADME Suite 5.0 software. These parameters are listed in Table D3 in Appendix D. The 'a, b, v, p, and r' terms are the coefficients obtained after regression and they quantify the relative contribution of each term to the dependent variable. The 'c' term is the regression constant. Multiple linear regressions were performed using SAS v.9.2 software. The generalized linear model (GLM) procedure of the software was applied to estimate the regression coefficients and the constant. The goodness of the fit was examined by the coefficient of determination (r^2). Prediction precision of the LSER models were quantified by the prediction error sum of squares (PRESS) values. A smaller PRESS value indicates a stronger prediction tendency of a model. PRESS values are used to quantify the internal validation strength of models by Leave-One-Out (LOO) internal validation technique.

4.3. Results and Discussion

4.3.1. Adsorption Isotherms

The liquid phase adsorption isotherms of ten halogenated aliphatic SOC_s onto SWCNT and MWCNT are illustrated in Figure 4.1. Freundlich isotherm parameters are provided in Table 4.3. The Freundlich model, a widely used non-linear isotherm model, fit the data reasonably well ($r^2 > 0.94$). The SOC uptake of SWCNT was higher than MWCNT. The total SSA of SWCNT was ~3 times higher than that of MWCNT (Table 4.1), while SWCNT had approximately 50 times higher $K_{F,m}$ values than MWCNT (Table 4.3), which suggests that SSA was not the only factor controlling the adsorption of aliphatic SOC_s by CNT_s.

A comparison of the Freundlich adsorption capacity descriptor ($K_{F,m}$) by SWCNT and MWCNT of each SOC is presented in Figure 4.2. SWCNT had higher adsorption capacity for all compounds tested. The specific surface area ($K_{F,m,SSA}$) and micropore volume (<1 nm) ($K_{F,m,micro PV}$) normalized $K_{F,m}$ values, respectively, are provided in Figure 4.2b and 4.2c. After SSA normalization, the differences between SWCNT and MWCNT adsorption affinities slightly decreased (Figure 4.2b), while micropore volume normalization reduced the differences completely and collapsed two lines to a single line (Figure 4.2c). This suggests that the microporous (<1 nm) regions of CNT bundles play an important role in the adsorption of aliphatic SOC_s. The analysis presented was based on the adsorption descriptors (represented by $K_{F,m}$) obtained at higher equilibrium concentration region of isotherms. At lower concentrations (represented by adsorption capacity descriptor $K_{F,\mu}$), on the other hand, the surface coverages (or amount of solute

adsorbed) were low; thus, there was an abundance of available sorption sites, and SSA or micropore volume was not the controlling factor for adsorption. The $K_{F,\mu}$ values of SWCNT and MWCNT values were not compared since the isotherm data at the very low concentration values for MWCNT were not available.

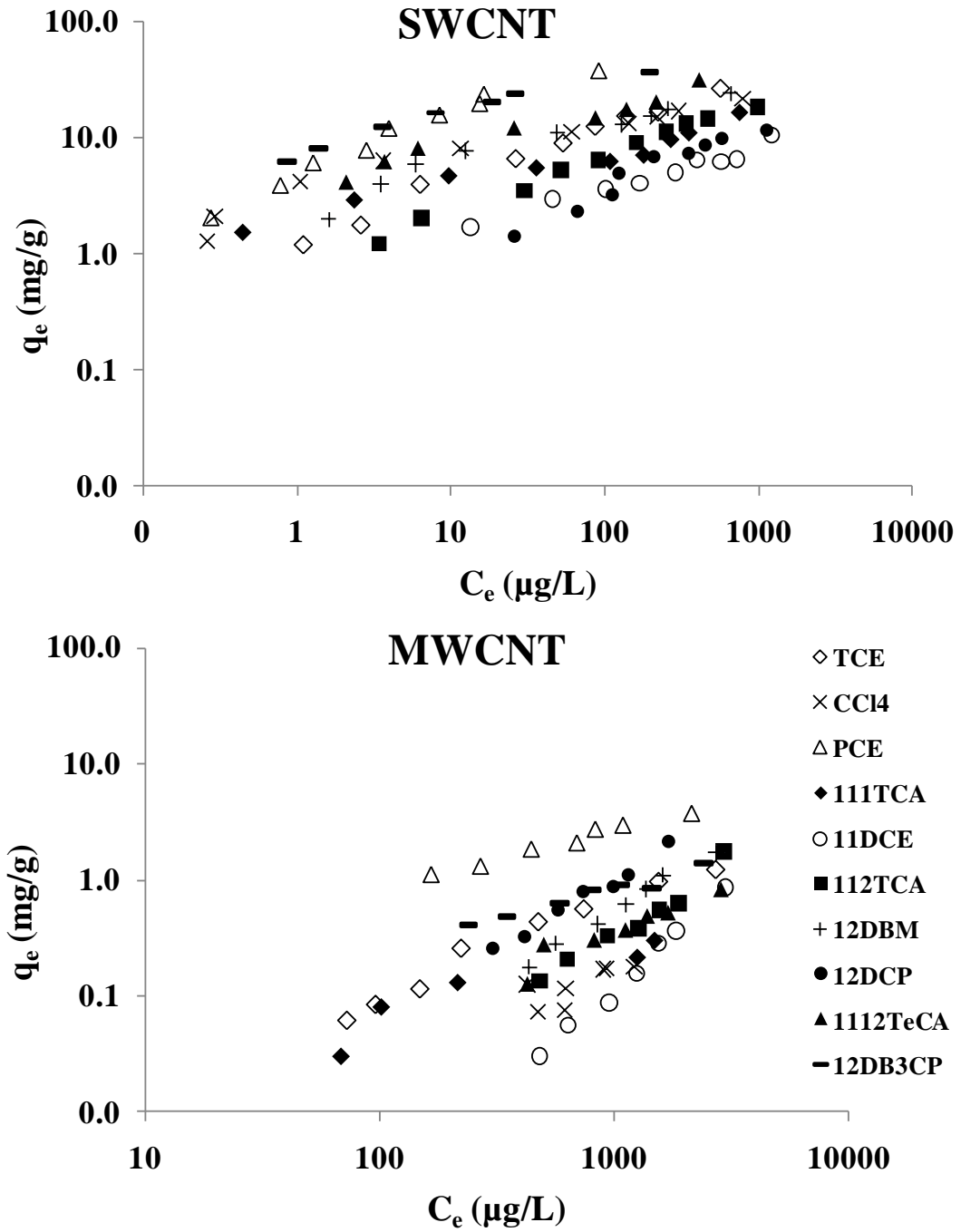


Figure 4.1. Adsorption isotherms of aliphatic SOCs by (a) SWCNT and (b) MWCNT

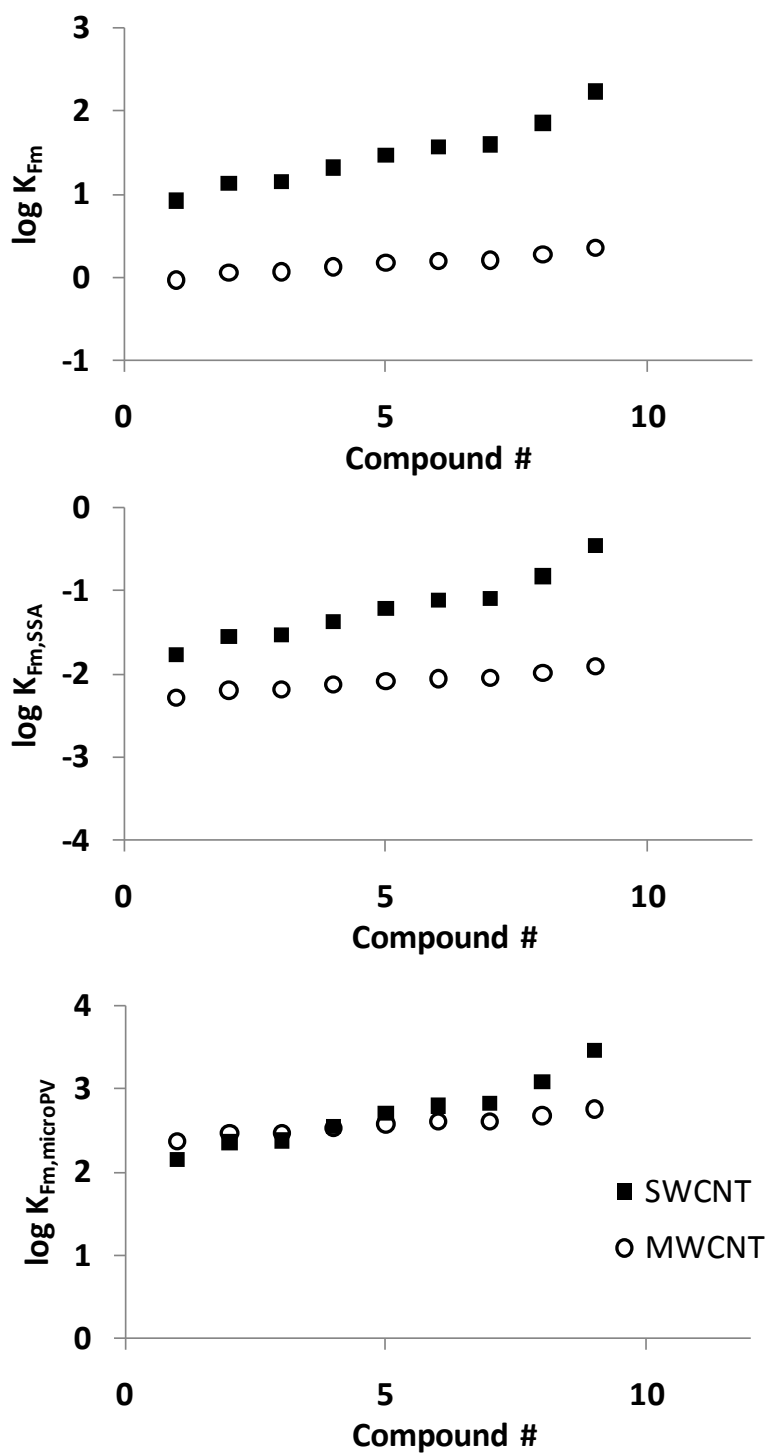


Figure 4.2. Comparison of adsorption affinities of SWCNT vs. MWCNTs depicted by (a) $\log K_{Fm}$ (b) $\log K_{Fm,SSA}$ - specific surface area normalized and (c) $\log K_{Fm,microPV}$ - micro pore volume normalized. Compound numbers are assigned according to Table 4.2.

Table 4.3. Freundlich model parameters of adsorption isotherms for aliphatic SOCs.

	SWCNT				MWCNT		
	$K_{F,m}$ (mg/g)/(mg/L) ⁿ	$K_{F,\mu}^*$ (mg/g)/(μg/L) ⁿ	n	r ²	$K_{F,m}$ (mg/g)/(mg/L) ⁿ	n	r ²
TCE	39.6	1.27	0.50	0.987	0.66	0.84	0.971
CCl₄	25.9	3.15	0.30	0.939	NA	NA	NA
PCE	172.5	4.80	0.52	0.970	2.69	0.50	0.977
1,1,1-TCA	14.2	2.06	0.28	0.952	0.23	0.59	0.858
1,1-DCE	8.40	0.67	0.36	0.967	0.12	1.83	0.992
1,1,2-TCA	21.0	0.75	0.48	0.993	0.34	1.29	0.961
1,2-DBM	29.9	2.46	0.36	0.942	0.54	1.25	0.991
1,2-DCP	13.6	0.22	0.60	0.946	1.02	1.18	0.982
1,1,1,2-TeCA	37.5	3.91	0.33	0.964	0.70	0.83	0.894
1,2-DB-3-CP	72.9	7.63	0.33	0.972	0.84	0.50	0.955

*: only calculated for SWCNT since the isotherm data for very low concentrations were not available for MWCNT

All isotherms were also normalized by the DFT surface area in the 0.5 – 0.8 nm pore size region (Figure D1a). The isotherms converged to a narrower range (Figure D1b). Previously, TCE adsorption by activated carbon was reported to correlate with the micropore volume less than 1 nm especially in the 0.5 – 0.8 nm range [Dastgheib et al. 2004]. The tighter aggregation of SWCNT bundles than MWCNT bundles in the aqueous phase were also reported to form smaller pores resulting in better accommodation of flexible low-molecular weight aromatic SOCs [Zhang et al. 2010a]. Our isotherm results also suggest that aliphatic SOCs adsorb preferentially in micropore openings of CNT bundles. Due to their small molecular sizes, aliphatic SOCs tested in this study are expected to align better in microporous interstices closer to their sizes favoring adsorption on SWCNT over MWCNT.

The Freundlich n values for MWCNT ranged between 0.50 – 1.84, higher than those of SWCNT ranging 0.28 – 0.60 (Table 4.3). Lower n values indicate a less homogeneous surface with adsorption sites distributed evenly [Carter et al. 1995]. Lower n values suggest that the presence of microporous spaces in the SWCNT bundle structure presents high energy sorption sites leading to more heterogeneous adsorption, whereas MWCNT structure was deficient in micropores, and the abundance of meso- and macropore size spaces appear to create a network of pores with similar sorption energies leading to a more homogenous adsorption sites for aliphatic SOCs.

4.3.2. Interpretation of Adsorption Interactions

Hydrophobic repulsion of SOCs from the aqueous phase to the adsorbent surface is a key driving force for adsorption. To investigate the hydrophobicity effect, solubility normalized adsorption isotherms were examined (Figure D2). Solubility normalization converged the isotherms to a narrower band for both SWCNT and MWCNT; however, they did not come together on a single line. Therefore, the hydrophobic driving force was an influential but not the sole factor controlling adsorption. To quantify the influence of the hydrophobicity effect, correlations between the K_{ow} and adsorption descriptors (K_D) of aliphatic SOCs were investigated (i.e. single parameter linear regression) and determination of coefficients (r^2) are tabulated in Table 4.4. In general, 40 – 60% correlation was observed for both SWCNTs and MWCNTs indicating some influence of the hydrophobicity effect on the sorption of aliphatics. Both SWCNT and MWCNT had relatively comparable correlations between adsorption (K_D) and hydrophobicity (K_{ow}) (Table 4.4), which was attributed to the similar oxygen contents, suggesting comparable polarities, of the CNTs.

Other important attractive forces between CNTs and SOCs are nonspecific interactions, also known as *van der Waals* interactions. Any molecule can have nonspecific attraction regardless of its chemical structure. The superposition of various components of *van der Waals* interactions can be influenced by size and/or polarizability of a molecule [Schwarzenbach et al. 2003]. To further investigate these interactions, three aliphatic SOCs (PCE, TCE and 1,1-DCE) with similar molecular structures (Table D1) but different sizes and polarizabilities were selected. As expected, solubility

normalization (Figure 4.3b) reduced the pronounced differences in mass-basis isotherms (Figure 4.3a), but adsorption capacities were still in the order of the molecular sizes of the adsorbates: PCE > TCE > 1,1-DCE. The correlation of molar volumes and polarizability vs. solubility normalized adsorption capacity descriptors of these three compounds indicated an increase in adsorption capacities with increasing size and increasing polarizability (Figure D3).

Table 4.4. Single parameter linear correlation between hydrophobicity and adsorption descriptors

	Dependent Variable	Independent Variable	r²	slope	intercept
SWCNT	Log K _{D,500}	Log K _{OW}	0.61	0.50	-2.53
	Log K _{D,750}		0.60	0.50	-2.63
	Log K _{D,1000}		0.59	0.49	-2.70
MWCNT	Log K _{D,500}	Log K _{OW}	0.62	0.49	-4.29
	Log K _{D,750}		0.48	0.39	-4.04
	Log K _{D,1000}		0.36	0.30	-3.86

adsorption descriptors at 500 ppb, 750 ppb and 1000 ppb represented by K_{D,500}, K_{D,750} and K_{D,1000}, respectively.

To further investigate the individual contributions of polarizability and size on adsorption, two isomer SOCs (1,1,1-TCA and 1,1,2-TCA) with identical molecular weights but different polarizabilities were also examined. Comparison of solubility normalized adsorption isotherms (Figure 4.4) showed that 1,1,2-TCA has slightly more adsorption affinity than 1,1,1-TCA on both CNTs even though the molar volume of 1,1,2-TCA is slightly smaller due to its molecular configuration. This difference was attributed to the difference in polarizabilities of the isomers captured by *P* values (0.41

vs. 0.68). It should be noted that influence of polarity (which is different than polarizability) was not discussed hence the solubility normalization captures polarity as well. Making direct observations regarding the attractions between time-varying uneven electron distributions is very difficult yet these findings may be viewed as an indirect evidence for the phenomena.

Aromatic SOCs possess resonating π -electrons in their benzene rings; therefore, they possess a strong π - π attraction towards the graphitic surface of CNTs. Unlike aromatic CNTs, the π -electrons in the structure of aliphatic SOCs may or may not contribute to the overall adsorption. Testing the effect of π -electron donor and acceptor interactions on aliphatic adsorption is not straightforward because presence of a π -bond alters the solubility, polarizability and size of the molecule. In this regard, further investigations are required for understanding the contribution of π - π electron donor-acceptor interactions for adsorption of aliphatic SOCs by CNTs. Comparison of 1,1,2-TCA vs. TCE and 1,1,1,2-TCA vs. PCE is presented in Figure D4 and Figure D5 in Appendix D, respectively. The solubility normalized isotherms showed no difference indicating that there was no observable effect of π -electron on adsorption of aliphatics by CNTs.

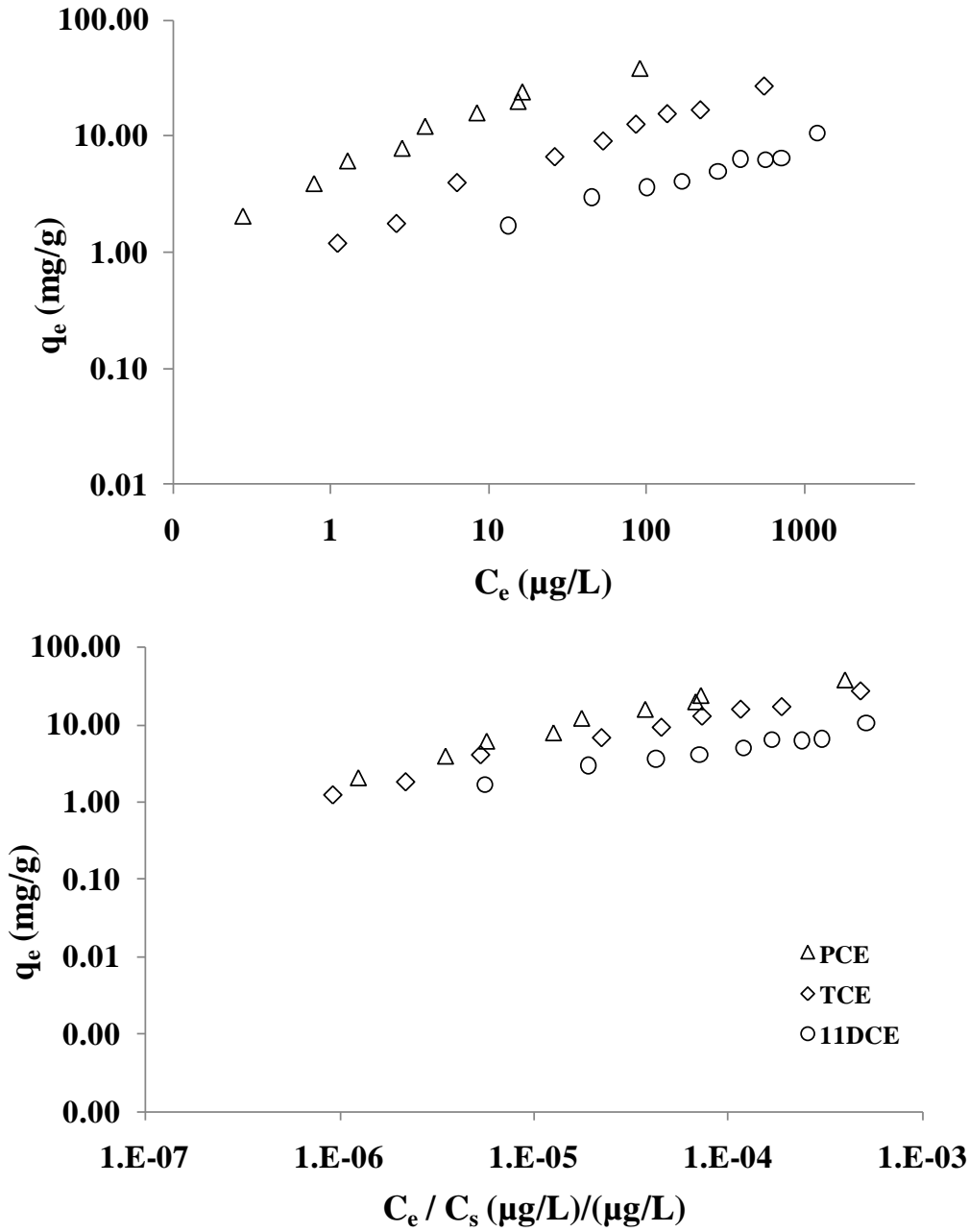


Figure 4.3. PCE, TCE and 1,1-DCE adsorption isotherms (top) and after solubility normalization (bottom)

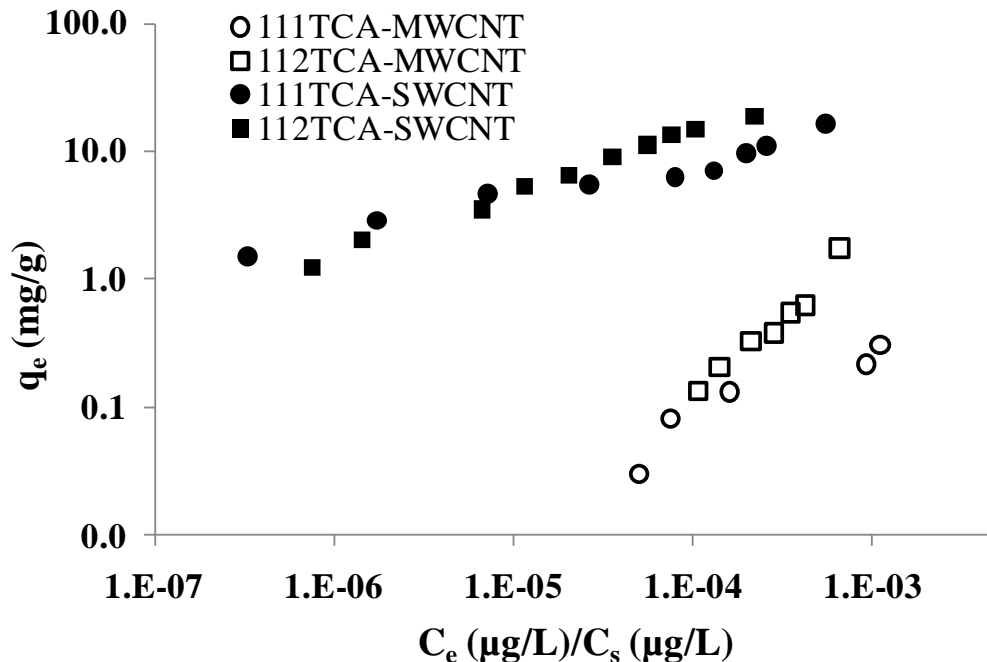


Figure 4.4. Comparison of 1,1,1-TCA and 1,1,2-TCA adsorption isotherms on CNTs

4.3.3. Poly-parameter LSER for Adsorption of Aliphatic SOCs by CNTs

Poly-parameter LSER equations for adsorption of aliphatic SOCs by CNTs were developed using five solvatochromic descriptors (A , B , V , P and R). Since the adsorption isotherms for SWCNT and MWCNT were covering different concentration ranges (see Figure 4.1), adsorption by SWCNT was modeled using nine adsorption descriptors (K_D) ranging between 5 – 1000 $\mu\text{g/L}$; whereas, adsorption by MWCNT was modeled using three adsorption descriptors (500, 750 and 1000 $\mu\text{g/L}$). The coefficients of the LSER model parameters are tabulated in Table 4.5. The detailed SAS outputs of multiple regression including p-values and ANOVA tables are presented in Appendix D. The r^2 of

LSER models ranged between 0.82 – 0.95 indicating better linearity than the single parameter models ($r^2 = 0.36 - 0.62$). For both SWCNT and MWCNT, the B parameter, capturing the hydrogen bond accepting ability, had a strong negative correlation with the adsorption descriptors. The negative dependence of adsorption on B indicates; as the hydrogen bond accepting ability of an aliphatic compound increases it becomes less likely to be adsorbed by the CNTs. The negative dependence of adsorption to B was attributed to the partitioning of contaminants with water molecules via hydrogen bonding [Luehrs et al. 1996]. The B parameter was higher for MWCNTs than SWCNTs. Among the positively correlated parameters, the V and R parameters were two notable parameters for SWCNTs and P was notable for MWCNT. The positive correlation of these parameters indicates that size and polarizability favors adsorption [Schwarzenbach et al. 2003]; however, differences in the SWCNT and MWCNT models indicate that the individual contribution of each parameter depends on the CNT type. The LSER parameter coefficients for SWCNT versus MWCNTs vary and the reasons behind these variations are not known yet. However these results show that there was not a single predominant parameter contribution to the overall adsorption of aliphatics by CNTs.

Table 4.5. Poly-parameter linear solvation energy relationship coefficients for SWCNTs and MWCNTs

	Dependent Variable	Independent Variables	r²	A	B	V	P	R	c
SWCNT	Log K _{D,5}	<i>A, B, V, P, R</i>	0.88	1.00	-1.69	2.06	-1.16	1.69	-1.95
	Log K _{D,10}		0.91	0.90	-2.13	1.95	-0.90	1.63	-2.11
	Log K _{D,25}		0.93	0.77	-2.72	1.81	-0.56	1.55	-2.32
	Log K _{D,50}		0.95	0.67	-3.17	1.70	-0.29	1.48	-2.48
	Log K _{D,100}		0.95	0.57	-3.62	1.60	-0.03	1.42	-2.64
	Log K _{D,250}		0.93	0.44	-4.21	1.45	0.31	1.33	-2.86
	Log K _{D,500}		0.91	0.35	-4.65	1.35	0.57	1.27	-3.02
	Log K _{D,750}		0.89	0.29	-4.92	1.29	0.72	1.23	-3.11
	Log K _{D,1000}		0.87	0.25	-5.10	1.24	0.83	1.20	-3.17
MWCNT	Log K _{D,500}		0.82	-2.34	-9.82	0.60	3.52	0.02	-4.57
	Log K _{D,750}		0.83	-2.56	-10.2	-0.25	3.98	-0.00	-4.11
	Log K _{D,1000}		0.84	-2.72	-10.5	-0.86	4.31	-0.02	-3.78

The profiles of the LSER model parameter coefficients for adsorption onto SWCNTs versus aqueous equilibrium concentration are presented in Figure D6. As seen from the figure, all parameters were slightly or moderately concentration dependent. The absolute value of B parameter was increasing with increasing SOC concentration, indicating that the relative contribution of hydrogen bond accepting ability for adsorption of aliphatics by SWCNTs increase with increasing concentration. The B parameter is negatively correlated; therefore, compounds with larger B values can be expected to adsorb less at elevated concentrations. The relative contribution of other parameters (A , V , P and R) showed minor changes with respect to concentration changes. The r^2 of the LSER model for adsorption onto SWCNTs versus aqueous equilibrium concentration is plotted in Figure D7. The r^2 of LSER models ranged between 0.88 – 0.95 indicating the success of the LSER model; and there were no notable fluctuations leading to the conclusion that LSER modeling approach can be valid for data fitting in a concentration range for adsorption of aliphatics by CNTs.

In Chapter III, poly-parameter LSER equations were generated for adsorption of aromatic SOCs by MWCNTs. The molecular refraction parameter (R) capturing the molecular forces of lone-pair electrons was not accounted in the aforementioned study, because the dataset was exclusively aromatic and lone pair electrons are assumed to be enclosed within the π -electron clouds of aromatic rings [Xia et al. 2010a]. Since aliphatic compounds do not contain resonating π -electron clouds, the relative contribution of R was tested in this study for the modeling of aliphatic SOC adsorption (eq. 2). In Table D4, coefficients of the LSER parameters without R were presented. The comparison of

LSER equation r^2 values with and without the R parameter is also plotted in Figure D7. The elimination of R from the LSER model reduced the r^2 to ~0.70 from ~0.90. This reduction indicates the influence of R for modeling of aliphatic SOC adsorption by SWCNTs. On the other hand, there were no notable differences for MWCNTs with or without R at the three concentrations tested. The contribution of R to adsorption onto MWCNTs may be overshadowed by other interactions because the adsorption affinity of MWCNTs are much lower than SWCNTs since the contribution was notable for strongly adsorbing SWCNTs at similar or lower concentrations.

Previously, LSER modeling for adsorption of aromatic SOCs by MWCNTs yielded good linear fits indicated by $r^2 = 0.83 - 0.93$. The V parameter was statistically significant ($p \leq 0.05$) and it was persistent at higher concentrations. The V parameter represents the molecular volume, which captures *van der Waals* interactions and hydrophobically driven adsorption. On the other hand, the LSER modeling for adsorption of aliphatic SOCs by MWCNTs did not show a single parameter that governs overall adsorption. Adsorption of aromatic SOCs by MWCNTs strongly depend on the hydrophobicity; while for aliphatic SOCs, in addition to hydrophobic driving force, other interactions can also be playing a role such as polarizability. To further compare the adsorption of aromatic and aliphatic SOCs by CNTs, the LSER models obtained in Chapter III were regenerated including the R parameter. LSER model parameters for adsorption of aromatic SOCs by MWCNTs with and without R are presented in Table D5 in Appendix D. There was an increase in the linearity of the models after the addition of R especially at higher concentrations but unlike the aliphatic models, the increase in r^2

was less than 10%. This supports the relatively weaker contribution of R to the overall adsorption of aromatic SOCs. The contribution of R in aromatic adsorption may be surpassed by the $\pi - \pi$ bond attraction as previously indicated by Xie et al. (2010a). However, the interactions should be investigated in a wider concentration range and also for SWCNTs because compound concentration and CNT type are likely to influence LSER modeling. A comprehensive investigation of LSER modeling for organic contaminants at different concentrations by both SWCNTs and MWCNTs can be subject to future investigation.

4.4. Conclusions

In the present study, adsorption of ten environmentally significant halogenated aliphatic SOCs onto CNTs was tested experimentally and LSER equations were developed to further investigate the adsorption mechanisms. Among the two types of CNTs, SWCNTs adsorbed more aliphatic SOCs than MWCNTs and their total SSA difference did not completely explain this difference. The surface area of CNTs in smaller pores i.e. micropores (especially in the 0.5 - 0.8 nm range) were found to be more influential than total SSA, which was attributed to the multiple attachment points of small aliphatic molecules in primary micropores (the pore-filling mechanism). Investigation of molecular level adsorption interactions indicated that hydrophobicity was influential in adsorption; however, non-specific *van der Waals* attraction and polarizability were also shown to contribute. Unlike aromatic SOCs, no effect of π -electron in the structure of aliphatic SOCs on adsorption was observed. However, further investigations are required

to understand the contribution of π - π electron donor-acceptor interactions for adsorption of aliphatic SOCs by CNTs.

Additionally, LSER models for adsorption of aliphatic SOCs by CNTs were generated and model parameters were investigated in concentrations ranging from 5 to 1000 $\mu\text{g/L}$ for SWCNTs and from 500 to 1000 $\mu\text{g/L}$ for MWCNTs. The r^2 of LSER models ranged between 0.88 – 0.95 indicating the validity of the LSER modeling. The LSER modeling approach can be valid for data fitting in a concentration range for adsorption of aliphatics by CNTs. The model parameters for SWCNTs and MWCNTs showed some variability indicating the influence of CNT type on LSER model development. The profiles of the LSER model parameter coefficients for adsorption onto SWCNTs versus aqueous equilibrium concentration showed the concentration dependence of LSER parameters. The molecular refraction (R), capturing the molecular forces of lone-pair electrons, was accounted for in the aliphatic modeling and the contribution of R was found notable. However, the comparison of LSER equations with and without R for aromatic SOCs indicated a much weaker contribution, which was attributed to the stronger π – π bond attraction surpassing the influence of lone-pair electrons to overall aromatic adsorption. In Chapter III, LSER models showed that molecular volume (V) was solely significant ($p \leq 0.05$) for adsorption of aromatics with persistent predominance even at higher concentrations. However, LSER models for adsorption of aliphatic SOCs indicated multiple interactions contributing to the adsorption of halogenated aliphatic SOCs by CNTs. Aliphatic SOCs are smaller in size and polarizability, but their size and polarizability still favors adsorption. The CNT type

and compound concentration were influential parameters and further investigations are required to improve our understanding of intermolecular interactions between aliphatic SOCs and CNTs.

CHAPTER V

**THE IMPACT OF CARBON NANOTUBE MORPHOLOGY ON
PHENANTHRENE AND NAPHTHALENE ADSORPTION****

5.1. Introduction

Carbon nanotubes, due to their remarkable electrical, thermal and physical properties, have attracted extensive attention since their discovery. They have been used in a wide range of applications in electronic, space, biomedical and other industries [Lam et al. 2006; Klaine et al. 2008]. The rapid growth in production and industrial use of CNTs have also raised serious concerns over their potential environmental and health risks, since they are very likely to enter the environment through multiple pathways. Due to their highly hydrophobic surfaces, CNTs exhibit strong adsorption affinities to organic compounds. Consequently, CNTs may exhibit toxicological effects and/or increased toxicity due to the adsorbed chemicals, and the fate and transport of organic contaminants can be significantly altered in the presence of CNTs in the environment. Therefore, understanding organic compound-CNT interactions has important implications.

** Apul, O.G., Shao, T., Zhang, S. and Karanfil, T. 2012. The impact of carbon nanotube morphology on phenanthrene adsorption. *Environmental Toxicology and Chemistry*, 31(1):73-78.

Adsorption of SOC by CNTs has been examined in several previous studies. The fundamentals of SOC adsorption by CNTs and activated carbons (ACs) are the same. Adsorption is a heterogeneous process, and consists of a combination of physical, chemical and electrostatic interactions. The chemical interactions involve mainly four mechanisms: hydrophobic interaction, π - π interaction, π - π electron-donor-acceptor (EDA) interaction, and H-bonding. However, unlike AC particles, CNTs are prone to aggregate, and form bundles or randomly tangled agglomerates due to the strong *van der Waals* forces along the length axis [Girifalco et al. 2000]. The outermost surface, inner cavities, interstitial channels and peripheral grooves of CNTs constitute the four possible sites for adsorption. The aggregation of CNTs reduces the specific surface area especially for single walled nanotubes (SWCNTs), and generates nanopores through formation of interstitial channels [Zhang et al. 2009]. The aggregation of CNTs and the availability of sites for SOC adsorption have been related to the physicochemical characteristics of CNTs (e.g., diameter, length, chirality, number of walls, surface functional groups, surface curvature and defects) and the composition of the background solution matrix [Pan and Xing 2008; Zhang et al. 2009]. The complexity in aggregation increases the difficulty in examining and explaining the already complex adsorption interactions between SOC and CNTs. Although no single characteristic of CNTs has been proven to be the main factor controlling SOC adsorption, in recent studies, strong (linear) relationships have been reported between the maximum SOC adsorption capacities of CNTs in water and their bulk phase specific surface areas measured with N₂ gas adsorption [Yang et al. 2006a; Pan et al. 2008].

In this chapter, our objective was examining the roles of CNT surface area, diameter, and length on the adsorption of phenanthrene (PNT) by analyzing the adsorption isotherms obtained with several CNTs in our laboratory and available in the literature. Phenanthrene was the SOC specifically selected for the present study because it has the most isotherm data available in the literature. Furthermore, it is a planar and hydrophobic polyaromatic hydrocarbon with a relatively simple adsorption mechanism. The main driving force of adsorption of PNT on CNTs is hydrophobic affinity and π - π dispersion interactions [Zhang et al. 2009].

5.2. Materials and Methods

5.2.1. Materials

Adsorption of PNTs by CNTs was examined on eight different CNTs for this study: Two SWCNTs, long (SWCNT-L) and short (SWCNT-S), were purchased from Cheap Tube Inc. Three multi walled nanotubes (MWCNTs) with different diameters, small (MWCNT-SD), medium (MWCNT-MD) and long (MWCNT-LD), were obtained from Nanostructured & Amorphous Materials Inc. Three MWCNTs with different lengths, short (MWCNT-SL), medium (MWCNT-ML) and long (MWCNT-LL) were obtained from Nanoshel Inc. All CNTs were used as received. Phenanthrene (PNT, 99.5+%) was obtained from Sigma-Aldrich Chemical Co. In addition, fourteen PNT isotherm results with different CNTs were obtained from previous studies [Zhang et al. 2009; Yang et al. 2006b; Wang et al. 2008] that created an overall data set of sixteen isotherms for PNT to examine and analyze.

5.2.2. Characterization of CNTs

Nitrogen adsorption at 77 K was performed with a physisorption analyzer (Micromeritics ASAP 2010) to characterize the surface areas and pore size distributions of CNTs. The Brunauer-Emmett-Teller (BET) equation and t-plot method were used to calculate surface areas, pore volumes from adsorption isotherms. The details of characterization methods have been reported previously (Dastgheib et al. 2004). Some morphological characteristics such as length and outer/inner diameter of the CNTs were provided by the manufacturers. For diameter and length characterization, a transmission electron microscope (TEM, H7600T, Hitachi, Science Systems, Ltd.) was also used. The purities of the CNTs were determined with thermogravimetric analysis (Q5000 TGA, TA Instruments).

5.2.3. Adsorption Isotherms

Constant CNT dose liquid phase adsorption isotherms of PNT were conducted in distilled and deionized water (DDW) water using completely mixed batch reactors (CMBRs). Isotherm experiments were performed used the same approach by Zhang et al. 2009. In brief, 255 mL-glass bottles with Teflon-lined screw caps containing 1 mg CNT were almost completely filled with DDI water and PNT was spiked with predetermined volumes of stock solution. Stock solutions were prepared in methanol, which was used to eliminate the solubility limitations of PNT. The spiked methanol to DDI ratio in CMBRs was less than 0.1% (v/v) to prevent the co-solvent effect. After spiking, additional DDI

water was added to eliminate the headspace in CMBRs, which were then placed on a rotary tumbler for seven days of equilibrium time determined through kinetic experiments, as previously reported [Zhang et al. 2010a].

5.2.4. Isotherm Modeling

The Freundlich isotherm was employed to analyze the isotherm data. Our previous comparison of different isotherm models for PNT sorption showed that Freundlich isotherm was the best model to describe adsorption of PNT by CNTs [Zhang et al. 2010b].

5.3. Results and Discussion

5.3.1. Characterization of CNTs

Nitrogen gas adsorption experiments showed that the mean surface area of SWCNTs ($428 \pm 21 \text{ m}^2/\text{g}$) used in this study was significantly higher than that of MWCNTs ($168 \pm 74 \text{ m}^2/\text{g}$) (Table 5.1). Theoretical surface area calculations [Peigney et al. 2001] confirmed that SWCNTs have higher surface areas than MWCNTs due to the difference in the interstitial channel accessibility of SWCNTs and MWCNTs [Zhang et al. 2009]. However, the theoretical surface areas of SWCNTs were significantly higher than the experimentally measured values with N_2 gas adsorption. The difference was attributed to the state (close and/or open) of the nanotubes and their tight aggregation characteristics in water. However, the difference between theoretical and measured

values for MWCNTs was found to be much smaller as compared to SWCNTs, which was explained with the much less compact bundle structure formed by MWCNTs than SWCNTs [Zhang et al. 2009].

The outer diameter of the individual CNT impacts the specific surface areas of CNT aggregates. The average outer diameters of the six MWCNTs used in this study and the eight MWCNTs used from literature [Yang et al. 2006b; Wang et al. 2009] were plotted against their measured specific surface areas (Figure 5.1). The specific surface areas decreased with increasing outer diameter of CNTs. This trend is consistent with the theoretical calculations demonstrating that the specific surface areas of MWCNTs decrease with increasing outer diameter [Peigney et al. 2001].

Nitrogen gas adsorption experiments indicated that the total pore volumes ranged between 0.6 – 0.9 cm³/g for SWCNTs and 0.4 – 0.9 cm³/g for MWCNTs (Table 5.1). These values are also consistent with the ranges of total pore volumes reported in literature as ~ 0.3 – 0.8 cm³/g and ~ 0.4 – 0.9 cm³/g for SWCNTs and MWCNTs, respectively [Zhang et al. 2009; Yang et al. 2006b; Wang et al. 2009]. MWCNTs have higher pore volume/surface area ratios than SWCNTs, which is due to the formation of large interstices between individual MWCNTs during aggregation, whereas SWCNTs tend to form tight bundle structures with some pore volume trapped as interstitial channels resulting in lower pore volume/surface area ratios [Zhang et al. 2009].

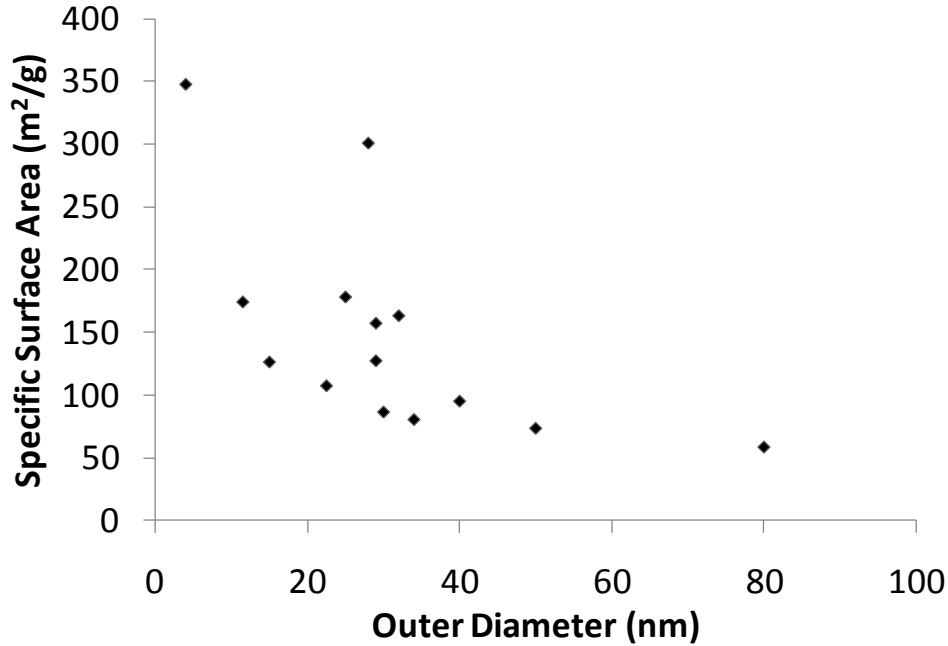


Figure 5.1. Average outer diameter and specific surface area (SSA) relationship for multi-walled carbon nanotubes (MWCNTs). (For the six MWCNTs used in the present study, the mean outer diameters were obtained from Transmission Electron Microscopy)

Table 5.1. Physical characteristics of carbon nanotubes

CNT	SSA ^a	V _{TOTAL} ^a	Purity ^a	O.D. ^b	I.D. ^b	Length ^b	No. of Walls ^b
	(m ² /g)	(cm ³ /g)	(%)	(nm)	(nm)	(μm)	
SWCNT-S	413	0.613	97.3	1-2	0.8-1.6	0.5-2	1
SWCNT-L	442	0.917	96.0	1-2	0.8-1.6	5-30	1
MWCNT-SD	178	0.848	99.1	10-20	5-10	10-30	7-15
MWCNT-MD	127	0.722	97.1	20-30	5-10	10-30	20-30
MWCNT-LD	157	0.702	98.6	30-50	5-15	10-20	40-50
MWCNT-SL	163	0.728	95.0	4-12	NR	3-10	NR
MWCNT-ML	80	0.367	99.2	4-12	NR	5-15	NR
MWCNT-LL	301	0.978	95.3	4-12	NR	15-30	NR

NR: Not Reported, O.D: Outer Diameter, I.D: Inner Diameter

^aThe data represent the average of triplicate measurements.

^bprovided by the manufacturer

Many techniques [e.g., atomic force microscopy (AFM), scanning tunneling microscopy (STM), raman spectroscopy, X-ray diffraction and transmission electronic microscopy (TEM)] have been reported to examine the diameters and lengths of CNTs [Belin and Epron 2005]. In this chapter, TEM was employed since it was readily available. Example TEM images of the MWCNTs used in the present study are shown in Figure E1 in Appendix E. For each MWCNT, at least ten different TEM images were obtained, and on each image at least three different readings were taken for diameter measurements. The distributions of the MWCNT diameters are shown in Figure E2 in Appendix E. Despite the narrow ranges reported by the manufacturer (Table 5.1), all three MWCNTs, in fact, had larger distribution of outer diameters. This discrepancy can also explain the scatter in the correlation obtained between the specific surface areas and average outer diameters in Figure 5.1. The outer diameters (mean of measurements \pm standard deviation) of MWCNT-SD, MWCNT-MD and MWCNT-LD were measured as 25 ± 10 nm, 29 ± 10 nm and 29 ± 13 nm, respectively.

It was not possible to obtain an accurate length determination for CNTs from the TEM pictures (Figure E1, Appendix E). Similar difficulties were also reported by Su and Lu (2007). The researchers reported the lengths of CNTs as “hundreds of nanometers to micrometers” obtained by TEM images. Most of the time the lengths of MWCNTs have not been measured and reported in other studies [e.g., Wang et al. 2008; 2009; Pyrznska et al. 2007; Peng et al. 2003]; usually researchers have relied on the data provided by the manufacturers, ranging from 0.5 to 500 μ m [Chen et al. 2007; Lu et al. 2006; Yan et al. 2008; Lin and Xing 2008a; 2008b]. Cho et al. (2008) reported AFM results for length

distribution of MWCNTs with a mean (\pm standard deviation) of $1.9 \pm 1.7 \mu\text{m}$, while the length data provided by manufacturers of the CNTs was from 1 to 5 μm . Carbon nanotube specific surface areas is expected to decrease with increasing lengths because a higher degree of aggregation is expected to occur with the increase in the length due to higher degree of *van der Waals* forces along the length axis [Zhang et al. 2009]. Among the three MWCNTs (MWCNT-SL, MWCNT-ML and MWCNT-LL) and the two SWCNTs (SWCNT-L and SWCNT-S) examined in the present study, there was no clear trend between the specific surface area and the CNT lengths (Table 5.1). The lack of a clear trend was attributed to the more heterogeneous nature of CNTs as observed with the TEM images (Figure E1, Appendix E) than the specifications provided by the manufacturer (Table 5.1).

These results confirm that the morphology of CNTs impacts their aggregation and plays an important role in their available surface area and pore volume for adsorption. It is evident that characterization of CNTs and, when necessary, their purification (i.e., production of CNTs with more uniform diameters and/or lengths) are necessary to systematically examine and explain the behavior of CNTs (e.g., adsorption, transport) in environmental systems. Manufacturer's data may not always represent the characteristics of CNTs in a particular batch.

5.3.2. Adsorption of PNT on CNTs

Freundlich isotherm results for adsorption of PNT by CNTs are tabulated in Table 5.2. For each isotherm, ten points were employed to fit the Freundlich model. On a mass

basis, SWCNTs exhibited significantly higher PNT adsorption capacities than MWCNTs, as indicated by the K_F values, which was attributed to the higher specific surface areas of SWCNTs than MWCNTs. The n values for SWCNT ($n = 0.45 \pm 0.01$) were also higher than MWCNT ($n = 0.28 \pm 0.02$), indicating that SWCNTs had more homogeneous surfaces for PNT adsorption than MWCNTs. Specific surface area has been reported as one of the important CNT and AC characteristics controlling their maximum or saturation SOC adsorption capacities [Yang et al. 2006b; Wang et al. 2009; Zhang et al. 2010a]. Surface area normalization of the isotherms decreased the difference between the adsorption capacities of different MWCNTs and SWCNTs; however, SWCNTs still exhibited higher adsorption capacities [e.g. surface area-based $K_{F,SSA}$ values (0.59 ± 0.04 in $(\text{mg}/\text{m}^2)/(\text{mg}/\text{L})^n$] than MWCNTs (0.30 ± 0.06)] (Table 5.2). The higher adsorption capacities of SWCNTs after SSA normalization indicated that there were other factors, in addition to specific surface area, affecting the adsorption on SWCNTs and MWCNTs. Our previous work showed also that SWCNTs had higher affinity to PNT than MWCNTs, since SWCNTs showed higher adsorption energies than MWCNTs due to the planar configuration of PNT molecules [Zhang et al. 2009]. These results also suggest that the loose entangled structure of MWCNTs was not as favorable as SWCNT for the adsorption of PNT.

Three MWCNTs, labeled as different diameter MWCNTs (MWCNT-SD, MWCNT-MD and MWCNT-LD) by their manufacturer, were used to examine the impact of diameter on PNT adsorption. No major difference was obtained for PNT adsorption on both mass and surface area based isotherms (Table 5.2). The lack of a clear

impact on adsorption due to diameter was attributed to the wide range and overlapping diameters of CNTs (Figure E2, Appendix E), which resulted in relatively similar surface areas (Table 5.2). To further evaluate the impact of diameter, PNT isotherms in the literature obtained with MWCNTs of different diameters were also examined (Table 5.3). Although outer diameter data of the MWCNTs were provided by the manufacturers in those studies, the decreasing trend of specific surface area with increasing outer diameter in each set of MWCNTs [Yang et al. 2006b; Wang et al. 2009] was consistent with both experimental observation (Figure 5.1) and theoretical calculations.

Table 5.2. Freundlich isotherm parameters (mass and specific surface area (SSA) basis) for phenanthrene (PNT) adsorption by carbon nanotubes (CNTs)

CNT	K_F (95% C.I.)	SSA	$K_{F,SSA}$ (95% C.I.)	n (95% C.I.)	r^2
	(mg/g)/(mg/L) ⁿ	(m ² /g)	(mg/m ²)/(mg/L) ⁿ		
SWCNT-S	256.93 (194.33 – 339.68)	413	0.62 (0.47 – 0.82)	0.44 (0.38 – 0.50)	0.96
SWCNT-L	246.40 (217.31 – 279.38)	442	0.56 (0.49 – 0.63)	0.46 (0.43 – 0.49)	0.99
MWCNT-SD	52.84 (45.18 – 61.79)	178	0.30 (0.25 – 0.35)	0.26 (0.21 – 0.31)	0.93
MWCNT-MD	45.85 (38.65 – 54.39)	127	0.36 (0.30 – 0.43)	0.26 (0.21 – 0.32)	0.91
MWCNT-LD	42.48 (37.90 – 47.61)	157	0.27 (0.24 – 0.30)	0.28 (0.24 – 0.33)	0.96
MWCNT-SL	58.04 (54.03 – 62.36)	163	0.36 (0.33 – 0.38)	0.29 (0.27 – 0.32)	0.99
MWCNT-ML	16.24 (12.44 – 21.20)	80	0.20 (0.16 – 0.26)	0.29 (0.24 – 0.47)	0.99
MWCNT-LL	97.07 (84.31 – 111.76)	301	0.32 (0.28 – 0.37)	0.30 (0.26 – 0.34)	0.97

C.I.: Confidence Interval, $K_{F,SSA}$: Specific surface area normalized K_F .

The trends for the Freundlich K_F values of the first eight isotherms in Table 5.3 showed that PNT adsorption decreased with increasing MWCNT diameter or decreasing specific surface area in each set of MWCNTs. The surface area normalized PNT

adsorption capacities on the eleven MWCNTs in Table 5.3 were examined at different equilibrium concentrations in the range of 1 $\mu\text{g/L}$ to 1 mg/L (Figure 5.2). Some correlations were obtained at low equilibrium concentrations, showing an increase of PNT adsorption on a surface area basis with increasing average MWCNT outer diameter.

The correlations became independent of diameters at high equilibrium concentrations, which were close to the saturation capacity or solubility of PNT. However, more data are required to confirm these findings. Surface coverage calculations, assuming the area occupied by a PNT molecule is 0.816 nm^2 (calculated by dividing the molar volume of PNT ($167.67 \text{ cm}^3/\text{g}$) by the smallest dimension of the molecule assuming it is the thickness of the molecule (3.4 \AA) [Zhang et al. 2009]), showed that the average specific surface areas occupied by PNT on the MWCNTs were 9.3 ± 4.4 , 19.9 ± 5.5 , 44.1 ± 5.5 , and $101.1 \pm 21.5 \%$ at 1, 10, 100, and 1000 $\mu\text{g/L}$ equilibrium concentrations, respectively. These observations show that at high equilibrium concentrations, the CNT surface was mostly covered and surface area became the controlling parameter. However, at low surface coverage, since surface curvature decreases with increasing diameter, it appears that there were better interactions between the flat surfaces of MWCNTs and planar PNT molecules for adsorption.

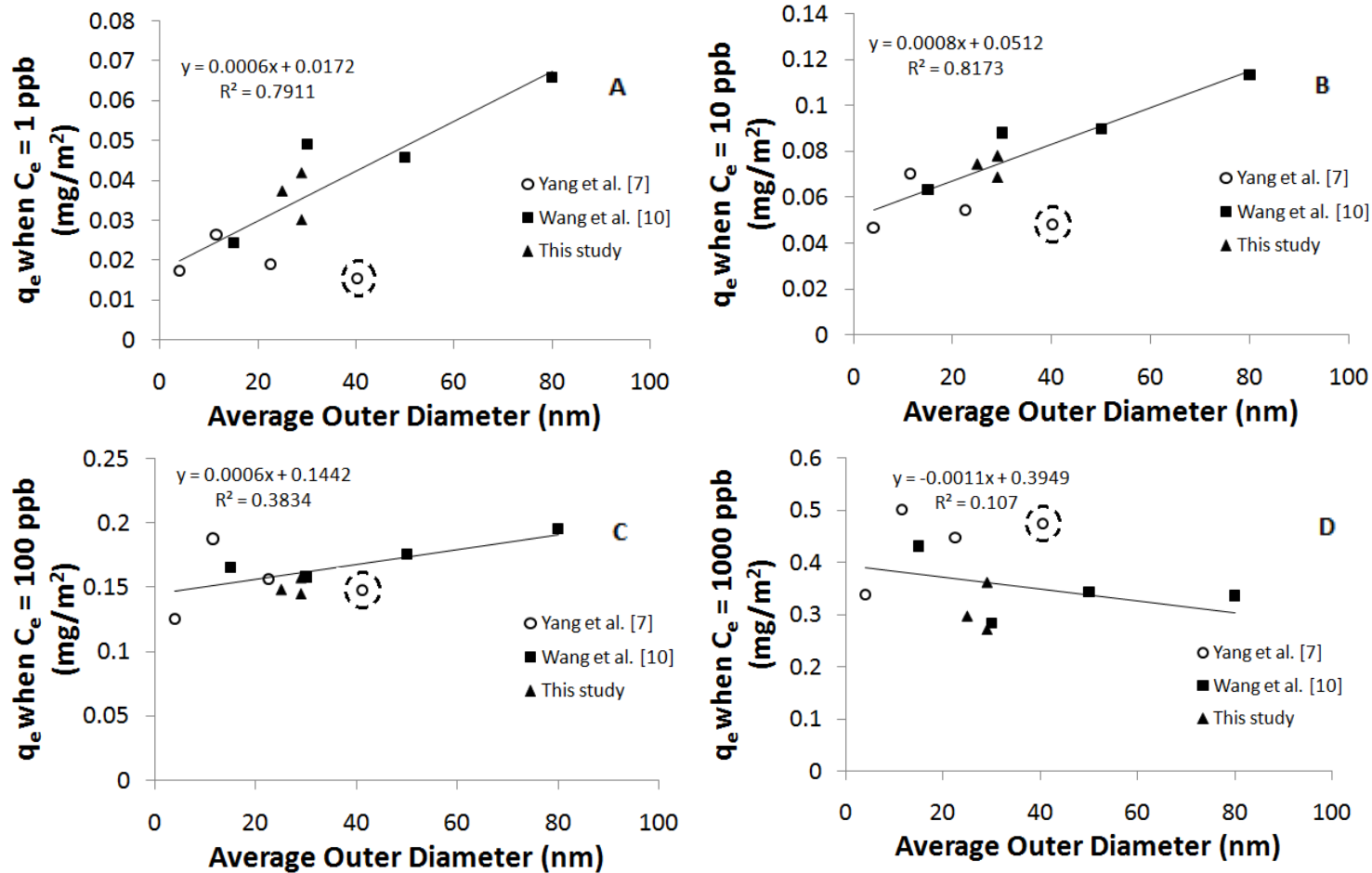


Figure 5.2. Specific surface area (SSA) normalized Phenanthrene (PNT) adsorption capacities of multi-walled carbon nanotubes (MWCNTs) at the equilibrium concentration of 1, 10, 100 and 1000 ppb (A, B, C and D, respectively). The data point in the dashed circle was excluded from the linear regression

Table 5.3. Comparison of phenanthrene (PNT) adsorption capacities of carbon nanotubes (CNTs) with different diameters

CNT	Reference	Outer Diameter*	K_F	SSA	$K_{F,SSA}$	n
		(nm)	(mg/g)/(mg/L) ⁿ	(m ² /g)	(mg/m ²)/(mg/L) ⁿ	(-)
MWCNT 8	Yang et al. (2006b)	<8	117.5	348	0.34	0.429
MWCNT 15	Yang et al. (2006b)	8-15	87.1	174	0.50	0.426
MWCNT 30	Yang et al. (2006b)	15-30	47.9	107	0.45	0.457
MWCNT 50	Yang et al. (2006b)	30-50	43.7	94.7	0.46	0.500
MWCNT 20	Wang et al. (2009)	10-20	54.3	126	0.43	0.416
MWCNT 40	Wang et al. (2009)	20-40	24.4	86	0.28	0.254
MWCNT 60	Wang et al. (2009)	40-60	25.1	73	0.34	0.292
MWCNT 100	Wang et al. (2009)	60-100	19.5	58	0.34	0.236
MWCNT-SD	This study	25 ± 10	52.8	178	0.30	0.262
MWCNT-MD	This study	29 ± 10	45.9	127	0.36	0.265
MWCNT-LD	This study	29 ± 13	42.5	157	0.27	0.285

*Manufacturer values reported in references [Yang et al. 2006b] and [Wang et al. 2009] while measured with Transmission Electron Microscopy (TEM) in this study

To further examine the impact of MWCNT diameter on SOC adsorption, the adsorption data for naphthalene (NPT) on MWCNTs in the literature was also examined. The NPT adsorption data was obtained on the same MWCNTs used for PNT on Table 5.3 [Yang et al. 2006b; Wang et al. 2009]. Naphthalene is also a planar molecule, and has one less benzene ring but twenty times higher solubility than PNT. Both on a mass and surface area basis, higher adsorption capacities of PNT than NPT were observed on the same MWCNTs, mainly due to the difference in the solubility. In the equilibrium concentration range of 1 µg/L to 20 mg/L, there was no clear correlation between outer

diameter of MWCNTs and specific surface area normalized adsorption capacities (Figure E3, Appendix E). It appears that with increased solubility and thus decreased adsorption capacity on a surface area basis, the diameter (or surface curvature) effect observed in PNT adsorption has become insignificant in the adsorption of NPT.

To examine the impact of length, three multi-walled (MWCNT-SL, MWCNT-ML and MWCNT-LL) and two single-walled (SWCNT-S and SWCNT- L) CNTs with different lengths (according to the manufacturer data) were selected and used in the experiments (Table 5.1). As mentioned before, TEM measurements were not applicable to obtain the length distribution of CNTs due to lack of uniformity. Therefore, the only information available about the length was from the manufacturer. On both mass and specific surface area bases, adsorption capacities of SWCNTs were higher than those of MWCNTs at different lengths (Table 5.2). Specific surface area normalized isotherms did not show a correlation between length and the PNT adsorption on SWCNTs and MWCNTs. The PNT adsorption on the MWCNT-ML was significantly lower than all other CNTs tested in this study (Table 5.2). During the isotherm experiments, a much more compact aggregate structure was observed for the MWCNT-ML, as compared to other MWCNTs. Considering the low adsorption capacity of the MWCNT-ML, it was hypothesized that the tighter aggregation of this CNT, causing a decrease in available surface area, may be related to the purity of the material. Thermogravimetric analysis showed that MWCNT-ML has the highest average purity (99.2 %) among all MWCNTs tested (Table 5.1).

5.4. Conclusions

The roles of CNT surface area, diameter, and length on the adsorption of phenanthrene (PNT) were analyzed by adsorption isotherms obtained with several single (SWCNT) and multi (MWCNT) walled CNTs in the laboratory and available in the literature. At low (e.g., 1 $\mu\text{g/L}$) equilibrium concentrations, MWCNTs with the larger outer diameters exhibited higher PNT adsorption capacity on a surface area basis than those with smaller diameters. With increasing equilibrium concentration, adsorption on a surface area basis became independent of MWCNT diameter, and maximum adsorption capacity was controlled by the total surface area. A similar analysis for the adsorption of naphthalene (NPT), a planar molecule with one less benzene ring but twenty times higher solubility than PNT, showed no correlation with respect to MWCNT outer diameter at both low and high equilibrium concentrations. The results indicated that the surface curvature of MWCNT was more important to the adsorption of PNT than to the adsorption of NPT, having smaller molecular size and exhibiting lower adsorption capacity than PNT. Surface area normalized isotherms did not show a correlation between PNT adsorption and lengths of SWCNTs and MWCNTs. CNT characterization results showed that the morphology of CNTs impacts their aggregation because the theoretical surface area calculations are considerably higher than the measured surface areas. Aggregation also plays an important role on the available surface area and pore volume for adsorption. Manufacturer's data may not always represent the characteristics of CNTs in a particular batch. Therefore, careful characterization of CNTs is critical to

systematically examine the behavior of CNTs (e.g., adsorption, transport) in environmental systems.

CHAPTER VI

CONCLUSIONS AND RECOMMENDATIONS

In this study, adsorption of synthetic organic contaminants (SOCs) by carbon nanotubes (CNTs) was investigated to gain a molecular-level mechanistic insight and statistical predictive models were generated. The important conclusions and recommendations of this study are as follows:

Phase (1): Predictive model development for adsorption of aromatic contaminants by multi-walled carbon nanotubes

QSAR and LSER equations were generated for adsorption of low-molecular weight (< 200 g/mol) aromatic SOCs by MWCNTs (with less than 5% oxygen content) in distilled and deionized water. Data was obtained from literature and combined with the data generated in our lab. Overall 58 low molecular weight aromatic compounds were compiled and used for training the most comprehensive predictive models in the literature.

Both QSAR and LSER models were generated at three different saturation concentrations and coefficient of determinations indicated the data fitting ability of the modeling approaches ($r^2 > 0.83$). In addition, an independent dataset was employed to externally validate the prediction accuracy of predictive models. The model predicted

values were compared with experimental values and the prediction strength of models were presented.

Models demonstrated the significance of hydrophobicity and nonspecific attractions for CNT adsorption captured by the V term. This finding was consistent with the activated carbon literature. At higher concentrations, the results showed that although V parameter was still dominant, the A and B parameters also became significant. The increasing significance of A and B parameters showed the influence of hydrogen bonding interactions at higher saturation concentrations.

Phase (2): Adsorption of halogenated aliphatic contaminants by carbon nanotubes

Adsorption of ten halogenated aliphatic SOC_s by SWCNT_s and MWCNT_s in distilled and deionized water were tested. Among the two types of CNT_s, SWCNT adsorbed more halogenated aliphatic SOC_s than MWCNT and their total SSA difference did not completely explain this difference. The surface area of CNT_s in micropores (especially in the 0.5 - 0.8 nm range) were found to be more influential than total SSA, which was attributed to the pore-filling mechanism.

Predictive models were generated using LSER approach for adsorption of aliphatic SOC_s by CNT_s for the first time in the literature. According to the models, hydrophobicity was influential in adsorption of halogenated aliphatics; however, non-specific *van der Waals* attraction and polarizability were also shown to contribute. Unlike

aromatic SOCs, no effect of π -electron in the structure of aliphatic SOCs on adsorption were observed. The r^2 of LSER models ranged between 0.88 – 0.95 indicating the validity of LSER modeling for adsorption of aliphatics by CNTs.

Molecular refraction (R), capturing the molecular forces of lone-pair electrons, was included in aliphatic modeling and the contribution of R was found notable. However, the comparison of LSER equations with and without R for aromatic SOCs indicated a much weaker contribution, which was attributed to the stronger $\pi - \pi$ bond attraction surpassing the influence of lone-pair electrons to overall aromatic adsorption.

For aromatic SOCs that molecular volume (V) was solely significant ($p \leq 0.05$) for adsorption of aromatics with persistent predominance even at higher concentrations. However, LSER models for adsorption of aliphatic SOCs indicated multiple interactions contributing to the adsorption of halogenated aliphatic SOCs by CNTs. Aliphatic SOCs are smaller in size and polarizability, but their size and polarizability still favors adsorption..

Phase (3): Impact of carbon nanotube morphology on phenanthrene and naphthalene adsorption

The outer diameter of CNTs plays an important role in their available specific surface area and pore volume for adsorption. Therefore, phenanthrene (PNT) and naphthalene (NPT) were selected as probe SOC to examine the impact of carbon morphology on adsorption MWCNT specific surface areas decreased with increasing

average outer diameter of MWCNTs. The distribution of MWCNT outer diameters measured with TEM was much larger than the range reported by the manufacturer.

Specific surface area normalized isotherms showed that SWCNTs exhibited higher adsorption capacities than MWCNTs, which was attributed to the external surfaces and interstitial channels of SWCNTs providing more adsorption sites than MWCNTs, which have loose entangled structures.

At low equilibrium concentrations, MWCNTs with larger outer diameter exhibited higher PNT adsorption capacity on a specific surface area basis than those with smaller diameters. With increasing equilibrium concentration, adsorption on a surface area basis became independent of MWCNT diameter, and maximum adsorption capacity was mainly controlled by the total available specific surface area.

Adsorption of naphthalene (NPT) showed no clear correlation with respect to the outer diameter of MWCNTs. The results suggested that the observed MWCNT diameter effect on PNT adsorption was an insignificant factor in the adsorption of NPT having a smaller molecular size and exhibiting lower adsorption capacity than PNT.

Recommendations

Adsorption of higher molecular weight SOCs with branched and complex structures (such as dyes, antibiotics, pesticides etc.) should be investigated and predictive LSER models can be generated. The model parameter coefficients can be compared with

LSERs of low-molecular weight SOC adsorption. Thus, a molecular-level mechanistic insight to the adsorption of large and complex SOCs can be acquired.

Our findings indicate that SWCNTs and MWCNTs show different SOC adsorption trends. However, there are significantly much more data for MWCNT than SWCNTs in the literature. Therefore, future data generation should be focused on the adsorption of SOCs by SWCNTs, and LSER models should be generated for SWCNTs. The comparison LSER equations generated for adsorption of SOCs by SWCNT and MWCNT can reveal certain mechanistic differences, and combination of two models, if possible, may generate a more comprehensive predictive tool.

The surface of CNTs may be oxidized intentionally during manufacturing or accidentally after its release to the environment. The oxygen on CNT surface may inhibit SOC adsorption because of the hydrophilic moieties or it can increase the dispersion of CNTs and expose more sorption sites. Therefore, testing the adsorption of SOCs by CNTs with higher surface oxygen content and examining adsorption mechanisms is warranted. Predictive models can be generated for adsorption of aromatics SOCs by CNTs with higher oxygen content (> 5%) to examine the impact on the LSER parameters and adsorption mechanisms.

Our LSER models indicate that different interactions dominate the adsorption of aromatic and aliphatic SOCs by CNTs. Further investigations should be conducted to understand and sort out the contribution of intermolecular interactions (such as π - π electron donor-acceptor interactions). Testing CNT surface before and after SOC

adsorption using Fourier transform infrared spectroscopy (FTIR) may reveal the contribution of π bonding in aromatic adsorption.

Further investigations are required to explain and predict the influence of other morphological characteristics such as chirality, number of walls and open/closed ended structure of CNTs. The bulk characterization parameters such as specific surface area or pore volume may be conventionally sufficient to predict adsorption capacity; however, CNTs have unique structural properties and the influence of their morphological properties should be subject to research.

Natural organic matter is ubiquitous in natural waters. Thus, in natural aqueous environments, the behavior of CNTs and the interactions between organic compounds and CNTs are further complicated due to the presence of NOM. The effect of NOM and NOM characteristics should be investigated on the adsorption of SOCs by CNTs and the predictive model development..

Manufacturer's data may not always represent the characteristics of CNTs in a particular batch. Therefore characterization of CNTs is critical to systematically examine and explain the behavior of CNTs (e.g., adsorption, transport) in environmental systems.

APPENDICES

Appendix A

Supplementary information for Chapter I

Table A1. List of SOCs that were used as adsorbate in aqueous phase CNT adsorption studies

No	Aromatic Compounds	SWCNT	SWCNT-Oxidized	MWCNT	MWCNT-Oxidized
1	Phenanthrene	[1-3]	[1, 2, 4-8]	[2]	[2, 5, 7-9]
2	Pyrene		[1, 4]		
3	Naphthalene	[3, 10]	[1, 4-6, 10-12]		[5, 11]
4	1-naphthol		[5, 6, 13]		[5]
5	Biphenyl	[2]	[2]	[2]	[2]
6	2-phenylphenol	[2]	[2, 13]	[2]	[2]
7	Toluene	[14]			
8	Benzene	[3, 14]	[14]		
9	Chlorobenzene	[14],[3]	[14]		
10	1,2- dichlorobenzene	[14]			
11	1,2,4-trichlorobenzene	[14]	[14]		
12	1,2,4,5-tetrachlorobenzene	[14]	[14]		
13	Nitrobenzene	[14, 15]	[14-16]	[15]	[15, 16]
14	4-nitrotoluene	[14]			
15	Atrazine	[3, 17, 18]	[3, 7, 17-19]		[7, 19]
16	Dicamba		[20]		
17	2,4,5-t		[20]		
18	EE2	[21]	[21]		
19	BPA	[21]	[21]		
20	Phenol	[15]	[8, 13, 15, 22, 23]	[15]	[8, 15, 23]
21	Catechol		[13]		
22	Pyrogallol		[13]		
23	1,3-dichlorobenzen	[24]		[24]	
24	2,4-dichlorobenzene	[24]		[24]	
25	2-naphthol	[24]	[9]	[24]	[9]
26	1-naphthylamine	[24]	[9]	[24]	[9]
27	1,3-dinitrobenzene	[25]	[16]	[25]	[16]
28	1,3,5-trinitrobenzene	[25]		[25]	
29	2,4,6-trichlorophenol		[26]		[26]
30	Tetracycline	[10, 15]	[10, 15]	[15]	[15]
31	3-nitrotoluene		[16]		[16]
32	4-nitrophenol		[16]		[16]
33	Aniline		[22]		
34	4-chloroaniline		[12, 22]		
35	2-nitroaniline		[22]		
36	3-nitroaniline		[22]		
37	4-nitroaniline		[22]		
38	2-chlorophenol		[22, 27]		[27]
39	4-chlorophenol		[22, 27]		[27]
40	2,4-dichlorophenol		[12, 22]		
41	2-nitrophenol		[22]		
42	3-nitrophenol		[22]		
43	4-nitrophenol		[22]		
44	4-methylphenol		[22]		
45	Pentachlorophenol		[28]		[28]
46	Oxytetracycline		[29, 30]		
47	Carbamazepine		[29]		
48	2-xylene	[31]		[31]	
49	1,4-dichlorobenzene	[3]			
50	Methylbenzene	[3]			
51	3-chlorophenol		[23, 27]		[23, 27]
52	2,4-dichlorophenoxyacetic acid		[32]		[32]
53	Dimethyl phthalate	[33]	[33]		
54	Diethyl phthalate	[33]	[33]		
55	Dibutyl phthalate	[33]	[33]		
56	M-xylene				
57	Ethylbenzene				
58	Sulfamethoxazole	[15]	[15, 34]	[15]	[15]
59	Sulfapyridine		[34]		
60	Benzoic acid				
61	Acridine orange		[35]		
62	Alizarin red		[35]		
63	Anthracene		[35]		
64	Rhodamine B		[35]		

65	Xylenol orange		[35]		
66	Diiodofluorescein		[35]		
67	Bromothymol blue		[35]		
68	Orange g		[35]		
69	1-(2-pyridylazo)-2-naphthol		[35]		
70	Methylene blue		[36]		
71	Methyl violet		[36]		
72	Ci direct yellow 86		[37]		
73	Ci direct red 224		[37]		
74	Procion red mx-5b		[38]		
75	Safranin O		[39]		
76	Bromothymol blue				[40]
77	Reactive blue 4	[41]	[41]		
78	Reactive red m-2be		[42]		
79	Alizarin red s		[43]		
80	Morin		[43]		
81	Direct congo red				[44]
82	Reactive green HE4BD				[44]
83	Golden yellow MR				[44]
84	Orange II		[36]		
85	4-n-nonylphenol		[32]		[32]
86	Tylosin	[15]	[15]	[15]	[15]
No	Aliphatic compounds				
		SWCNT	SWCNT-Oxidized	MWCNT	MWCNT-Oxidized
1	Dibromochloromethane		[45]		
2	Bromoform		[45]		
3	Cyclohexane	[14]			
4	Cyclohexanol		[13]		
5	Trichloroethene	[3]			
6	Cyclohexene	[3]			
7	Perfluorooctane sulfonate		[32]		[32]
8	Perfluorooctanoic acid		[32]		[32]
9	Perfluorooctane-sulfonamide		[32]		[32]
10	Lindane		[7]		[7]

Compounds listed with no reference indicates that the type of CNT was not revealed in the source.

References used in Table A1

1. Yang, K., Zhu, L.Z. and Xing, B.S. Adsorption of polycyclic aromatic hydrocarbons by carbon nanomaterials. *Environmental Science and Technology*, 2006. **40**(6): p. 1855-1861.
2. Zhang, S., Shao, T., Kaplan, S.K.K. and Karanfil, T. The impacts of aggregation and surface chemistry of carbon nanotubes on the adsorption of synthetic organic compounds. *Environmental Science and Technology*, 2009. **43**(15): p. 5719-5725.
3. Brooks, A.J., Lim, H. and Kilduff, J.E. Adsorption uptake of synthetic organic chemicals by carbon nanotubes and activated carbons. *Nanotechnology*, 2012. **23**(29).
4. Yang, K., Wang, X., Zhu, L. and Xing, B.S. Competitive sorption of pyrene, phenanthrene, and naphthalene on multiwalled carbon nanotubes. *Environmental Science and Technology*, 2006. **40**(18): p. 5804-5810.
5. Wang, X., Lu, J. and Xing, B.S. Sorption of organic contaminants by carbon nanotubes: Influence of adsorbed organic matter. *Environmental Science and Technology*, 2008. **42**(9): p. 3207-3212.
6. Wang, X., Tao, S. and Xing, B.S. Sorption and Competition of Aromatic Compounds and Humic Acid on Multiwalled Carbon Nanotubes. *Environmental Science and Technology*, 2009. **43**(16): p. 6214-6219.
7. Wang, X., Liu, Y., Tao, S. and Xing, B.S. Relative importance of multiple mechanisms in sorption of organic compounds by multiwalled carbon nanotubes. *Carbon*, 2010. **48**(13): p. 3721-3728.

8. Li, M., Hsieh, T.C., Doong, R.A. and Huang, C.P. Tuning the adsorption capability of multi-walled carbon nanotubes to polar and non-polar organic compounds by surface oxidation. *Separation and Purification Technology*, 2013. 117: p. 98-103.
9. Hou, L., Zhu, D., Wang, X., Wang, L., Zhang, C. and Chen, W., Adsorption of phenanthrene, 2-naphthol, and 1-naphthylamine to colloidal oxidized multiwalled carbon nanotubes: Effects of humic acid and surfactant modification. *Environmental Toxicology and Chemistry*, 2013. **32**(3): p. 493-500.
10. Ji, L., Chen, W., Duan, L. and Zhu, D. Mechanisms for strong adsorption of tetracycline to carbon nanotubes: A comparative study using activated carbon and graphite as adsorbents. *Environmental Science and Technology*, 2009. **43**(7): p. 2322-2327.
11. Cho, H.H., Smith, B.A., Wnuk, J.D., Fairbrother, D.H. and Ball, W.P. Influence of surface oxides on the adsorption of naphthalene onto multiwalled carbon nanotubes. *Environmental Science and Technology*, 2008. **42**(8): p. 2899-2905.
12. Yang, K., Wang, X., Zhu, L. and Xing, B.S. Competitive adsorption of naphthalene with 2,4-dichlorophenol and 4-chloroaniline on multiwalled carbon nanotubes. *Environmental Science and Technology*, 2010. **44**(8): p. 3021-3027.
13. Lin, D. and Xing, B.S. Adsorption of phenolic compounds by carbon nanotubes: Role of aromaticity and substitution of hydroxyl groups. *Environmental Science and Technology*, 2008. **42**(19): p. 7254-7259.
14. Chen, W., Duan, L. and Zhu, D. Adsorption of polar and nonpolar organic chemicals to carbon nanotubes. *Environmental Science and Technology*, 2007. **41**(24): p. 8295-8300.

15. Ji, L., Shao, Y., Xu, Z., Zheng, S. and Zhu, D. Adsorption of Monoaromatic Compounds and Pharmaceutical Antibiotics on Carbon Nanotubes Activated by KOH Etching. *Environmental Science and Technology*, 2010. **44**(16): p. 6429-6436.
16. Shen, X.E., Shan, X.Q., Dong, D.M., Hua, X.Y. and Owens, G. Kinetics and thermodynamics of sorption of nitroaromatic compounds to as-grown and oxidized multiwalled carbon nanotubes. *Journal of Colloid and Interface Science*, 2009. **330**(1): p. 1-8.
17. Yan, X.M., Shi, B.Y., Lu, J.J., Feng, C.H., Wang, D.S. and Tang, H.X. Adsorption and desorption of atrazine on carbon nanotubes. *Journal of Colloid and Interface Science*, 2008. **321**(1): p. 30-38.
18. Shi, B.Y., Zhuang, X., Yan, X., Lu, J. and Tang, H. Adsorption of atrazine by natural organic matter and surfactant dispersed carbon nanotubes. *Journal of Environmental Sciences-China*, 2010. **22**(8): p. 1195-1202.
19. Chen, G.C., Shan, X.Q., Zhou, Y.Q., Shen, X., Huang, H.L. and Khan, S.U. Adsorption kinetics, isotherms and thermodynamics of atrazine on surface oxidized multiwalled carbon nanotubes. *Journal of Hazardous Materials*, 2009. **169**(1-3): p. 912-918.
20. Pyrzynska, K., Stafiej, A. and Biesaga, M. Sorption behavior of acidic herbicides on carbon nanotubes. *Microchimica Acta*, 2007. **159**(3-4): p. 293-298.
21. Pan, B., Lin, D., Mashayekhi, H. and Xing, B.S. Adsorption and hysteresis of bisphenol A and 17 alpha-ethinyl estradiol on carbon nanomaterials. *Environmental Science and Technology*, 2008. **42**(15): p. 5480-5485.

22. Yang, K., Wu, W., Jing, Q. and Zhu, L. Aqueous Adsorption of Aniline, Phenol, and their Substitutes by Multi-Walled Carbon Nanotubes. *Environmental Science and Technology*, 2008. **42**(21): p. 7931-7936.
23. Toth, A., Torocsik, A., Tombacz, E. and Laszlo, K. Competitive adsorption of phenol and 3-chlorophenol on purified MWCNTs. *Journal of Colloid and Interface Science*, 2012. **387**: p. 244-249.
24. Chen, W., Duan, L., Wang, L. and Zhu, D. Adsorption of hydroxyl- and amino-substituted aromatics to carbon nanotubes. *Environmental Science and Technology*, 2008. **42**(18): p. 6862-6868.
25. Chen, J., Chen, W. and Zhu, D. Adsorption of nonionic aromatic compounds to single-walled carbon nanotubes: Effects of aqueous solution chemistry. *Environmental Science and Technology*, 2008. **42**(19): p. 7225-7230.
26. Chen, G.C., Shan, X.Q., Wang, Y.S., Wen, B., Pei, Z.G., Xie, Y.N., Liu, T. and Pignatello, J.J. Adsorption of 2,4,6-trichlorophenol by multi-walled carbon nanotubes as affected by Cu(II). *Water Research*, 2009. **43**(9): p. 2409-2418.
27. Liao, Q., Sun, J. and Gao, L. Adsorption of chlorophenols by multi-walled carbon nanotubes treated with HNO₃ and NH₃. *Carbon*, 2008. **46**(3): p. 553-555.
28. Salam, M.A. and Burk, R.C. Thermodynamics of pentachlorophenol adsorption from aqueous solutions by oxidized multi-walled carbon nanotubes. *Applied Surface Science*, 2008. **255**(5): p. 1975-1981.
29. Oleszczuk, P., Pan, B. and Xing, B.S. Adsorption and desorption of oxytetracycline and carbamazepine by multiwalled carbon nanotubes. *Environmental Science and Technology*, 2009. **43**(24): p. 9167-9173.

30. Oleszczuk, P. and Xing, B.S. Influence of anionic, cationic and nonionic surfactants on adsorption and desorption of oxytetracycline by ultrasonically treated and non-treated multiwalled carbon nanotubes. *Chemosphere*, 2011. **85**(8): p. 1312-1317.
31. Chin, C.J.M., Shih, L.C., Tsai, H.J. and Liu, T.K. Adsorption of o-xylene and p-xylene from water by SWCNTs. *Carbon*, 2007. **45**(6): p. 1254-1260.
32. Li, X., Zhao, H., Quan, X., Chen, S., Zhang, Y. and Yu, H. Adsorption of ionizable organic contaminants on multi-walled carbon nanotubes with different oxygen contents. *Journal of Hazardous Materials*, 2011. **186**(1): p. 407-415.
33. Wang, F., Yao, J., Sun, K. and Xing, B.S. Adsorption of dialkyl phthalate esters on carbon nanotubes. *Environmental Science and Technology*, 2010. **44**(18): p. 6985-6991.
34. Ji, L., Chen, W., Duan, L. and Zhu, D. Mechanisms for strong adsorption of tetracycline to carbon nanotubes: A comparative study using activated carbon and graphite as adsorbents. *Environmental Science and Technology*, 2009. **43**(7): p. 2322-2327.
35. Liu, C.H., Li, J.J., Zhang, H.L., Li, B.R. and Guo, Y. Structure dependent interaction between organic dyes and carbon nanotubes. *Colloids and Surfaces a-Physicochemical and Engineering Aspects*, 2008. **313**: p. 9-12.
36. Rodriguez, A., Ovejero, G., Sotelo, J.L., Mestanza, M. and Garcia, J. Adsorption of dyes on carbon nanomaterials from aqueous solutions. *Journal of Environmental Science and Health Part a-Toxic/Hazardous Substances and Environmental Engineering*, 2010. **45**(12): p. 1642-1653.
37. Kuo, C.Y., Wu, C.H. and Wu, J.Y. Adsorption of direct dyes from aqueous solutions by carbon nanotubes: Determination of equilibrium, kinetics and thermodynamics parameters. *Journal of Colloid and Interface Science*, 2008. **327**(2): p. 308-315.

38. Wu, C.H. Adsorption of reactive dye onto carbon nanotubes: Equilibrium, kinetics and thermodynamics. *Journal of Hazardous Materials*, 2007. **144**(1-2): p. 93-100.
39. Ghaedi, M., Haghdoost, S., Nasiri-Korkhdan, S., Mihandoost, A., Sahraie, R. and Daneshfar, A. Comparison of activated carbon, multiwalled carbon nanotubes, and cadmium hydroxide nanowire loaded on activated carbon as adsorbents for kinetic and equilibrium study of removal of safranin o. *Spectroscopy Letters*, 2012. **45**(7): p. 500-510.
40. Ghaedi, M., Khajehsharifi, H., Yadkuri, A.H., Roosta, M. and Asghari, A. Oxidized multiwalled carbon nanotubes as efficient adsorbent for bromothymol blue. *Toxicological and Environmental Chemistry*, 2012. **94**(5): p. 873-883.
41. Machado, F.M., Bergmann, C.P., Lima, E.C., Royer, B., de Souza, F.E., Jauris, I.M., Calvete, T. and Fagan S.B. Adsorption of reactive blue 4 dye from water solutions by carbon nanotubes: experiment and theory. *Physical Chemistry Chemical Physics*, 2012. **14**(31): p. 11139-11153.
42. Machado, F.M., Bergmann, C.P., Fernandes, T.H., Lima, E.C., Royer, B., Calvete, T. and Fagan, S.B. Adsorption of Reactive Red M-2BE dye from water solutions by multi-walled carbon nanotubes and activated carbon. *Journal of Hazardous Materials*, 2011. **192**(3): p. 1122-1131.
43. Ghaedi, M., Hassanzadeh, A. and Kokhdan, S.N. Multiwalled carbon nanotubes as adsorbents for the kinetic and equilibrium study of the removal of alizarin red S and morin. *Journal of Chemical and Engineering Data*, 2011. **56**(5): p. 2511-2520.

44. Mishra, A.K., Arockiadoss, T. and Ramaprabhu, S. Study of removal of azo dye by functionalized multi walled carbon nanotubes. *Chemical Engineering Journal*, 2010. **162**(3): p. 1026-1034.
45. Lu, C., Chung, Y.L. and Chang, K.F. Adsorption thermodynamic and kinetic studies of trihalomethanes on multiwalled carbon nanotubes. *Journal of Hazardous Materials*, 2006. **138**(2): p. 304-310.

Appendix B

Supplementary information for Chapter II

Table B1. Manufacturer and supplier full names and countries provided by the articles compiled for CNT adsorption studies tabulated in Table 2.1

Manufacturer Short Name	Manufacturer Full Name	Country
Chengdu	Chinese Academy of Sciences, Chengdu Organic Chemistry Co. Ltd.	China
Shenzen NAM	Shenzen Nanotech Port Co. Ltd. Nanostructured and Amorphous Materials, Inc.	China TX, USA
Nanoshel Cheap Tube	Nanoshel LLC Cheap Tubes Inc.	DE, USA VT, USA
Nanolab Aldrich	NanoLab Inc. Sigma-Aldrich	MA, USA International Corporation
Sun Nanotech Nanothinx	Sun Nanotech Co. Ltd Nanothinx: Nanotubes, Nanomaterials, and Nanotechnology R&D	China Greece
R.I.P.I	Research Institute of Petroleum Industry	Iran
Merck Carbon Solutions	Merck & Co. Inc. Carbon solutions, Inc.	International Corporation CA, USA

Appendix C

Supplementary information for Chapter III

Determination of K_{∞} , $K_{0.01}$, and $K_{0.1}$ values for adsorbates

Procedure for determining K_{∞}

- The isotherm plots were magnified, copied and printed to a separate sheet.
- The smallest data point (C_e , q_e) tested for the isotherm was picked from magnified plot (See illustration below).
- The K_{∞} value was calculated using the smallest tested data point (i.e. $K_{\infty} = q_e/C_e$)
- If there are multiple isotherms available for a single compound an average value for K_{∞} values excluding the extreme outliers was calculated.
- The number of available data for each compound and the average ratios of lowest dilution concentrations to saturation concentrations were tabulated in Table C1.

Procedure for determining $K_{0.01}$ and $K_{0.1}$

The isotherm plots were magnified, copied and printed to a separate sheet.

- The points at 1% and 10% of aqueous saturation concentrations were picked from magnified plot.
- If there are multiple isotherms available for a single compound an average value for K_{∞} values excluding the extreme outliers was calculated.
- The $K_{0.01}$ and $K_{0.1}$ values were calculated using these points accordingly as described in K_{∞} value determination procedure (i.e. $K_{0.01} = q_e/C_e$ at 0.01 S_w and $K_{0.1} = q_e/C_e$ at 0.1 S_w).

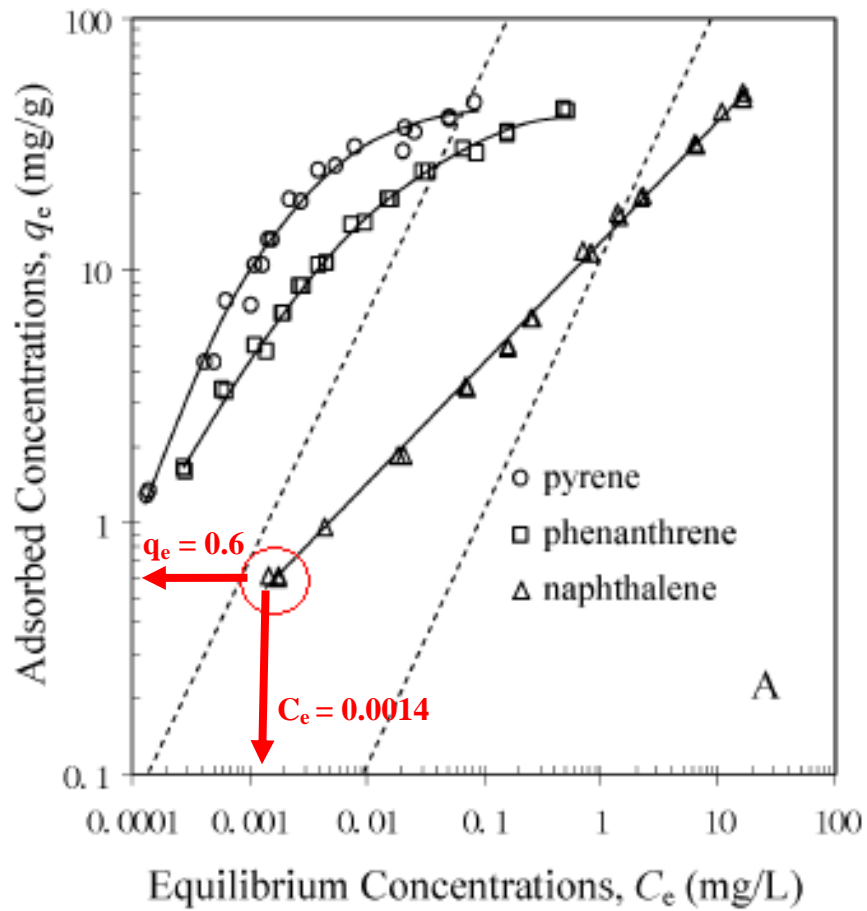


Illustration. A sample isotherm plot for naphthalene ($S_w = 32$ mg/L) to explain the data selection procedure for infinite dilution condition. Approximately, 120 adsorption isotherm and 350 data points were processed as described above to compile the database used in the present study (Figure was obtained from Yang et al. 2006b)

Table C1. The percentage of solubility at infinite dilution conditions concentrations

No	Compounds	Number of data points	C_{∞}/S_w^* (%)
1	Phenanthrene	16	0.567
2	Pyrene	1	0.290
3	Naphthalene	12	0.524
4	1-naphthol	6	0.524
5	Biphenyl	4	0.500
6	2-phenylphenol	5	1.898
7	Benzene	2	0.123
8	Chlorobenzene	2	0.412
9	1,2,4-trichlorobenzene	1	0.361
10	Nitrobenzene	3	0.088
11	2,4-dinitrotoluene	1	0.002
12	Phenol	3	0.011
13	Catechol	2	0.021
14	Pyrogallol	2	0.001
15	2,4,6-trichlorophenol	6	0.097
16	3-nitrotoluene	2	0.101
17	4-nitrophenol	3	0.012
18	Aniline	1	0.013
19	4-chloroaniline	1	0.076
20	2-nitroaniline	1	0.002
21	3-nitroaniline	1	0.058
22	4-nitroaniline	1	0.128
23	4-methylphenol	1	0.021
24	2-chlorophenol	1	0.030
25	4-chlorophenol	1	0.007
26	2,4-dichlorophenol	1	0.019
27	2-nitrophenol	1	0.170
28	3-nitrophenol	1	0.006
29	1,3-dinitrobenzene	2	0.059
	AVERAGE*		0.211

*If there is more than one data point, the average was provided

**Average for all 29 compounds

Table C2. Surface area normalized adsorption descriptors (K_{SA} values)

	Compound	Log $K_{SA,\infty}$	Log $K_{SA,0.01}$	Log $K_{SA,0.1}$
1	Phenanthrene	1.13	0.88	0.21
2	Pyrene	1.77	1.56	1.06
3	Naphthalene	-0.45	-0.75	-1.32
4	1-naphthol	-1.24	-1.09	-1.80
5	Biphenyl	-0.17	-0.30	-0.74
6	2-phenylphenol	-1.16	-1.97	-2.97
7	Benzene	-2.47	N.A	N.A
8	Chlorobenzene	-2.35	-1.38	-2.38
9	1,2,4-trichlorobenzene	-1.00	-0.94	-1.30
10	Nitrobenzene	-1.86	N.A	N.A
11	2,4-dinitrotoluene	0.21	-1.60	-2.35
12	Phenol	-2.73	-3.77	-4.46
13	Catechol	-1.95	N.A	N.A
14	Pyrogallol	-0.98	N.A	N.A
15	2,4,6-trichlorophenol	-0.81	-2.80	-2.36
16	3-nitrotoluene	-1.17	N.A	N.A
17	4-nitrophenol	-1.45	N.A	N.A
18	Aniline	-3.01	-3.67	-4.11
19	4-chloroaniline	-2.90	-2.54	-3.08
20	2-nitroaniline	-0.64	-2.03	-2.80
21	3-nitroaniline	-1.53	-2.05	-2.74
22	4-nitroaniline	-1.30	-1.81	-2.50
23	4-methylphenol	-2.18	-3.05	-3.80
24	2-chlorophenol	-2.16	N.A	N.A
25	4-chlorophenol	-1.50	N.A	N.A
26	2,4-dichlorophenol	-1.28	-2.23	-2.99
27	2-nitrophenol	-1.69	-2.10	-2.70
28	3-nitrophenol	-1.32	-2.02	-2.71
29	1,3-dinitrobenzene	-0.75	N.A	N.A

N.A: Data was not available within the experimental isotherm range. *: K_{SA} is in mg/m^2

Table C3. The solvatochromic descriptors of training dataset*

No	Compounds	A	B	V	P
1	Phenanthrene	0.00	0.29	1.45	1.29
2	Pyrene	0.00	0.25	1.58	1.52
3	Naphthalene	0.00	0.20	1.09	0.92
4	1-naphthol	0.60	0.37	1.14	1.05
5	Biphenyl	0.00	0.26	1.32	0.99
6	2-phenylphenol	0.56	0.49	1.38	1.40
7	Benzene	0.00	0.14	0.72	0.52
8	Chlorobenzene	0.00	0.07	0.84	0.65
9	1,2,4-trichlorobenzene	0.00	0.00	1.08	0.81
10	Nitrobenzene	0.00	0.28	0.98	1.11
11	2,4-dinitrotoluene	0.00	0.49	1.21	1.61
12	Phenol	0.60	0.30	0.78	0.89
13	Catechol	0.88	0.47	0.83	1.10
14	Pyrogallol	1.35	0.62	0.89	1.35
15	2,4,6-trichlorophenol	0.42	0.15	1.14	1.14
16	3-nitrotoluene	0.00	0.25	1.03	1.10
17	4-nitrophenol	0.82	0.26	0.95	1.72
18	Aniline	0.26	0.41	0.82	0.96
19	4-chloroaniline	0.30	0.31	0.94	1.13
20	2-nitroaniline	0.30	0.36	0.99	1.37
21	3-nitroaniline	0.40	0.35	0.99	1.71
22	4-nitroaniline	0.46	0.35	0.99	1.93
23	4-methylphenol	0.57	0.31	0.92	0.87
24	2-chlorophenol	0.32	0.31	0.90	0.88
25	4-chlorophenol	0.67	0.20	0.90	1.08
26	2,4-dichlorophenol	0.53	0.19	1.02	0.84
27	2-nitrophenol	0.05	0.37	0.95	1.05
28	3-nitrophenol	0.79	0.23	0.95	1.57
29	1,3-dinitrobenzene	0.00	0.47	1.06	1.60

*Obtained from the Absolv Module of ADME 5.0 software

Table C4. The solvatochromic descriptors of validation dataset*

No	Compounds	A	B	V	P
1	Ethylbenzene	0.00	0.15	1.00	0.51
2	4-xylene	0.00	0.16	1.00	0.52
3	Bromobenzene	0.00	0.09	0.89	0.73
4	Propylbenzene	0.00	0.15	1.14	0.5
5	4-chlorotoluene	0.00	0.05	0.98	0.67
6	Benzonitrile	0.00	0.33	0.87	1.11
7	4-fluorophenol	0.63	0.23	0.79	0.98
8	Benzyl alcohol	0.39	0.56	0.92	0.87
9	Iodobenzene	0.00	0.12	0.97	0.82
10	Acetophenone	0.00	0.48	1.01	1.01
11	3-methylphenol	0.57	0.34	0.92	0.88
12	Methyl benzoate	0.00	0.46	1.07	0.85
13	4-chloroanisole	0.00	0.24	1.04	0.86
14	Phenethyl alcohol	0.31	0.65	1.06	0.86
15	3-methylbenzyl alcohol	0.39	0.59	1.06	0.9
16	4 ethylphenol	0.55	0.36	1.06	0.9
17	3,5-dimethylphenol	0.57	0.36	1.06	0.82
18	Ethyl benzoate	0.00	0.46	1.21	0.85
19	Methyl 2-methylbenzoate	0.00	0.43	1.21	0.87
20	3-chlorophenol	0.69	0.15	0.90	1.06
21	4-nitrotoluene	0.00	0.28	1.03	1.11
22	4-chloroacetophenone	0.00	0.44	1.14	1.09
23	3-bromophenol	0.70	0.16	0.95	1.13
24	1-methylnaphthalene	0.00	0.2	1.23	0.92
25	2-dichlorobenzene	0.00	0.04	0.96	0.78
26	3-dichlorobenzene	0.00	0.02	0.96	0.73
27	4-dichlorobenzene	0.00	0.02	0.96	0.75
28	Isophorone	0.00	0.53	1.24	1.12
29	2-chloronaphthalene	0.00	0.17	1.21	1.1
30	Azobenzene	0.00	0.4	1.48	1.2

*Obtained from the Absolv Module of ADME 5.0 software

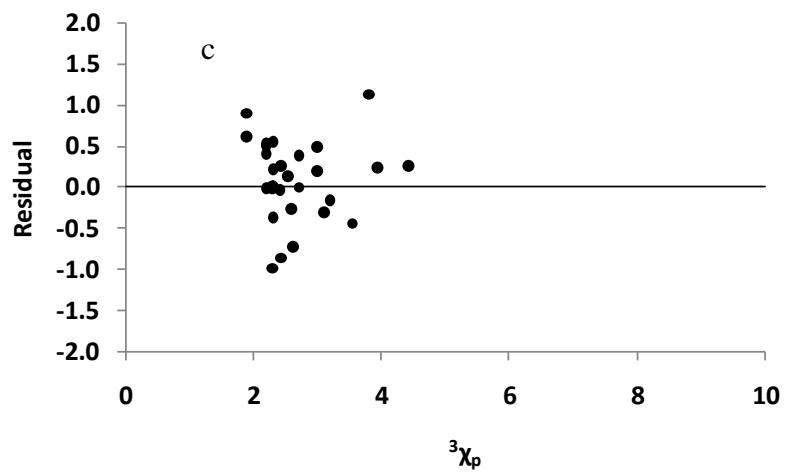
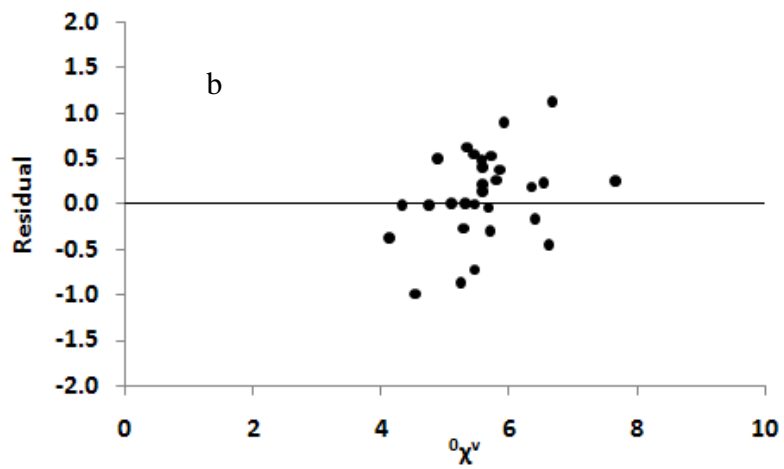
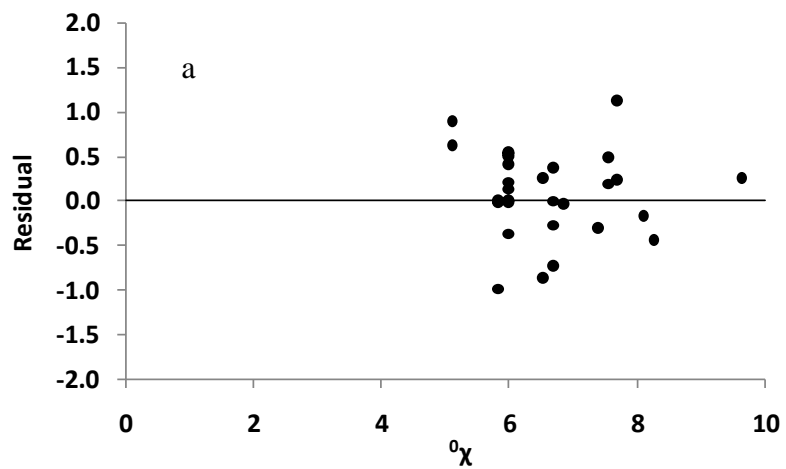


Figure C1. Residual analyses of QSAR model independent variables for (a) ${}^0\chi$, (b) ${}^0\chi^v$, and (c) ${}^3\chi_p$

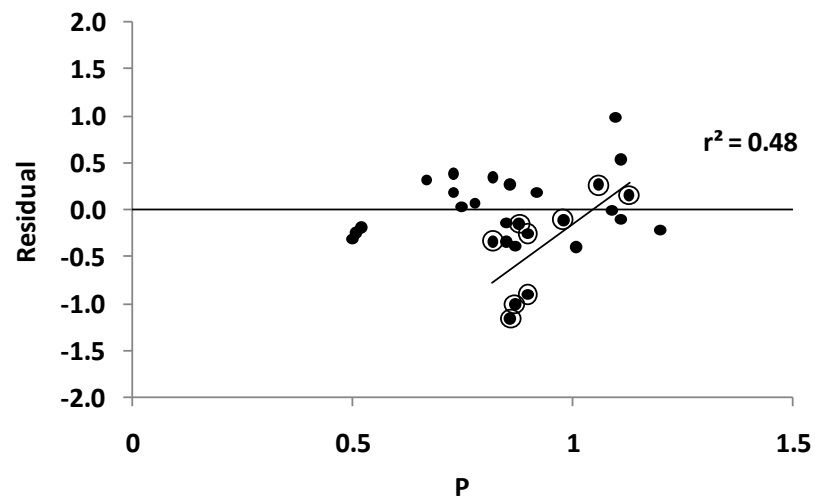
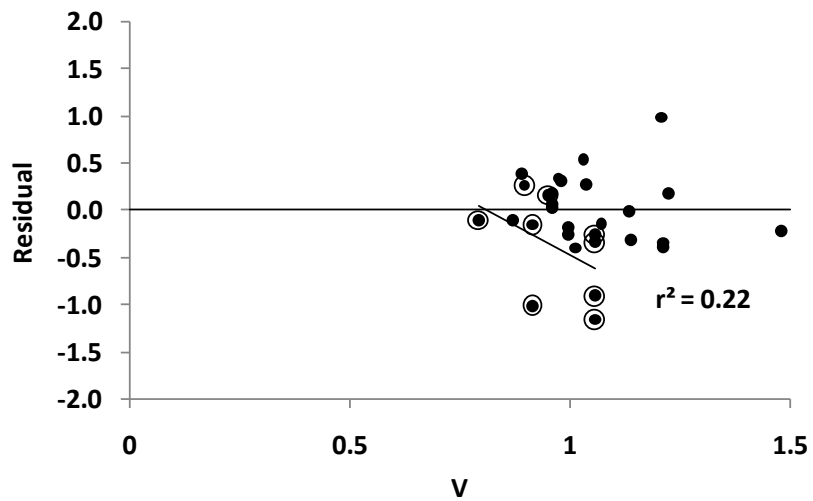
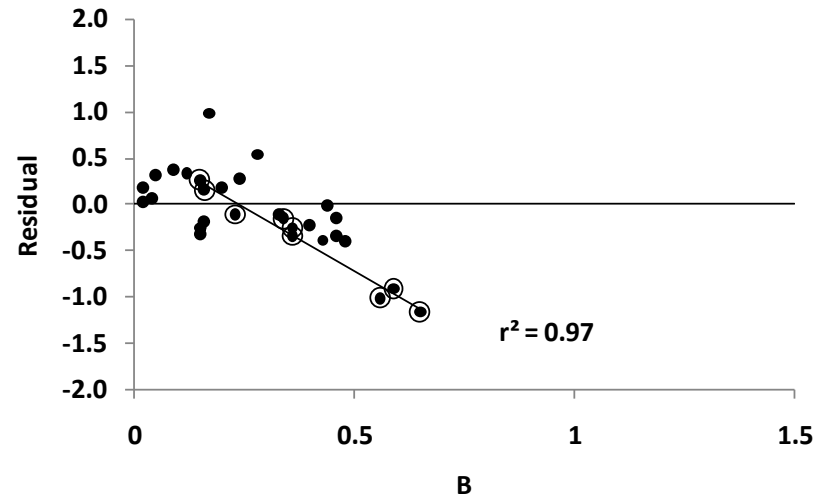
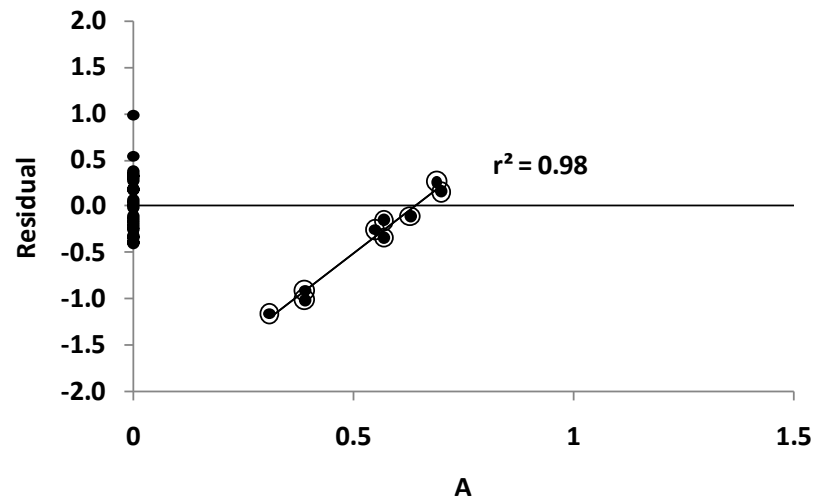


Figure C2. Residual analyses of LSER model independent variables for (a) A (b) B (c) V, and (d) P. The circled points are for phenolic compounds in the dataset following a trend represented by the regression line and coefficient of determination (r^2)

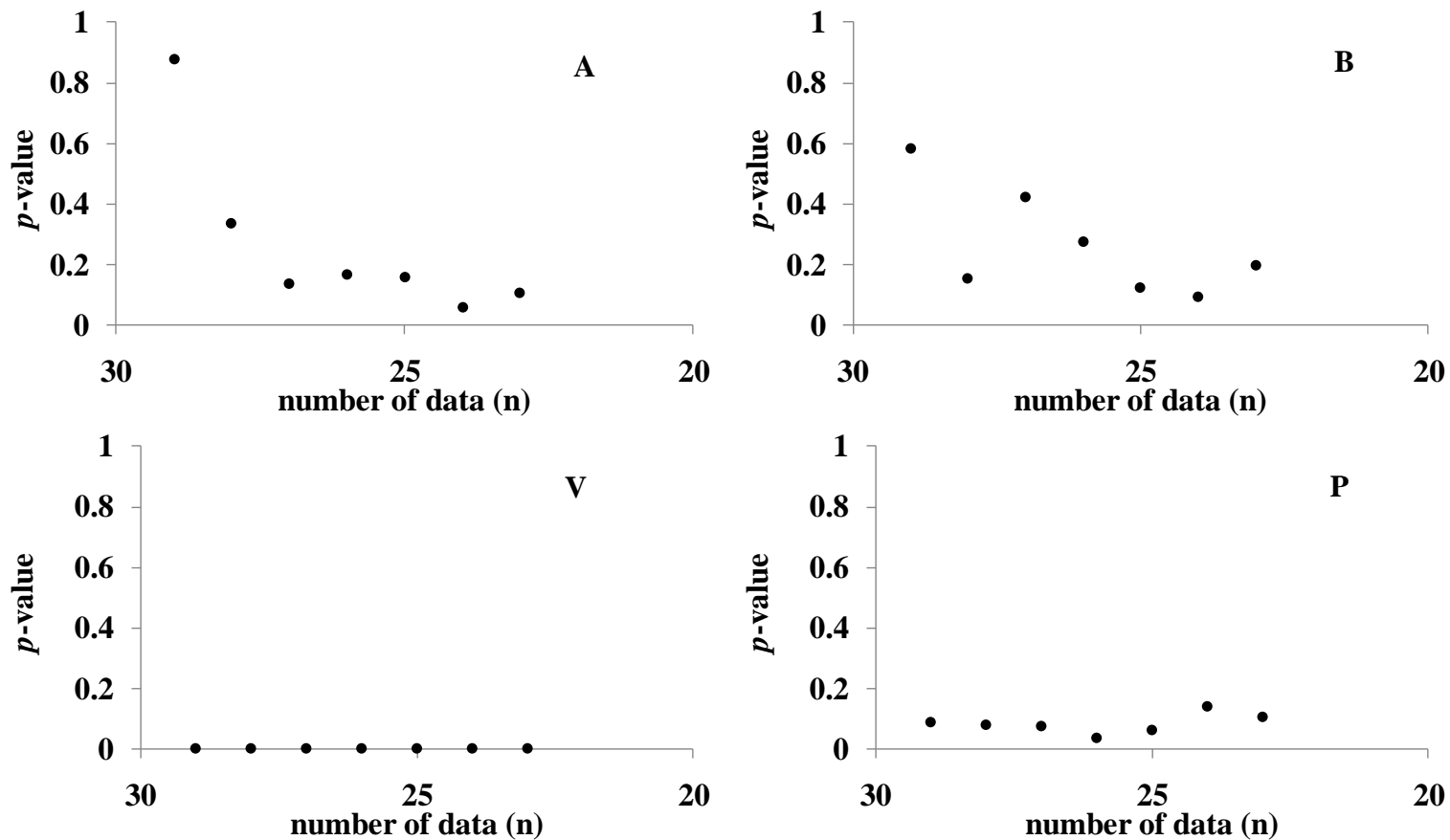


Figure C3. Examination of p -values for each LSER parameter by one by one elimination of highest descriptor values from the independent parameter list

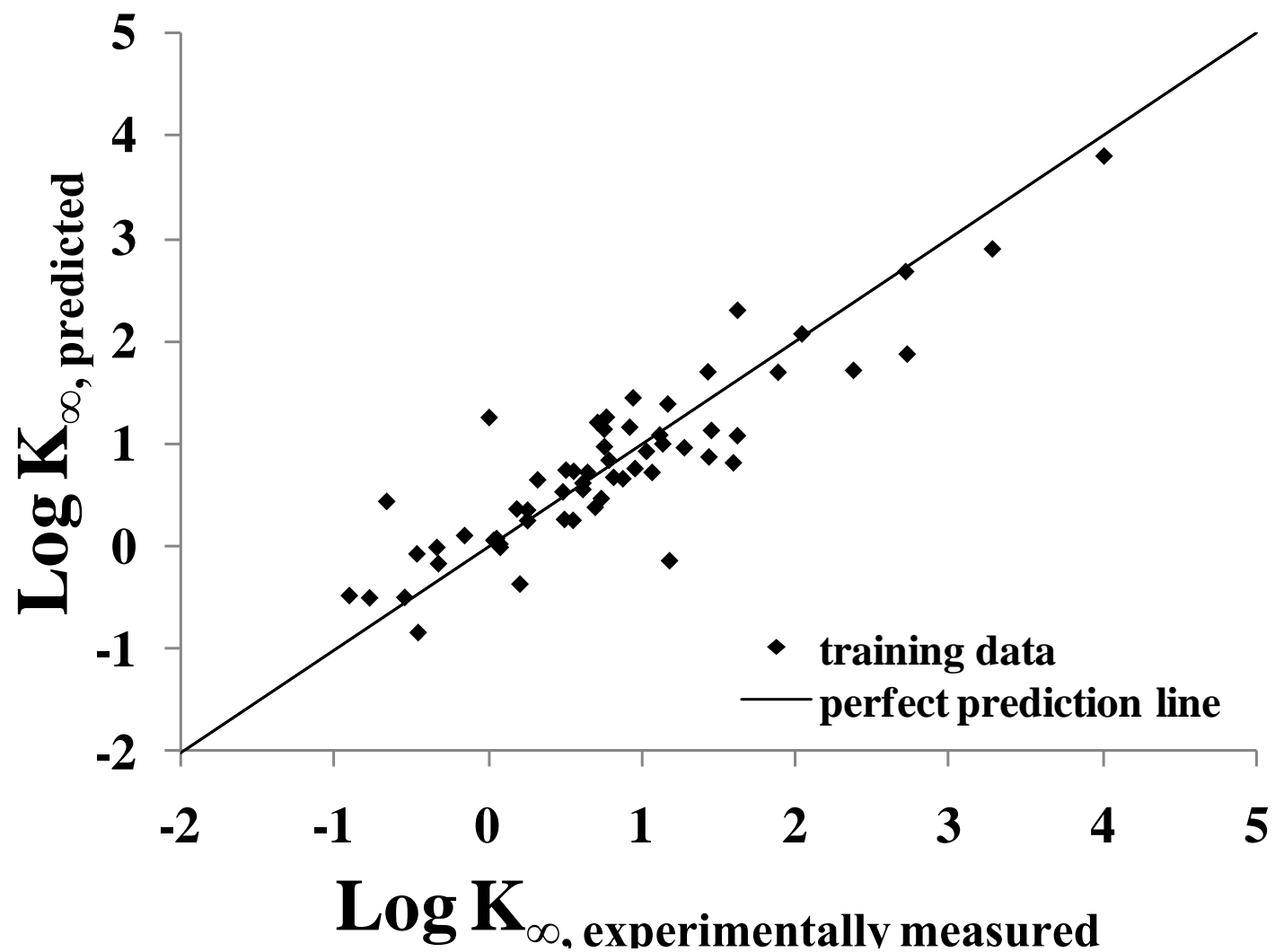


Figure C4. Experimentally measured adsorption descriptors vs. the predicted adsorption descriptors by LSER model generated by combination of training and validation datasets

Table C5. Comparison of residual values (actual- predicted) and RMSE* values for three models
 (i) the model developed by Xia et al.¹⁷, (ii) the model developed for 29 compounds (eq. 3) and
 (iii) the combined model (eq. 5)

No	Compounds	(i)	(ii)	(iii)
1	Phenanthrene	0.11	0.36	0.41
2	Pyrene	-0.23	0.33	0.23
3	Naphthalene	0.35	0.56	0.53
4	1-naphthol	-0.26	-0.60	-0.37
5	Biphenyl	-0.15	-0.12	0.00
6	2-phenylphenol	-0.69	-0.97	-0.66
7	Benzene	0.35	0.38	0.36
8	Chlorobenzene	-0.45	-0.17	-0.33
9	1,2,4-trichlorobenzene	-0.43	0.09	-0.21
10	Nitrobenzene	-0.60	-0.34	-0.32
11	2,4-dinitrotoluene	0.20	0.48	0.64
12	Phenol	0.03	-0.16	-0.08
13	Catechol	0.78	0.26	0.58
14	Pyrogallol	1.65	0.86	1.32
15	2,4,6-trichlorophenol	-0.43	-0.08	-0.26
16	3-nitrotoluene	-0.18	0.12	0.10
17	4-nitrophenol	-0.85	-0.18	-0.50
18	Aniline	-0.31	-0.55	-0.30
19	4-chloroaniline	-1.26	-1.15	-1.11
20	2-nitroaniline	0.51	0.75	0.78
21	3-nitroaniline	-0.96	-0.35	-0.49
22	4-nitroaniline	-1.09	-0.25	-0.50
23	4-methylphenol	0.09	-0.18	-0.04
24	2-chlorophenol	0.09	-0.07	0.07
25	4-chlorophenol	0.22	0.40	0.26
26	2,4-dichlorophenol	0.28	0.21	0.19
27	2-nitrophenol	0.13	0.11	0.29
28	3-nitrophenol	-0.54	0.05	-0.25
29	1,3-dinitrobenzene	-0.13	0.20	0.35
30	Ethylbenzene	-0.14	-0.25	-0.19
31	4-xylene	-0.06	-0.18	-0.11
32	Bromobenzene	0.08	0.38	0.23
33	Propylbenzene	-0.13	-0.32	-0.22
34	4-chlorotoluene	0.02	0.32	0.14
35	Benzonitrile	-0.29	-0.11	-0.02
36	4-fluorophenol	-0.13	-0.11	-0.15
37	Benzyl alcohol	-0.24	-1.01	-0.45
38	Iodobenzene	0.05	0.34	0.23
39	Acetophenone	-0.06	-0.40	0.02
40	3-methylphenol	0.18	-0.15	0.03
41	Methyl benzoate	0.35	-0.14	0.32
42	4-chloroanisole	0.22	0.27	0.34

43	Phenethyl alcohol	-0.14	-1.16	-0.41
44	3-methylbenzyl alcohol	-0.04	-0.91	-0.28
45	4-ethylphenol	0.15	-0.25	-0.02
46	3,5-dimethylphenol	0.17	-0.34	-0.06
47	Ethyl benzoate	0.20	-0.34	0.15
48	Methyl 2-methylbenzoate	0.07	-0.39	0.04
49	3-chlorophenol	0.01	0.26	0.05
50	4-nitrotoluene	0.30	0.54	0.57
51	4-chloroacetophenone	0.16	-0.01	0.30
52	3-bromophenol	-0.12	0.16	-0.06
53	1-methylnaphthalene	0.02	0.18	0.17
54	2-dichlorobenzene	-0.38	0.07	-0.17
55	3-dichlorobenzene	-0.25	0.18	-0.07
56	4-dichlorobenzene	-0.43	0.03	-0.23
57	2-chloronaphthalene	0.55	0.98	0.84
58	Azobenzene	-0.12	-0.22	0.05
*RMSE		0.45	0.45	0.40

$$* \text{RMSE} = \sqrt{\frac{\sum(\text{actual} - \text{predicted})^2}{n}}$$

SAS Outputs for Multiple Linear Regression Results

SAS Outputs for the QSAR Model (eq. 1)

Number of Observation	29
Independent Variable	Log K_{∞}
Dependent Variable(s)	χ^0 , χ^0 , χ^3
r^2	0.88
$r_{adj.}^2$	0.87
PRESS	4.97

Parameter Estimates for QSAR Model (eq. 1)

Variable	Estimated Coefficient	Standard Error	p-value	VIF
χ^0	0.17	0.15	0.2552	5.83
χ^0	0.18	0.12	0.1505	5.64
χ^3	0.55	0.20	0.0125	8.60
intercept	-2.98	0.52	<0.0001	0.00

ANOVA Table for QSAR Model (eq. 1)

	Degrees of Freedom	Sum of Squares	Mean Square	F	p
Model	3	30.2	10.1	63.4	<0.0001
Error	25	3.97	0.16		
Total	28	34.2			

SAS Outputs for the QSAR Model (eq. 2)

Number of Observation	29
Independent Variable	Log $K_{SA,\infty}$
Dependent Variable(s)	$\chi^0_v, \chi^0, \chi^3_p$
r^2	0.84
$r_{adj.}^2$	0.83
PRESS	6.65

Parameter Estimates for QSAR Model (eq. 2)

Variable	Estimated Coefficient	Standard Error	p-value	VIF
χ^0_v	0.14	0.17	0.4253	5.83
χ^0	0.12	0.14	0.3712	5.64
χ^3_p	0.62	0.23	0.0132	8.60
intercept	-4.85	0.59	<0.0001	0.00

ANOVA Table for QSAR Model (eq. 2)

	Degrees of Freedom	Sum of Squares	Mean Square	F	p
Model	3	28.1	9.37	45.1	<0.0001
Error	25	5.19	0.21		
Total	28	33.3			

SAS Outputs for the LSER Model (eq. 3)

Number of Observation	29
Independent Variable	Log K_{∞}
Dependent Variable(s)	A, B, V, P
r^2	0.82
$r_{adj.}^2$	0.79
PRESS	9.20

Parameter Estimates for LSER Model (eq. 3)

Variable	Estimated Coefficient	Standard Error	p-value	VIF
A	0.05	0.32	0.8763	1.47
B	-0.48	0.86	0.5843	1.48
V	4.56	0.55	<0.0001	1.43
P	0.49	0.31	0.0883	1.60
intercept	-4.30	0.55	<0.0001	0.00

ANOVA Table for LSER Model (eq. 3)

	Degrees of Freedom	Sum of Squares	Mean Square	F	p
Model	4	28.2	7.05	28.4	<0.0001
Error	24	5.96	0.25		
Total	28	34.2			

SAS Outputs for the LSER Model (eq. 4)

Number of Observation	29
Independent Variable	Log $K_{SA, \infty}$
Dependent Variable(s)	A, B, V, P
r^2	0.77
$r_{adj.}^2$	0.73
PRESS	12.4

Parameter Estimates for LSER Model (eq. 4)

Variable	Estimated Coefficient	Standard Error	p-value	VIF
A	-0.03	0.37	0.9357	1.47
B	-0.65	0.97	0.5109	1.48
V	4.31	0.63	<0.0001	1.43
P	0.58	0.39	0.1486	1.60
intercept	-6.19	0.63	<0.0001	0.00

ANOVA Table for LSER Model (eq. 4)

	Degrees of Freedom	Sum of Squares	Mean Square	F	p
Model	4	25.6	6.41	20.1	<0.0001
Error	24	7.66	0.32		
Total	28	33.3			

SAS Outputs for the LSER Model using the combination of training and validation datasets (eq. 5)

Number of Observation	58
Independent Variable	Log K_{∞}
Dependent Variable(s)	A, B, V, P
r^2	0.83
$r_{adj.}^2$	0.82
PRESS	11.9

Parameter Estimates for LSER Model using the combination of training and validation datasets (eq. 5)

Variable	Estimated Coefficient	Standard Error	p-value	VIF
A	-0.01	0.21	0.9564	1.55
B	-1.91	0.39	<0.0001	1.25
V	4.45	0.38	<0.0001	1.42
P	1.06	0.21	<0.0001	1.43
intercept	-4.11	0.37	<0.0001	0.00

ANOVA Table for LSER Model using the combination of training and validation datasets (eq. 5)

	Degrees of Freedom	Sum of Squares	Mean Square	F	p
Model	4	44.3	11.1	64.6	<0.0001
Error	53	9.07	0.17		
Total	57	53.3			

SAS Outputs for the LSER Model (eq. 6)

Number of Observation	20
Independent Variable	Log $K_{0.01}$
Dependent Variable(s)	A, B, V, P
r^2	0.85
$r_{adj.}^2$	0.82
PRESS	4.61

Parameter Estimates for LSER Model (eq. 6)

Variable	Estimated Coefficient	Standard Error	p-value	VIF
A	-1.31	0.56	0.0321	1.31
B	-2.86	1.22	0.0335	1.38
V	4.41	0.70	<0.0001	1.39
P	0.67	0.47	0.1734	1.57
intercept	-3.81	0.78	0.0002	0.00

ANOVA Table for LSER Model (eq. 6)

	Degrees of Freedom	Sum of Squares	Mean Square	F	p
Model	4	28.2	1.05	22.1	<0.0001
Error	15	4.79	0.32		
Total	19	33.0			

SAS Outputs for the LSER Model (eq. 7)

Number of Observation	20
Independent Variable	Log $K_{0.1}$
Dependent Variable(s)	A, B, V, P
r^2	0.93
$r_{adj.}^2$	0.91
PRESS	8.37

Parameter Estimates for LSER Model (eq. 7)

Variable	Estimated Coefficient	Standard Error	p-value	VIF
A	-1.29	0.40	0.0047	1.31
B	-3.81	0.85	0.0005	1.38
V	4.59	0.49	<0.0001	1.39
P	0.74	0.33	0.0399	1.57
intercept	-4.42	0.55	<0.0001	0.00

ANOVA Table for LSER Model (eq. 7)

	Degrees of Freedom	Sum of Squares	Mean Square	F	p
Model	4	31.2	7.81	49.9	<0.0001
Error	15	2.35	0.16		
Total	19	33.6			

Appendix D

Supplementary information for Chapter IV

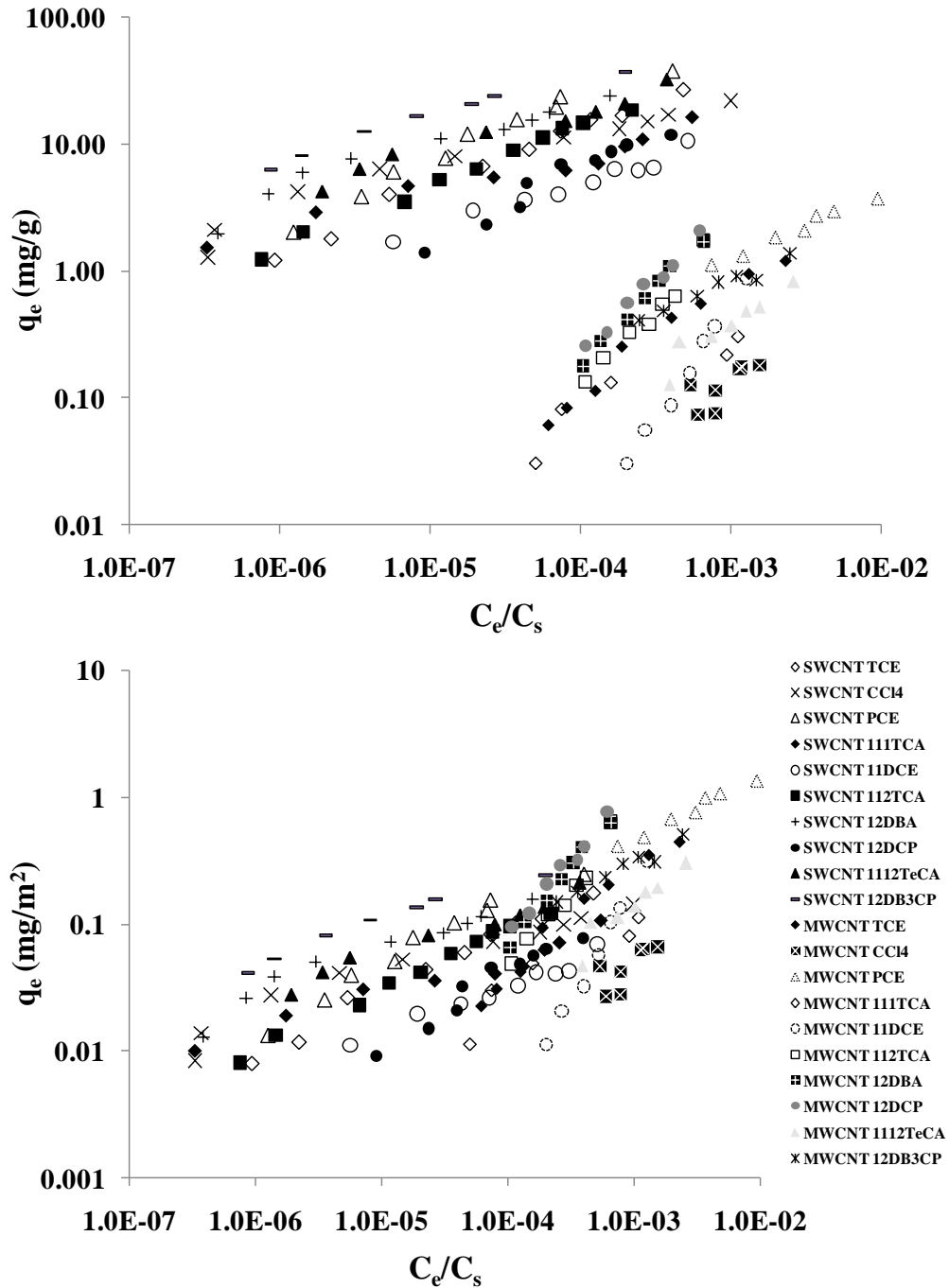


Figure D1. Comparison of SWCNT vs. MWCNT adsorption isotherms (top) and after surface area normalized within 0.5 – 0.8 nm pore size range (below) For comparison SWCNT and MWCNT adsorption isotherms were plotted on the same graph with the surface area normalized isotherms

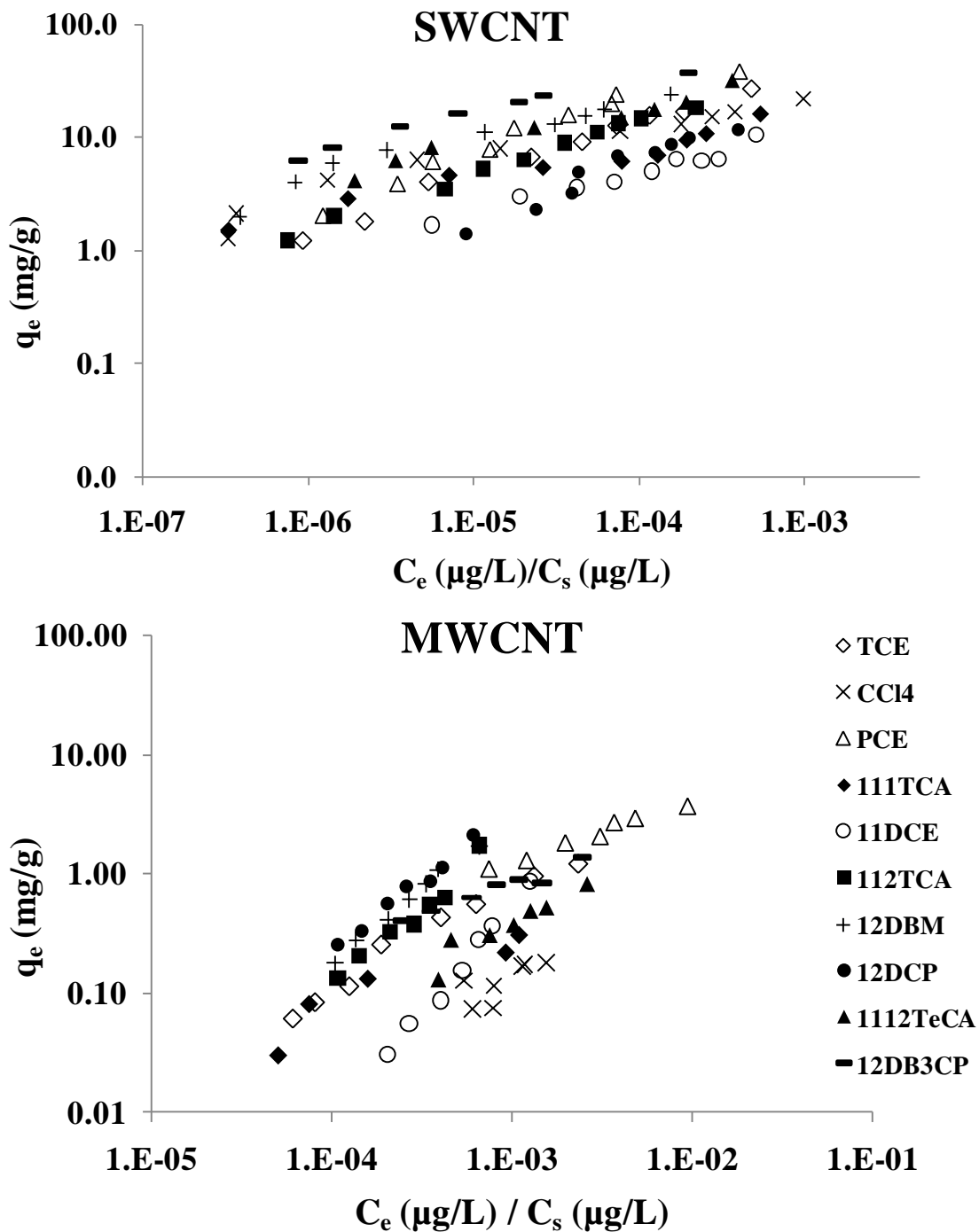


Figure D2. Solubility normalized adsorption isotherms of aliphatic SOCs by (a) SWCNT and (b) MWCNT

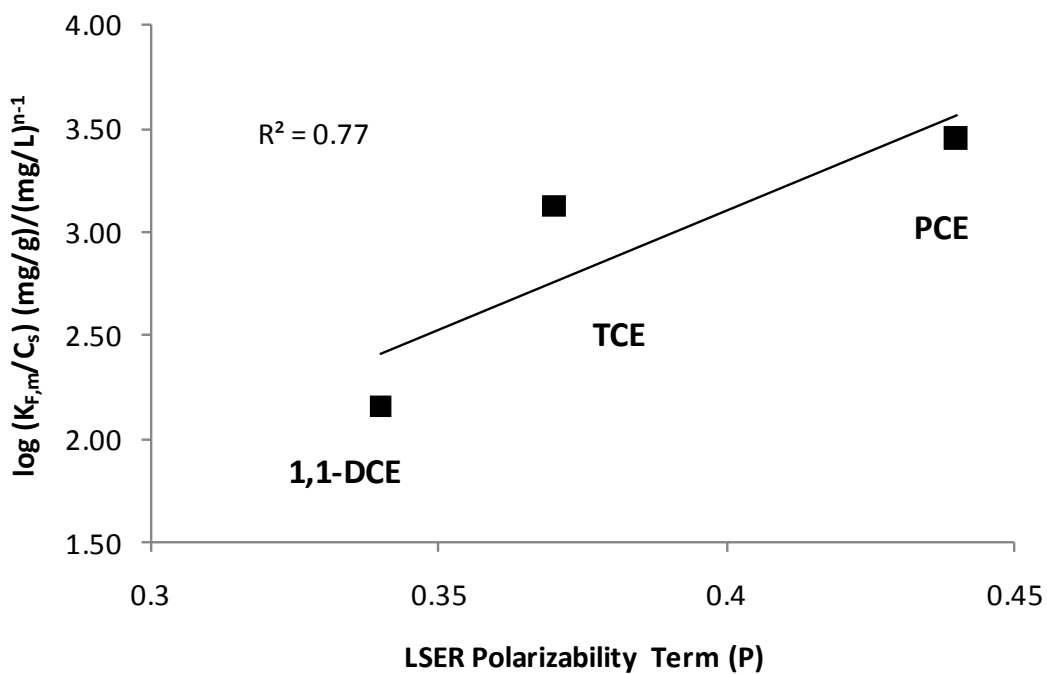
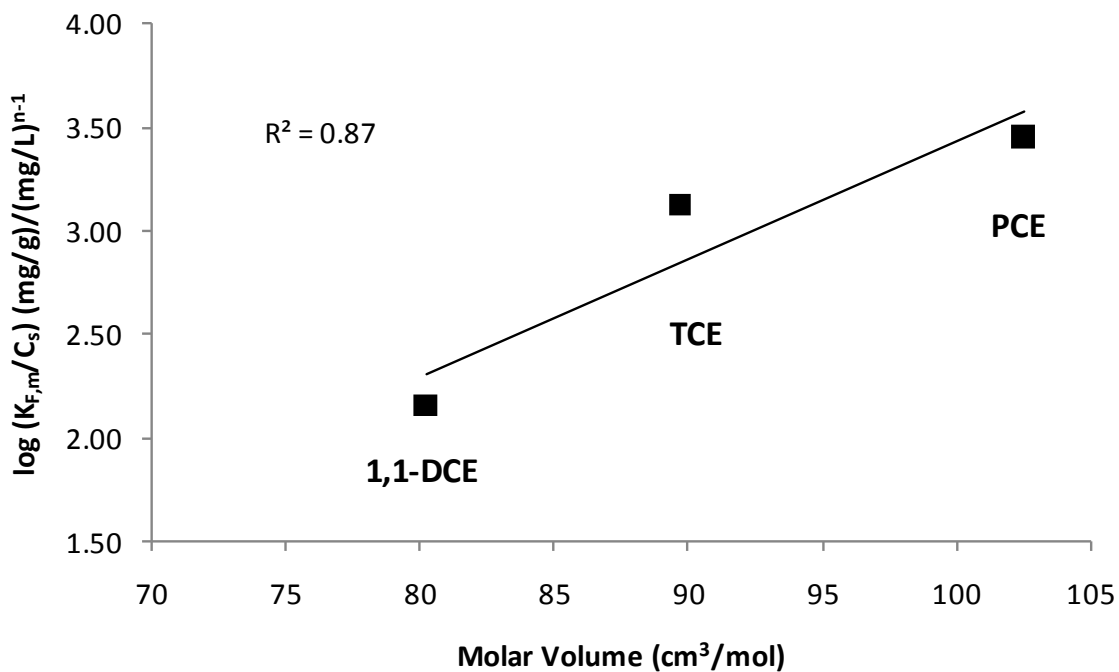


Figure D3. Correlation of molar volume (top) and polarizability (bottom) with solubility normalized adsorption descriptors ($K_{F,m}$) for PCE, TCE and 1,1-DCE

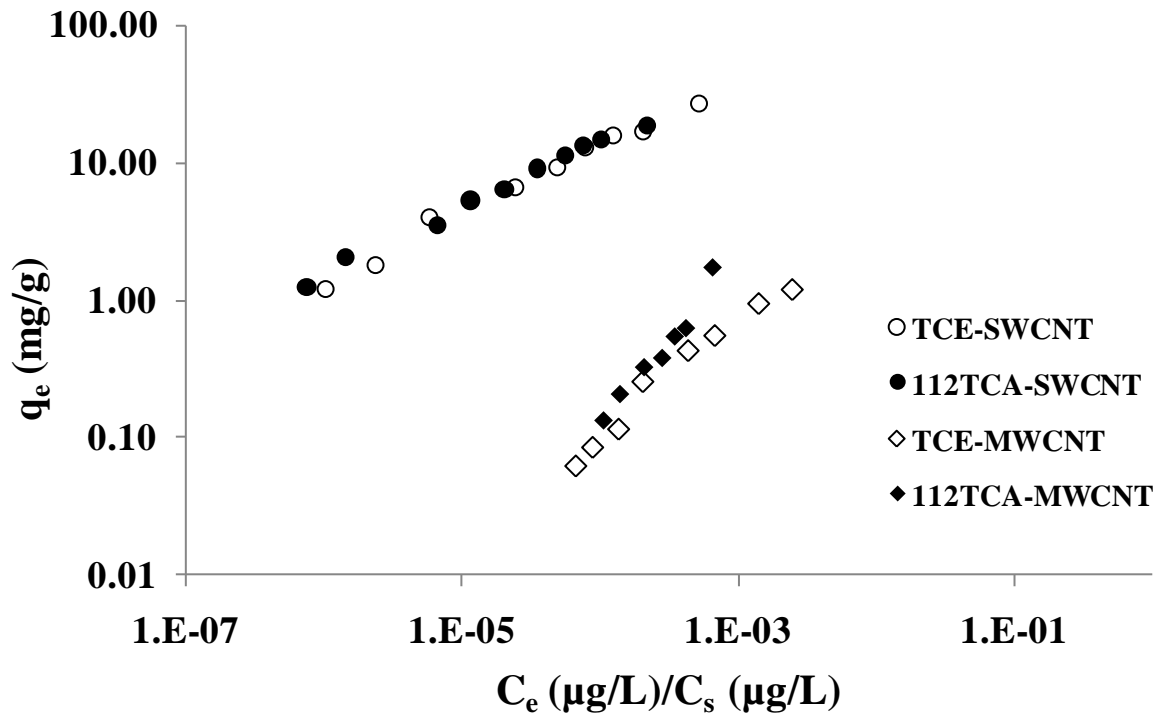


Figure D4. Solubility normalized adsorption isotherms of TCE and 1,1,2-TCA

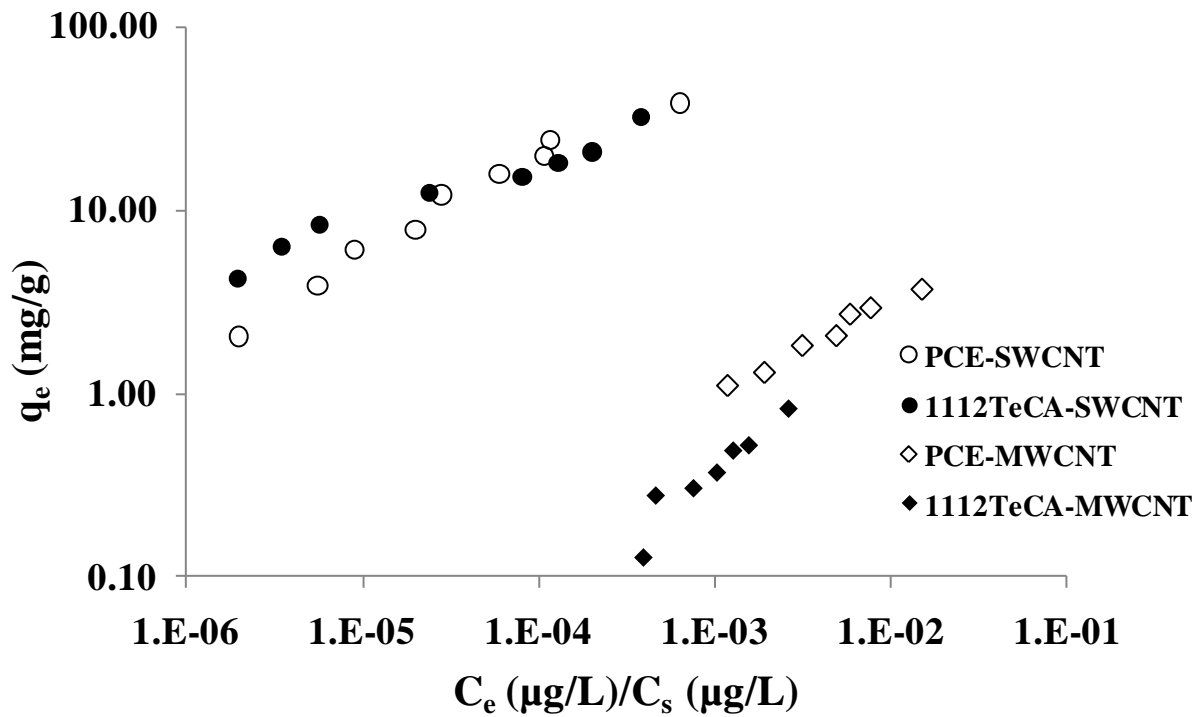


Figure D5. Solubility normalized adsorption isotherms of PCE and 1,1,1,2-TeCA

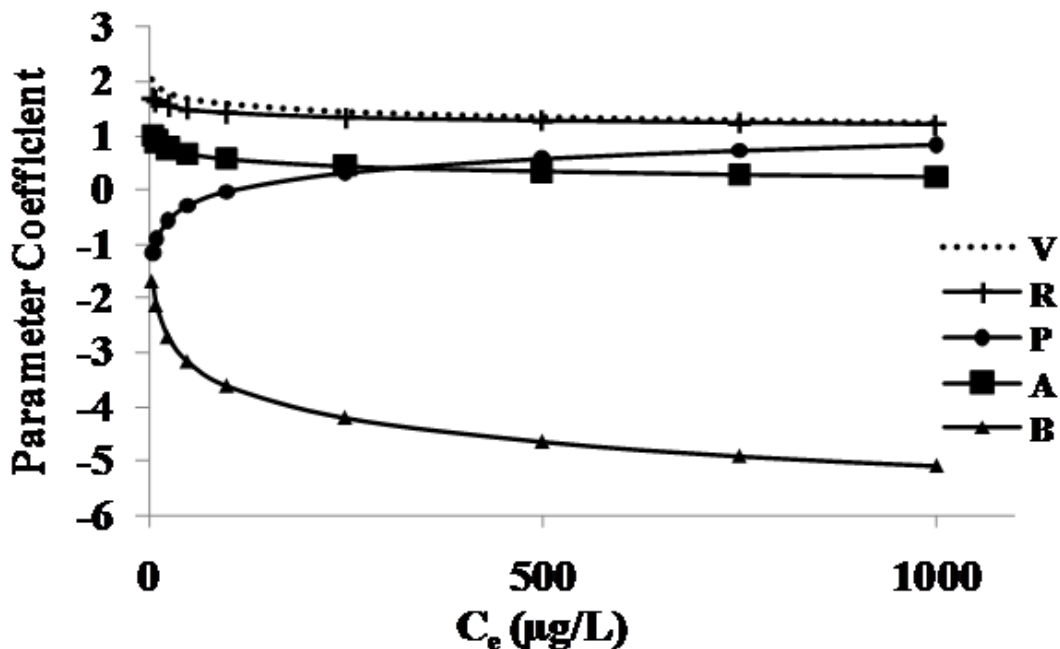


Figure D6. Change of LSER model parameter coefficients with aqueous equilibrium concentration

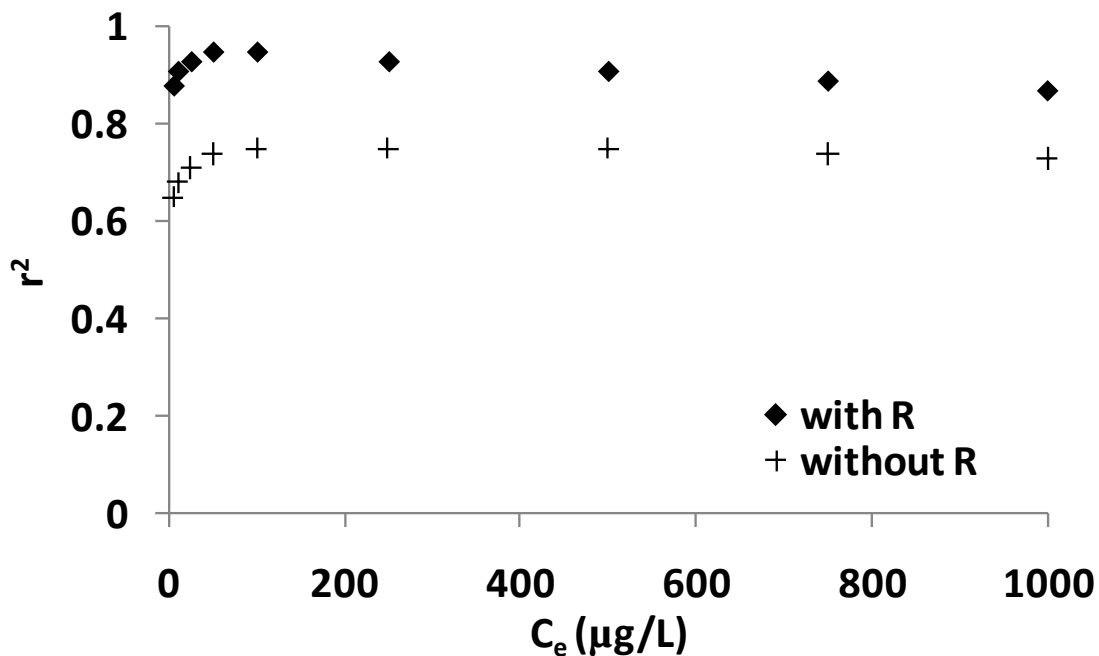


Figure D7. Change of LSER model coefficient of determination with increasing aqueous equilibrium concentration for adsorption of aliphatic SOCs by SWCNTs with and without R parameter

Table D1. Molecular structures of aliphatic SOCs

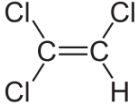
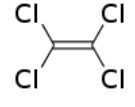
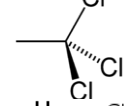
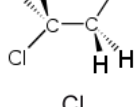
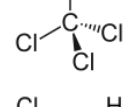
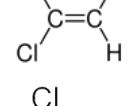
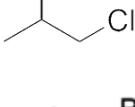
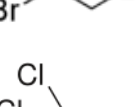
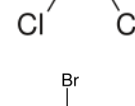
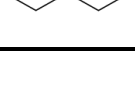
SOC	Abbreviation	Molecular Structure
Trichloroethylene	TCE	
Tetrachloroethylene	PCE	
1,1,1-Trichloroethane	1,1,1-TCA	
1,1,2-Trichloroethane	1,1,2-TCA	
Carbon Tetrachloride	CCL4	
1,1-Dichloroethylene	1,1-DCE	
1,2-Dichloropropane	1,2-DCP	
1,2-Dibromoethane	1,2-DBA	
1,1,1,2-Tetrachloroethane	1,1,1,2-TeCA	
1,2-Dibromo-3-Chloropropane	1,2-DB-3-CP	

Table D2. Adsorption descriptors for aliphatic SOCs

	SWCNT			MWCNT		
	Log $K_{D,500}$ (mg/g)/(µg/L)	Log $K_{D,750}$ (mg/g)/(mg/L)	Log $K_{D,1000}$ (mg/g)/(µg/L)	Log $K_{D,500}$ (mg/g)/(mg/L)	Log $K_{D,750}$ (mg/g)/(mg/L)	Log $K_{D,1000}$ (mg/g)/(mg/L)
TCE	-1.246	-1.334	-1.396	-3.13	-3.16	-3.18
CCl ₄	-1.391	-1.514	-1.602			
PCE	-0.614	-0.699	-0.759	-2.40	-2.48	-2.55
1,1,1-TCA	-1.629	-1.756	-1.846	-3.50	-3.58	-3.63
1,1-DCE	-1.901	-2.014	-2.094	-3.76	-3.61	-3.51
1,1,2-TCA	-1.528	-1.620	-1.685	-3.22	-3.17	-3.13
1,2-DBM	-1.336	-1.449	-1.529	-3.33	-3.28	-3.25
1,2-DCP	-1.737	-1.808	-1.858	-3.04	-3.01	-2.98
1,1,1,2-TeCA	-1.216	-1.334	-1.418	-3.10	-3.13	-3.15
1,2-DB3CP	-0.926	-1.044	-1.127	-2.93	-3.02	-3.09

Table D3. Solvatochromic parameters of aliphatic SOC_s

SOC	Abbreviation	A	B	V	P	R
Trichloroethylene	TCE	0.08	0.03	0.71	0.37	0.52
Carbon tetrachloride	CCL ₄	0.00*	0.00	0.74	0.38	0.46
Tetrachloroethylene	PCE	0.00	0.00	0.84	0.44	0.64
1,1,1-trichloroethane	111TCA	0.00	0.09	0.76	0.41	0.37
1,1-dichloroethylene	11DCE	0.00	0.05	0.59	0.34	0.36
1,1,2-trichloroethane	112TCA	0.13	0.13	0.76	0.68	0.50
1,2-dibromoethane	12DBM	0.10	0.17	0.74	0.76	0.75
1,2-dichloropropane	12DCP	0.00	0.15	0.78	0.68	0.37
1,1,1,2-tetrachloroethane	1112TeCA	0.10	0.08	0.88	0.63	0.54
1,2-dibromo-3-chloropropane	12DB3CP	0.00	0.17	1.00	0.78	0.93

*Minimum and maximum values per each parameter are indicated by the **bold** font

Table D4. LSER model parameters for adsorption of aliphatic SOCs by SWCNTs and MWCNTs without *R*

	Dependent Variable	Independent Variables	r²	A	B	V	P	R	c
SWCNT	Log K _{D,5}	<i>A, B, V, P</i>	0.65	1.19	-2.69	3.48	-0.31	-	-2.53
	Log K _{D,10}		0.68	1.09	-3.10	3.32	-0.08	-	-2.66
	Log K _{D,25}		0.71	0.95	-3.64	3.11	-0.22	-	-2.85
	Log K _{D,50}		0.74	0.84	-4.04	2.95	0.45	-	-2.99
	Log K _{D,100}		0.75	0.74	-4.45	2.79	0.67	-	-3.13
	Log K _{D,250}		0.75	0.60	-4.99	2.58	0.98	-	-3.31
	Log K _{D,500}		0.75	0.49	-5.40	2.42	1.21	-	-3.45
	Log K _{D,750}		0.74	0.43	-5.64	2.32	1.34	-	-3.53
	Log K _{D,1000}		0.73	0.39	-5.81	2.26	1.43	-	-3.59
MWCNT	Log K _{D,500}		0.82	-2.34	-9.83	0.61	3.53	-	-4.57
	Log K _{D,750}		0.83	-2.56	-10.2	-0.26	3.98	-	-4.11
	Log K _{D,1000}		0.84	-2.72	-10.5	-0.87	4.30	-	-3.77

Table D5. LSER model parameters for adsorption of aromatic SOCs by MWCNTs with and without *R*

	CNT	n	Independent	Dependent	r²	A	B	V	P	R	c
	type		Variables	Variable							
Without <i>R</i>	MWCNT	29	A,B,V,P	Log K _{D,inf}	0.83	0.05	-0.48	4.55	0.61	-	-4.34
	MWCNT	20	A,B,V,P	Log K _{D,0.01}	0.85	-1.31	-2.86	4.41	0.67	-	-3.81
	MWCNT	20	A,B,V,P	Log K _{D,0.1}	0.93	-1.29	-3.81	4.59	0.74	-	-4.42
With <i>R</i>	MWCNT	29	A,B,V,P,R	Log K _{D,inf}	0.83	0.00	-0.54	3.86	0.58	0.39	-4.00
	MWCNT	20	A,B,V,P,R	Log K _{D,0.01}	0.90	-1.24	-2.97	1.98	0.41	1.45	-2.65
	MWCNT	20	A,B,V,P,R	Log K _{D,0.1}	0.97	-1.23	-3.92	2.46	0.51	1.28	-3.41

*Data from Chapter III and remodeled with *R*

SAS Outputs for Multiparameter Linear Regression Results

SWCNT

SAS Outputs for the LSER Model

Number of Observation	10
Independent Variable	Log $K_{D,5}$
Dependent Variable(s)	A,B,V,P,R
r^2	0.88
$r_{adj.}^2$	0.73
PRESS	1.91

Parameter Estimates for LSER Model

Variable	Estimated Coefficient	Standard Error	p-value	VIF
A	0.99801	1.75801	0.6006	1.63666
B	-1.68646	3.02351	0.6067	7.20218
V	2.05683	1.24742	0.1745	3.33145
P	-1.1607	1.50941	0.4848	12.48908
R	1.69355	0.61636	0.0515	2.29913
intercept	-1.94928	0.61155	0.0333	0

ANOVA table for LSER Model

	Degrees of Freedom	Sum of Squares	Mean Square	F	p
Model	5	1.43788	0.28758	5.75	0.0575
Error	4	0.20009	0.05002		
Total	9	1.63797			

SAS Outputs for the LSER Model

Number of Observation	10
Independent Variable	Log $K_{D,10}$
Dependent Variable(s)	A,B,V,P,R
r^2	0.91
$r_{adj.}^2$	0.79
PRESS	1.49

Parameter Estimates for LSER Model

Variable	Estimated Coefficient	Standard Error	p-value	VIF
A	0.89975	1.48888	0.5782	1.63666
B	-2.13308	2.56065	0.4517	7.20218
V	1.95009	1.05645	0.1386	3.33145
P	-0.89997	1.27833	0.5202	12.48908
R	1.6296	0.522	0.0355	2.29913
intercept	-2.10979	0.51793	0.0152	0

ANOVA table for LSER Model

	Degrees of Freedom	Sum of Squares	Mean Square	F	p
Model	5	1.39077	0.27815	7.75	0.0348
Error	4	0.14352	0.03588		
Total	9	1.53429			

SAS Outputs for the LSER Model

Number of Observation	10
Independent Variable	Log $K_{D,25}$
Dependent Variable(s)	A,B,V,P,R
r^2	0.93
$r_{adj.}^2$	0.85
PRESS	1.09

Parameter Estimates for LSER Model

Variable	Estimated Coefficient	Standard Error	p-value	VIF
A	0.76986	1.19806	0.5555	1.63666
B	-2.72349	2.06048	0.2568	7.20218
V	1.80899	0.8501	0.1004	3.33145
P	-0.55532	1.02864	0.6179	12.48908
R	1.54507	0.42004	0.0212	2.29913
intercept	-2.32197	0.41676	0.0051	0

ANOVA table for LSER Model

	Degrees of Freedom	Sum of Squares	Mean Square	F	p
Model	5	1.33430	0.26686	11.5	0.0174
Error	4	0.09293	0.02323		
Total	9	1.42722			

SAS Outputs for the LSER Model

Number of Observation	10
Independent Variable	Log $K_{D,50}$
Dependent Variable(s)	A,B,V,P,R
r^2	0.95
$r_{adj.}^2$	0.88
PRESS	0.91

Parameter Estimates for LSER Model

Variable	Estimated Coefficient	Standard Error	p-value	VIF
A	0.6716	1.06157	0.5613	1.63666
B	-3.17011	1.82574	0.1575	7.20218
V	1.70225	0.75325	0.0867	3.33145
P	-0.29459	0.91145	0.7627	12.48908
R	1.48112	0.37219	0.0164	2.29913
intercept	-2.48248	0.36928	0.0026	0

ANOVA table for LSER Model

	Degrees of Freedom	Sum of Squares	Mean Square	F	p
Model	5	1.29596	0.25919	14.2	0.0118
Error	4	0.07296	0.01824		
Total	9	1.36892			

SAS Outputs for the LSER Model

Number of Observation	10
Independent Variable	Log $K_{D,100}$
Dependent Variable(s)	A,B,V,P,R
r^2	0.95
$r_{adj.}^2$	0.88
PRESS	0.82

Parameter Estimates for LSER Model

Variable	Estimated Coefficient	Standard Error	p-value	VIF
A	0.57334	1.03055	0.6076	1.63666
B	-3.61673	1.77239	0.1109	7.20218
V	1.5955	0.73124	0.0945	3.33145
P	-0.03387	0.88482	0.9713	12.48908
R	1.41717	0.36131	0.0172	2.29913
intercept	-2.64299	0.35849	0.0018	0

ANOVA table for LSER Model

	Degrees of Freedom	Sum of Squares	Mean Square	F	p
Model	5	1.26140	0.25228	14.7	0.0111
Error	4	0.06876	0.01719		
Total	9	1.33016			

SAS Outputs for the LSER Model

Number of Observation	10
Independent Variable	Log $K_{D,250}$
Dependent Variable(s)	A,B,V,P,R
r^2	0.93
$r_{adj.}^2$	0.85
PRESS	0.87

Parameter Estimates for LSER Model

Variable	Estimated Coefficient	Standard Error	p-value	VIF
A	0.44345	1.16188	0.7221	1.63666
B	-4.20714	1.99826	0.1030	7.20218
V	1.4544	0.82443	0.1525	3.33145
P	0.31079	0.99758	0.7709	12.48908
R	1.33264	0.40736	0.0307	2.29913
intercept	-2.85517	0.40418	0.0021	0

ANOVA table for LSER Model

	Degrees of Freedom	Sum of Squares	Mean Square	F	p
Model	5	1.22152	0.24430	11.2	0.0182
Error	4	0.08740	0.02185		
Total	9	1.30892			

SAS Outputs for the LSER Model

Number of Observation	10
Independent Variable	Log $K_{D,500}$
Dependent Variable(s)	A,B,V,P,R
r^2	0.91
$r_{adj.}^2$	0.80
PRESS	1.02

Parameter Estimates for LSER Model

Variable	Estimated Coefficient	Standard Error	p-value	VIF
A	0.34519	1.36033	0.8122	1.63666
B	-4.65376	2.33956	0.1176	7.20218
V	1.34766	0.96524	0.2352	3.33145
P	0.57151	1.16796	0.6502	12.48908
R	1.26869	0.47693	0.0564	2.29913
intercept	-3.01568	0.47321	0.0031	0

ANOVA table for LSER Model

	Degrees of Freedom	Sum of Squares	Mean Square	F	p
Model	5	1.19574	0.32915	7.98	0.033
Error	4	0.11980	0.02995		
Total	9	1.31554			

SAS Outputs for the LSER Model

Number of Observation	10
Independent Variable	Log $K_{D,750}$
Dependent Variable(s)	A,B,V,P,R
r^2	0.89
$r_{adj.}^2$	0.75
PRESS	1.16

Parameter Estimates for LSER Model

Variable	Estimated Coefficient	Standard Error	p-value	VIF
A	0.28771	1.50206	0.8574	1.63666
B	-4.91502	2.58331	0.1298	7.20218
V	1.28522	1.0658	0.2943	3.33145
P	0.72403	1.28965	0.6045	12.48908
R	1.23129	0.52662	0.0795	2.29913
intercept	-3.10957	0.52251	0.004	0

ANOVA table for LSER Model

	Degrees of Freedom	Sum of Squares	Mean Square	F	p
Model	5	1.18241	0.23648	6.48	0.0472
Error	4	0.14607	0.03652		
Total	9	1.32848			

SAS Outputs for the LSER Model

Number of Observation	10
Independent Variable	Log $K_{D,1000}$
Dependent Variable(s)	A,B,V,P,R
r^2	0.87
$r_{adj.}^2$	0.72
PRESS	1.27

Parameter Estimates for LSER Model

Variable	Estimated Coefficient	Standard Error	p-value	VIF
A	0.24693	1.61076	0.8856	1.63666
B	-5.10038	2.77026	0.1394	7.20218
V	1.24092	1.14293	0.3387	3.33145
P	0.83224	1.38298	0.5798	12.48908
R	1.20474	0.56473	0.0998	2.29913
intercept	-3.17619	0.56033	0.0048	0

ANOVA table for LSER Model

	Degrees of Freedom	Sum of Squares	Mean Square	F	p
Model	5	1.17374	0.23475	5.59	0.0602
Error	4	0.16797	0.04199		
Total	9	1.34171			

MWCNT

SAS Outputs for the LSER Model

Number of Observation	9
Independent Variable	Log $K_{D,500}$
Dependent Variable(s)	A,B,V,P,R
r^2	0.82
$r_{adj.}^2$	0.52
PRESS	1.90

Parameter Estimates for LSER Model

Variable	Estimated Coefficient	Standard Error	p-value	VIF
A	-2.33656	2.2217	0.3702	1.72177
B	-9.81879	4.09491	0.0961	7.3642
V	0.59776	1.52274	0.7209	3.45747
P	3.52075	1.92301	0.1645	12.74214
R	0.01526	0.7332	0.9847	2.24286
intercept	-4.56863	0.74198	0.0086	0

ANOVA table for LSER Model

	Degrees of Freedom	Sum of Squares	Mean Square	F	p
Model	5	0.95281	0.19056	2.70	0.2216
Error	3	0.21176	0.07059		
Total	8	1.16457			

SAS Outputs for the LSER Model

Number of Observation	9
Independent Variable	Log $K_{D,750}$
Dependent Variable(s)	A,B,V,P,R
r^2	0.83
$r_{adj.}^2$	0.55
PRESS	1.22

Parameter Estimates for LSER Model

Variable	Estimated Coefficient	Standard Error	p-value	VIF
A	-2.56256	1.88658	0.2675	1.72177
B	-10.2306	3.47723	0.0604	7.3642
V	-0.25415	1.29304	0.8567	3.45747
P	3.9843	1.63294	0.0925	12.74214
R	-0.0026	0.6226	0.9969	2.24286
intercept	-4.10632	0.63006	0.0073	0

ANOVA table for LSER Model

	Degrees of Freedom	Sum of Squares	Mean Square	F	p
Model	5	0.74336	0.14867	2.92	0.2034
Error	3	0.15269	0.05090		
Total	8	0.89606			

SAS Outputs for the LSER Model

Number of Observation	9
Independent Variable	Log $K_{D,1000}$
Dependent Variable(s)	A,B,V,P,R
r^2	0.84
$r_{adj.}^2$	0.58
PRESS	0.90

Parameter Estimates for LSER Model

Variable	Estimated Coefficient	Standard Error	p-value	VIF
A	-2.72291	1.68448	0.2044	1.72177
B	-10.5228	3.10473	0.0428	7.3642
V	-0.8586	1.15453	0.5110	3.45747
P	4.3132	1.45801	0.0596	12.74214
R	-0.01526	0.55591	0.9798	2.24286
intercept	-3.7783	0.56256	0.0067	0

ANOVA table for LSER Model

	Degrees of Freedom	Sum of Squares	Mean Square	F	p
Model	5	0.64348	0.12870	3.17	0.1855
Error	3	0.12173	0.04058		
Total	8	0.76521			

SWCNT (without R)

SAS Outputs for the LSER Model

Number of Observation	10
Independent Variable	Log $K_{D,5}$
Dependent Variable(s)	A,B,V,P
r^2	0.65
$r_{adj.}^2$	0.37
PRESS	2.21

Parameter Estimates for LSER Model

Variable	Estimated Coefficient	Standard Error	p-value	VIF
A	1.19299	2.66972	0.6737	1.63399
B	-2.68661	4.56185	0.5815	7.0978
V	3.48497	1.72347	0.0991	2.75306
P	-0.3136	2.24571	0.8944	11.96806
intercept	-2.52587	0.87303	0.0341	0

ANOVA table for LSER Model

	Degrees of Freedom	Sum of Squares	Mean Square	F	p
Model	4	1.06023	0.26506	2.29	0.1935
Error	5	0.57774	0.11555		
Total	9	1.63797			

SAS Outputs for the LSER Model

Number of Observation	10
Independent Variable	Log $K_{D,10}$
Dependent Variable(s)	A,B,V,P
r^2	0.68
$r_{adj.}^2$	0.42
PRESS	1.89

Parameter Estimates for LSER Model

Variable	Estimated Coefficient	Standard Error	p-value	VIF
A	1.08737	2.46664	0.6777	1.63399
B	-3.09546	4.21483	0.4957	7.0978
V	3.3243	1.59237	0.0912	2.75306
P	-0.08487	2.07487	0.969	11.96806
intercept	-2.6646	0.80662	0.0214	0

ANOVA table for LSER Model

	Degrees of Freedom	Sum of Squares	Mean Square	F	p
Model	4	1.04110	0.26028	2.64	0.1580
Error	5	0.49319	0.09864		
Total	9	1.53429			

SAS Outputs for the LSER Model

Number of Observation	10
Independent Variable	Log $K_{D,25}$
Dependent Variable(s)	A,B,V,P
r^2	0.71
$r_{adj.}^2$	0.49
PRESS	1.56

Parameter Estimates for LSER Model

Variable	Estimated Coefficient	Standard Error	p-value	VIF
A	0.94775	2.24148	0.69	1.63399
B	-3.63594	3.8301	0.3861	7.0978
V	3.11191	1.44701	0.0842	2.75306
P	0.21751	1.88548	0.9126	11.96806
intercept	-2.84801	0.73299	0.0116	0

ANOVA table for LSER Model

	Degrees of Freedom	Sum of Squares	Mean Square	F	p
Model	4	1.01996	0.25499	3.13	0.1212
Error	5	0.40726	0.08145		
Total	9	1.42722			

SAS Outputs for the LSER Model

Number of Observation	10
Independent Variable	Log $K_{D,50}$
Dependent Variable(s)	A,B,V,P
r^2	0.74
$r_{adj.}^2$	0.52
PRESS	1.38

Parameter Estimates for LSER Model

Variable	Estimated Coefficient	Standard Error	p-value	VIF
A	0.84213	2.11272	0.7066	1.63399
B	-4.0448	3.61007	0.3134	7.0978
V	2.95125	1.36389	0.0828	2.75306
P	0.44625	1.77716	0.8117	11.96806
intercept	-2.98674	0.69088	0.0075	0

ANOVA table for LSER Model

	Degrees of Freedom	Sum of Squares	Mean Square	F	p
Model	4	1.00711	0.25178	3.48	0.1020
Error	5	0.36181	0.07236		
Total	9	1.36892			

SAS Outputs for the LSER Model

Number of Observation	10
Independent Variable	Log $K_{D,100}$
Dependent Variable(s)	A,B,V,P
r^2	0.75
$r_{adj.}^2$	0.55
PRESS	1.26

Parameter Estimates for LSER Model

Variable	Estimated Coefficient	Standard Error	p-value	VIF
A	0.73651	2.02748	0.7313	1.63399
B	-4.45366	3.46443	0.2549	7.0978
V	2.79058	1.30886	0.0862	2.75306
P	0.67498	1.70547	0.7086	11.96806
intercept	-3.12548	0.66301	0.0053	0

ANOVA table for LSER Model

	Degrees of Freedom	Sum of Squares	Mean Square	F	p
Model	4	0.99695	0.24924	3.74	0.0903
Error	5	0.33321	0.06664		
Total	9	1.33016			

SAS Outputs for the LSER Model

Number of Observation	10
Independent Variable	Log $K_{D,250}$
Dependent Variable(s)	A,B,V,P
r^2	0.75
$r_{adj.}^2$	0.56
PRESS	1.19

Parameter Estimates for LSER Model

Variable	Estimated Coefficient	Standard Error	p-value	VIF
A	0.59688	1.99074	0.7764	1.63399
B	-4.99414	3.40165	0.202	7.0978
V	2.57819	1.28514	0.1011	2.75306
P	0.97736	1.67456	0.5848	11.96806
intercept	-3.30888	0.651	0.0038	0

ANOVA table for LSER Model

	Degrees of Freedom	Sum of Squares	Mean Square	F	p
Model	4	0.98768	0.24692	3.84	0.0861
Error	5	0.32124	0.06425		
Total	9	1.30892			

SAS Outputs for the LSER Model

Number of Observation	10
Independent Variable	Log $K_{D,500}$
Dependent Variable(s)	A,B,V,P
r^2	0.75
$r_{adj.}^2$	0.55
PRESS	1.21

Parameter Estimates for LSER Model

Variable	Estimated Coefficient	Standard Error	p-value	VIF
A	0.49126	2.02302	0.8178	1.63399
B	-5.403	3.4568	0.1788	7.0978
V	2.41752	1.30598	0.1234	2.75306
P	1.2061	1.70171	0.5101	11.96806
intercept	-3.44762	0.66155	0.0034	0

ANOVA table for LSER Model

	Degrees of Freedom	Sum of Squares	Mean Square	F	p
Model	4	0.9838	0.24595	3.71	0.0916
Error	5	0.3317	0.0663		
Total	9	1.3155			

SAS Outputs for the LSER Model

Number of Observation	10
Independent Variable	Log $K_{D,750}$
Dependent Variable(s)	A,B,V,P
r^2	0.74
$r_{adj.}^2$	0.53
PRESS	1.25

Parameter Estimates for LSER Model

Variable	Estimated Coefficient	Standard Error	p-value	VIF
A	0.42948	2.06512	0.8435	1.63399
B	-5.64216	3.52873	0.1707	7.0978
V	2.32354	1.33316	0.1418	2.75306
P	1.3399	1.73712	0.4754	11.96806
intercept	-3.52878	0.67532	0.0034	0

ANOVA table for LSER Model

	Degrees of Freedom	Sum of Squares	Mean Square	F	p
Model	4	0.9827	0.2457	3.55	0.0984
Error	5	0.3456	0.06914		
Total	9	1.3284			

SAS Outputs for the LSER Model

Number of Observation	10
Independent Variable	Log $K_{D,1000}$
Dependent Variable(s)	A,B,V,P
r^2	0.73
$r_{adj.}^2$	0.52
PRESS	1.29

Parameter Estimates for LSER Model

Variable	Estimated Coefficient	Standard Error	p-value	VIF
A	0.38564	2.10474	0.8618	1.63399
B	-5.81186	3.59644	0.167	7.0978
V	2.25686	1.35874	0.1576	2.75306
P	1.43484	1.77045	0.4545	11.96806
intercept	-3.58636	0.68827	0.0034	0

ANOVA table for LSER Model

	Degrees of Freedom	Sum of Squares	Mean Square	F	p
Model	4	0.98263	0.24566	3.42	0.1049
Error	5	0.35909	0.07182		
Total	9	1.34171			

MWCNT (without R)

SAS Outputs for the LSER Model

Number of Observation	9
Independent Variable	Log $K_{D,500}$
Dependent Variable(s)	A,B,V,P
r^2	0.82
$r_{adj.}^2$	0.64
PRESS	1.17

Parameter Estimates for LSER Model

Variable	Estimated Coefficient	Standard Error	p-value	VIF
A	-2.33564	1.92381	0.2915	1.72109
B	-9.82994	3.51604	0.049	7.23806
V	0.61021	1.21287	0.6413	2.92426
P	3.52913	1.6286	0.0961	12.18387
intercept	-4.57365	0.6078	0.0017	0

ANOVA table for LSER Model

	Degrees of Freedom	Sum of Squares	Mean Square	F	p
Model	4	0.95278	0.23819	4.50	0.0872
Error	4	0.21179	0.05295		
Total	8	1.16457			

SAS Outputs for the LSER Model

Number of Observation	9
Independent Variable	Log $K_{D,750}$
Dependent Variable(s)	A,B,V,P
r^2	0.83
$r_{adj.}^2$	0.66
PRESS	0.15

Parameter Estimates for LSER Model

Variable	Estimated Coefficient	Standard Error	p-value	VIF
A	-2.56272	1.63351	0.1918	1.72109
B	-10.2287	2.98547	0.0266	7.23806
V	-0.25627	1.02985	0.8157	2.92426
P	3.98288	1.38285	0.045	12.18387
intercept	-4.10547	0.51608	0.0014	0

ANOVA table for LSER Model

	Degrees of Freedom	Sum of Squares	Mean Square	F	p
Model	4	0.74336	0.18584	4.87	0.0772
Error	4	0.15270	0.03817		
Total	8	0.89606			

SAS Outputs for the LSER Model

Number of Observation	9
Independent Variable	Log $K_{D,1000}$
Dependent Variable(s)	A,B,V,P
r^2	0.84
$r_{adj.}^2$	0.68
PRESS	0.54

Parameter Estimates for LSER Model

Variable	Estimated Coefficient	Standard Error	p-value	VIF
A	-2.72383	1.4587	0.1353	1.72109
B	-10.5117	2.66598	0.0169	7.23806
V	-0.87105	0.91964	0.3972	2.92426
P	4.30482	1.23486	0.0252	12.18387
intercept	-3.77329	0.46085	0.0012	0

ANOVA table for LSER Model

	Degrees of Freedom	Sum of Squares	Mean Square	F	p
Model	4	0.64345	0.16086	5.28	0.0679
Error	4	0.12176	0.03044		
Total	8	0.76521			

Appendix E

Supplementary information for Chapter V

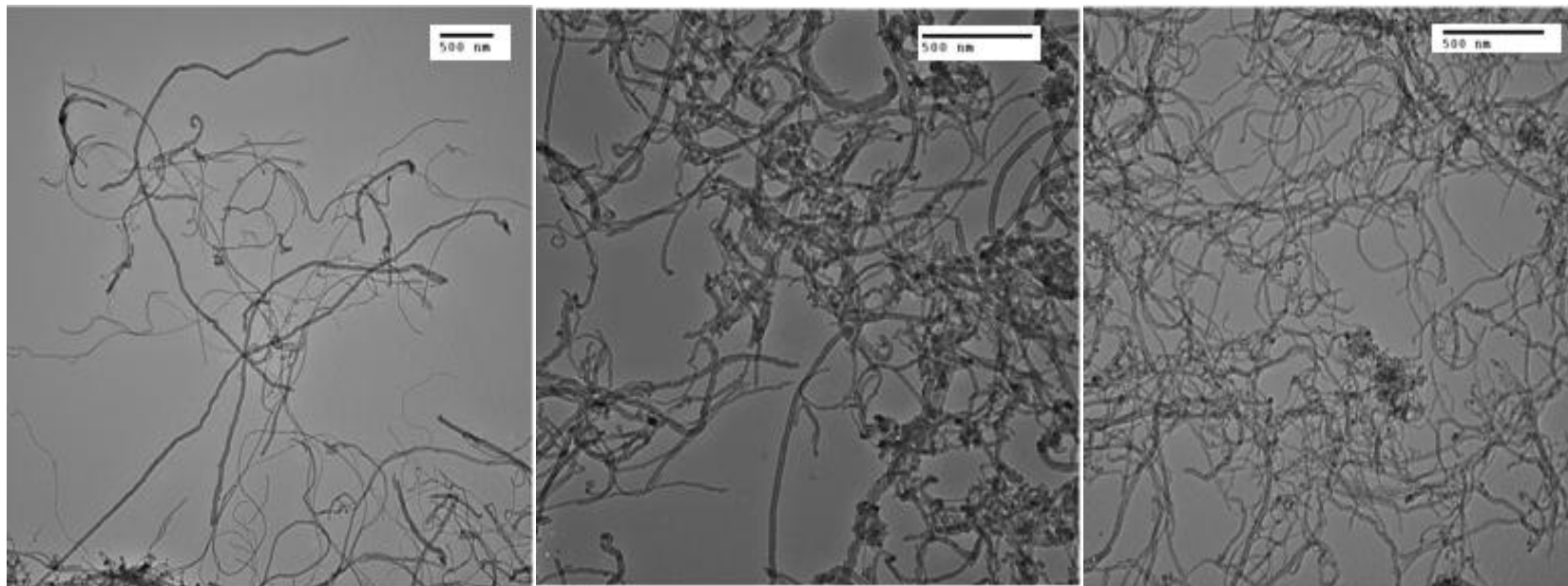


Figure E1. Sample transmission electron microscopy (TEM) images of multiwalled carbon nanotubes (MWCNTs). Small-diameter MWCNTs (left), medium-diameter MWCNTs (middle) and large-diameter MWCNTs (right)

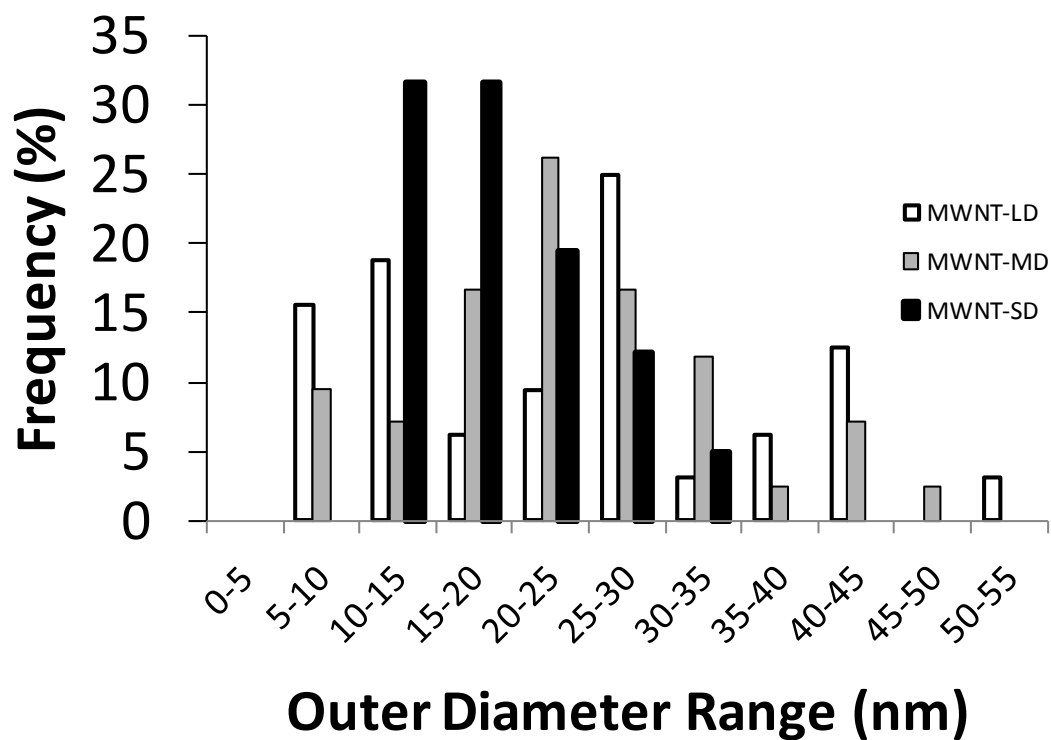


Figure E2. Diameter distribution of small-diameter multiwalled carbon nanotubes (MWCNTs), medium-diameter MWCNTs and large-diameter MWCNTs

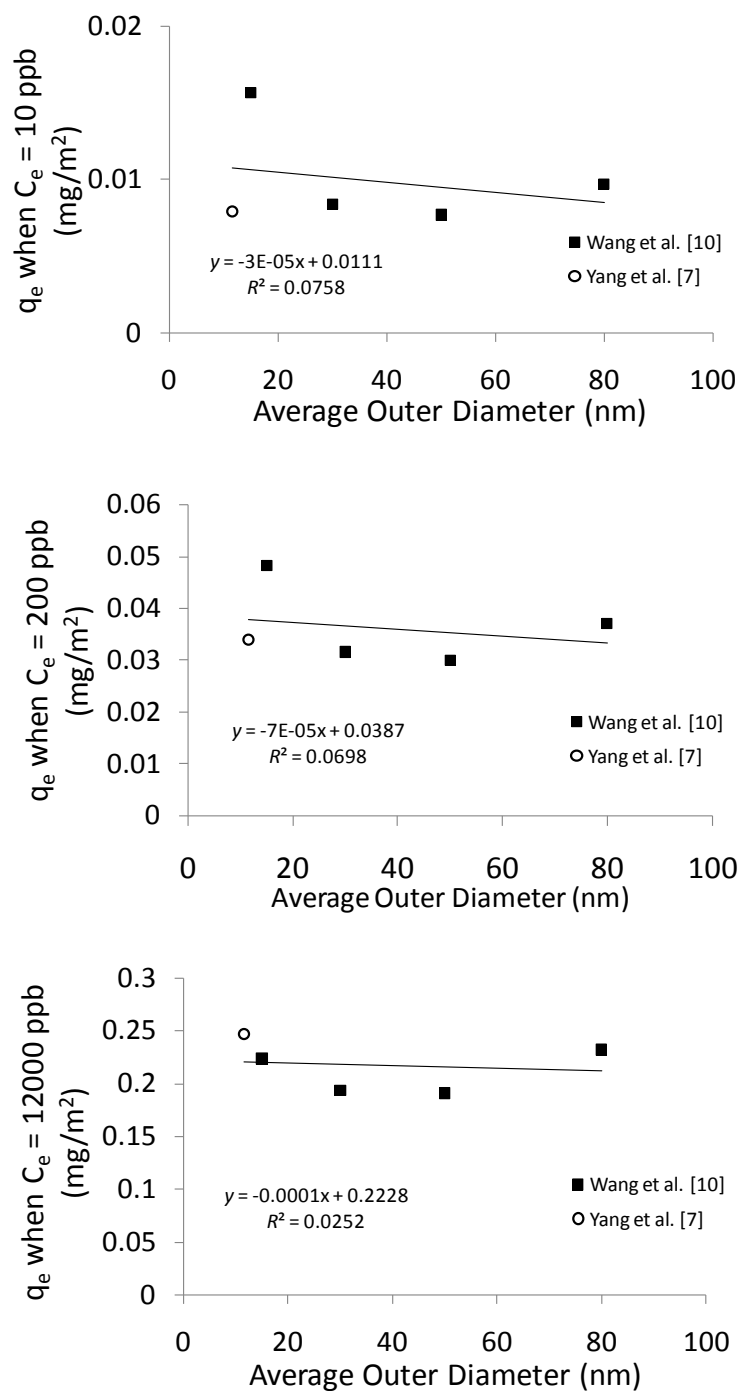


Figure E3. Specific surface area (SSA) normalized naphthalene adsorption capacities of multiwalled carbon nanotubes (MWCNTs) at the equilibrium concentrations of 10, 200, and 12,000 ppb, respectively

REFERENCES

Abe, I., Hayashi, K. and Kitagawa, M. Prediction of adsorption-isotherms of organic-compounds from water on activated carbons. Bulletin of the Chemical Society of Japan, 1981a. 54(9): p. 2819-2820.

Abe, I., Hayashi, K and Kitagawa, M. Prediction of adsorption-isotherms of organic-compounds from water on activated carbons .2. relative adsorbabilities of elements. Bulletin of the Chemical Society of Japan, 1981b. 54(12): p. 3857-3858.

Abe, I., Hayashi, K., Kitagawa, M. and Hirashima, T. Prediction of adsorbability of organic-compounds from aqueous-solution on activated carbon by means of the linear free-energy relationship. Bulletin of the Chemical Society of Japan, 1983. 56(4): p. 1002-1005.

Agnihotri, S., Kim, P., Zheng, Y., Mota, J.P. and Yang, L. Regioselective competitive adsorption of water and organic vapor mixtures on pristine single-walled carbon nanotube bundles. Langmuir, 2008. 24(11): p. 5746-5754.

Agnihotri, S., Mota, J.P.B., Rostam-Abadi, M. and Rood, M. Adsorption site analysis of impurity embedded single-walled carbon nanotube bundles. Carbon, 2006. 44(12): p. 2376-2383.

Ajayan, P.M. Nanotubes from carbon. Chemical Reviews, 1999. 99(7): p. 1787-1799.

Apul, O.G., Shao, T., Zhang, S. and Karanfil, T. The impact of carbon nanotube morphology on phenanthrene adsorption. Environmental Toxicology and Chemistry, 2012. 31(1):73-78

Apul, O.G., Wang, Q., Shao, T., Rieck J. and Karanfil, T. Predictive model development for adsorption of aromatic contaminants by multi walled carbon nanotubes. *Environmental Science and Technology*, 2013. 47(5):2295-230.

Apul, O.G., Wang, Q., Zhou, Y., and Karanfil, T. Adsorption of aromatic organic contaminants by graphene nanosheets: Comparison with carbon nanotubes and activated carbon. *Water Research*, 2013. 47(4): p. 1648-1654.

Belfort, G. Selective adsorption of organic homologues onto activated carbon from dilute aqueous solutions. Solvophobic interaction approach and correlations of molar adsorptivity with physicochemical parameters. *Environmental Science and Technology*, 1979. 13(8): p. 939-946.

Belin, T. and Epron, F. Characterization methods of carbon nanotubes: A review. *Material Science and Engineering B*. 2005 119(2):105-118.

Belsley, D.A., Kuh, E., Welsch, R.E. *Regression diagnostic: Identifying influential data and sources of collinearity*; Wiley-Interscience:New York, 1980.

Blum, D.J.W., Suffet, I.H. and Duguet, J.P. Quantitative structure-activity relationship using molecular connectivity for the activated carbon adsorption of organic-chemicals in water. *Water Research*, 1994. 28(3): p. 687-699.

Brasquet, C. and Le Cloirec, P. QSAR for organics adsorption onto activated carbon in water: What about the use of neural networks? *Water Research*, 1999, 33: p. 3603-3608.

Brooks, A.J., Lim, H.N. and Kilduff, J.E. Adsorption uptake of synthetic organic chemicals by carbon nanotubes and activated carbons. *Nanotechnology*, 2012. 23(29): p.1-13.

Carter, M.C., Kilduff, J.E. and Weber Jr., W.J. Site energy distribution analysis of preloaded adsorbents. *Environmental Science and Technology*, 1995. 29(7): p. 1773-1780.

Chen, W., Duan, L. and Zhu, D. Adsorption of polar and nonpolar organic chemicals to carbon nanotubes. *Environmental Science and Technology*, 2007. 41(24): p. 8295-8300.

Chen, J., Chen, W. and Zhu, D. Adsorption of nonionic aromatic compounds to single-walled carbon nanotubes: Effects of aqueous solution chemistry. *Environmental Science and Technology*, 2008a. 42(19): p. 7225-7230.

Chen, W., Duan, L., Wang, L. and Zhu, D. Adsorption of hydroxyl- and amino-substituted aromatics to carbon nanotubes. *Environmental Science and Technology*, 2008b. 42(18): p. 6862-6868.

Chen, G.C., Shan, X.Q., Wang, Y.S., Pei, Z.G., Shen, X.E., Wen, B and Owens, G. Effects of copper, lead, and cadmium on the sorption and desorption of atrazine onto and from carbon nanotubes. *Environmental Science and Technology*, 2008c. 42(22): p. 8297-8302.

Chen, G.C., Shan, X.Q., Wang, Y.S., Wen, B., Pei, Z.G., Xie, Y.N., Liu, T. and Pignatello, J.J. Adsorption of 2,4,6-trichlorophenol by multi-walled carbon nanotubes as affected by Cu(II). *Water Research*, 2009a. 43(9): p. 2409-2418.

Chen, G.C., Shan, X.Q., Zhou, Y.Q., Shen, X., Huang, H.L. and Khan, S.U. Adsorption kinetics, isotherms and thermodynamics of atrazine on surface oxidized multiwalled carbon nanotubes. *Journal of Hazardous Materials*, 2009b. 169(1-3): p. 912-918.

Chen, Z., Pierre, D., He, H., Tan, S., Pham-Huy, C., Honh, H. and Huang, J. Adsorption behavior of epirubicin hydrochloride on carboxylated carbon nanotubes. *International Journal of Pharmaceutics*, 2011. 405(1-2): p. 153-161.

Chin, C.J.M., Shih, L.C., Tsai, H.J. and Liu, T.K. Adsorption of o-xylene and p-xylene from water by SWCNTs. *Carbon*, 2007. 45(6): p. 1254-1260.

Cho, H.-H., Smith, B.A., Wnuk, J.D., Fairbrother, D.H. and Ball, W.P. Influence of surface oxides on the adsorption of naphthalene onto multiwalled carbon nanotubes. *Environmental Science and Technology*, 2008. 42(8): p. 2899-2905.

Dastgheib, S.A., Karanfil, T. and Cheng, W. Tailoring activated carbons for enhanced removal of natural organic matter from natural waters. *Carbon*, 2004. 42(3): p. 547-557.

Dickenson, E.R.V. and Drewes, J.E. Quantitative structure property relationships for the adsorption of pharmaceuticals onto activated carbon. *Water Science and Technology*, 2010. 62(10): p. 2270-2276.

Ferguson, P.L., Chandler, G.T., Templeton, R.C., DeMarco, A., Scrivens, W.A. and Englehart, B.A. Influence of sediment-amendment with single-walled carbon nanotubes and diesel soot on bioaccumulation of hydrophobic organic contaminants by

benthic invertebrates. *Environmental Science and Technology*, 2008. 42(10): p. 3879-3885.

Fu, H., Yang, L., Wan, Y., Xu, Z. and Zhu, D. Adsorption of pharmaceuticals to microporous activated carbon treated with potassium hydroxide, carbon dioxide, and steam. *Journal of Environmental Quality*, 2011. 40(6): p. 1886-1894.

Ghaedi, M., Hassanzadeh, A. and Kokhdan, S.N. Multiwalled carbon nanotubes as adsorbents for the kinetic and equilibrium study of the removal of alizarin red S and morin. *Journal of Chemical and Engineering Data*. 2011. 56(5): p. 2511-2520.

Ghaedi, M., Haghdoost, S., Nasiri-Korkhdan, S., Mihandoost, A., Sahraie, R. and Daneshfar, A. Comparison of activated carbon, multiwalled carbon nanotubes, and cadmium hydroxide nanowire loaded on activated carbon as adsorbents for kinetic and equilibrium study of removal of safranin-o. *Spectroscopy Letters*, 2012a. 45(7): p. 500-510.

Ghaedi, M., Khajehsharifi, H., Yadkuri, A.H., Roosta, M. and Asghari, A. Oxidized multiwalled carbon nanotubes as efficient adsorbent for bromothymol blue. *Toxicological and Environmental Chemistry*, 2012b. 94(5): p. 873-883.

Girifalco, L.A., Hodak, M. and Lee, R.S. 2000. Carbon nanotubes, buckyballs, ropes, and a universal graphitic potential. *Physical Review B*. 62:13104-13110.

Giusti, D.M., Conway, R.A. and Lawson, C.T. Activated carbon adsorption of petrochemicals. *Journal Water Pollution Control Federation*, 1974. 46(5): p. 947-965.

Gotovac, S., Hattori, Y., Noguchi, D., Miyamoto, J., Kanamaru, M., Utsumi, S., Kanoh, H. and Kaneko, K. Phenanthrene adsorption from solution on single wall carbon nanotubes. *Journal of Physical Chemistry B*, 2006. 110(33): p. 16219-16224.

Gotovac, S., Honda, H., Hattori, Y., Takahashi, K., Kanoh, H. and Kaneko K. Effect of nanoscale curvature of single-walled carbon nanotubes on adsorption of polycyclic aromatic hydrocarbons. *Nano Letters*, 2007a. 7(3): p. 583-587.

Gotovac, S., Yang, C.M., Hattori, Y., Takahashi, K., Kanoh, H. and Kaneko, K. Adsorption of polyaromatic hydrocarbons on single wall carbon nanotubes of different functionalities and diameters. *Journal of Colloid and Interface Science*, 2007b. 314(1): p. 18-24.

Gotovac, S., Song, L., Kanoh, H. and Kaneko, K. Assembly structure control of single wall carbon nanotubes with liquid phase naphthalene adsorption. *Colloids and Surfaces a-Physicochemical and Engineering Aspects*, 2007c. 300(1-2): p. 117-121.

Gupta, V.K., Kumar, R., Nayak, A., Salah, T.A. and Barakat, M.A. Adsorptive removal of dyes from aqueous solution onto carbon nanotubes: A review. *Advances in Colloid and Interface Science*, 2013. 193-194: p. 24-34.

Hickey, J.P. and Passinoreader, D.R. Linear solvation energy relationships - rules of thumb for estimation of variable values. *Environmental Science and Technology*, 1991. 25(10): p. 1753-1760.

Hou, L., Zhu, D., Wang, X., Wang, L., Zhang, C. and Chen, W. Adsorption of phenanthrene, 2-naphthol, and 1-naphthylamine to colloidal oxidized multiwalled carbon

nanotubes: Effects of humic acid and surfactant modification. *Environmental Toxicology and Chemistry*, 2013. 32(3): p. 493-500.

Hyung, H., Fortner, J.D., Hughes, J.B. and Kim, J.H. Natural organic matter stabilizes carbon nanotubes in the aqueous phase. *Environmental Science and Technology*, 2007. 41(1): p. 179-184.

Iijima, S. Helical Microtubules of graphitic carbon. *Nature*, 1991. 354(6348): p. 56-58.

Ji, L., Chen, W., Duan, L. and Zhu, D. Mechanisms for strong adsorption of tetracycline to carbon nanotubes: A comparative study using activated carbon and graphite as adsorbents. *Environmental Science and Technology*, 2009a. 43(7): p. 2322-2327.

Ji, L., Chen, W., Zheng, S., Xu, Z. and Zhu, D. Adsorption of sulfonamide antibiotics to multiwalled carbon nanotubes. *Langmuir*, 2009b. 25(19): p. 11608-11613.

Ji, L., Chen, W., Bi, J., Zheng, S., Xu, Z., Zhu, D. and Alvarez, P.J. Adsorption of tetracycline on single-walled and multi-walled carbon nanotubes as affected by aqueous solution chemistry. *Environmental Toxicology and Chemistry*, 2010a. 29(12): p. 2713-2719.

Ji, L., Shao, Y., Xu, Z., Zheng, S. and Zhu, D. Adsorption of monoaromatic compounds and pharmaceutical antibiotics on carbon nanotubes activated by KOH etching. *Environmental Science and Technology*, 2010b. 44(16): p. 6429-6436.

Johnston, H.J., Hutchison, G.R., Christensen, F.M., Peters, S., Hankin, S., Aschberger, A. and Stone, V. Critical review of the biological mechanisms underlying

the in vivo and in vitro toxicity of carbon nanotubes: The contribution of physico-chemical characteristics. *Nanotoxicology*, 2010. 4(2): p. 207-246.

Kamlet, M.J., Doherty, R.M., Abraham, M.H. and Taft, R.W. Linear solvation energy relationships .33. An analysis of the factors that influence adsorption of organic-compounds on activated carbon. *Carbon*, 1985. 23(5): p. 549-554.

Karanfil, T. and Kilduff, J. E. Role of granular activated carbon surface chemistry on the adsorption of organic compounds.1. priority pollutants. *Environmental Science and Technology*, 1999, 33: p. 3217-3224.

Kier, L.B., Hall, L.H. *Molecular connectivity in structure-activity analysis*; Wiley: New York, U.S.A, 1986.

Kilduff, J.E., Karanfil, T., Chin, Y. P., and Weber, W.J. Adsorption of natural organic polyelectrolytes by activated carbon: A size-exclusion chromatography study. *Environmental Science and Technology*, 1996. 30(4): p. 1336-1343.

Klaine, S.J., Alvarez, P.J.J., Batley, G.E., Fernandes, T.F., Handy, R.D., Lyon, D.Y., Mahendra, S., McLaughlin, M.J. and Lead, J.R. *Nanomaterials in the environment: Behavior, fate, bioavailability, and effects*. *Environmental Toxicology and Chemistry*, 2008. 27(9): p. 1825-1851.

Kotel, L.Y., Brichka, A.V. and Brichka, S.Y. Adsorption properties of modified multilayer carbon nanotubes with respect to benzoic acid. *Russian Journal of Applied Chemistry*, 2009. 82(4): p. 569-573.

Kuo, C.Y., Wu, C.H. and Wu, J.Y. Adsorption of direct dyes from aqueous solutions by carbon nanotubes: Determination of equilibrium, kinetics and

thermodynamics parameters. *Journal of Colloid and Interface Science*, 2008. 327(2): p. 308-315.

Kutics, K. and Suzuki, M. Adsorption of organics on surface-treated activated carbon-fibers. *Hungarian Journal of Industrial Chemistry*, 1993. 21(2): p. 93-99.

Lam, C.W., James, J.T., McCluskey, R., Arepalli, S. and Hunter, R.L. A review of carbon nanotube toxicity and assessment of potential occupational and environmental health risks. *Critical Reviews in Toxicology*, 2006. 36(3): p. 189-217.

Li, Y.H., Wang, S.G., Luan, Z.K., Ding, J., Xu, C.L. and Wu, D.H. Adsorption of cadmium(II) from aqueous solution by surface oxidized carbon nanotubes. *Carbon*, 2003. 41(5): p. 1057-1062.

Li, Y.H., Di, Z., Ding, J., Wu, D., Luan, Z. and Zhu, Y. Adsorption thermodynamic, kinetic and desorption studies of Pb^{2+} on carbon nanotubes. *Water Research*, 2005. 39(4): p. 605-609.

Li, X., Zhao, H., Quan, X., Chen, S., Zhang, Y. and Yu, H. Adsorption of ionizable organic contaminants on multi-walled carbon nanotubes with different oxygen contents. *Journal of Hazardous Materials*, 2011. 186(1): p. 407-415.

Li, M., Hsieh, T.C., Doong, R.A. and Huang, C.P. Tuning the adsorption capability of multi-walled carbon nanotubes to polar and non-polar organic compounds by surface oxidation. *Separation and Purification Technology*, 2013. 117: p.98-103

Liao, Q., Sun, J. and Gao, L. Adsorption of chlorophenols by multi-walled carbon nanotubes treated with HNO_3 and NH_3 . *Carbon*, 2008. 46(3): p. 553-555.

Lin, D. and Xing, B.S. Adsorption of phenolic compounds by carbon nanotubes: Role of aromaticity and substitution of hydroxyl groups. *Environmental Science and Technology*, 2008a. 42(19): p. 7254-7259.

Lin, D. and Xing, B.S. Tannic acid adsorption and its role for stabilizing carbon nanotube suspensions. *Environmental Science and Technology*, 2008b. 42(16): p. 5917-5923.

Liu, C.H., Li, J.J., Zhang, H.L., Li, B.R. and Guo, Y. Structure dependent interaction between organic dyes and carbon nanotubes. *Colloids and Surfaces a-Physicochemical and Engineering Aspects*, 2008. 313: p. 9-12.

Long, R.Q. and Yang, R.T. Carbon nanotubes as superior sorbent for dioxin removal. *Journal of the American Chemical Society*, 2001. 123(9): p. 2058-2059.

Lu, C., Chung, Y.L. and Chang, K.F. Adsorption thermodynamic and kinetic studies of trihalomethanes on multiwalled carbon nanotubes. *Journal of Hazardous Materials*, 2006. 138(2): p. 304-310.

Luehrs, D.C., Hickey, J.P., Nilsen, P.E., Godbole, K.A. and Rogers, T.N. Linear solvation energy relationship of the limiting partition coefficient of organic solutes between water and activated carbon. *Environmental Science and Technology*, 1996. 30(1): p. 143-152.

Ma, X., Tsige, M., Uddin, S. and Talapatra, S. Application of carbon nanotubes for removing organic contaminants from water. *Materials Express*, 2011. 1(3): p. 183-200.

Machado, F.M., Bergmann, C.P., Fernandes, T.H., Lima, E.C., Royer, B., Calvete, T. and Fagan, S.B. Adsorption of reactive red M-2BE dye from water solutions by multi-walled carbon nanotubes and activated carbon. *Journal of Hazardous Materials*, 2011. 192(3): p. 1122-1131.

Machado, F.M., Bergmann, C.P., Lima, E.C., Royer, B., de Souza, F.E., Jauris, I.M., Calvete, T. and Fagan S.B. Adsorption of reactive blue 4 dye from water solutions by carbon nanotubes: experiment and theory. *Physical Chemistry Chemical Physics*, 2012. 14(31): p. 11139-11153.

Manes, M. Polanyi adsorption potential theory and its application to liquid-phase adsorption. *Abstracts of Papers of the American Chemical Society*, 1978. 176: p. 4-4.

Mauter, M.S. and Elimelech, M. Environmental applications of carbon-based nanomaterials. *Environmental Science and Technology*, 2008. 42(16): p. 5843-5859.

Mishra, A.K., Arockiadoss, T. and Ramaprabhu, S. Study of removal of azo dye by functionalized multi walled carbon nanotubes. *Chemical Engineering Journal*, 2010. 162(3): p. 1026-1034.

Moreno-Castilla, C. Adsorption of organic molecules from aqueous solutions on carbon materials. *Carbon*, 2004. 42(1): p. 83-94.

Nanoposts, www.nanopostst.com, The global market for carbon nanotubes to 2015: A Realistic Assessment. 2010.

Nirmalakhandan, N. and Speece, R. Adsorption from aqueous phase by activated carbon - a simplified application of the solvophobic theory. *Environmental Science and Technology*, 1990. 24(4): p. 575-580.

Oleszczuk, P., Pan, B. and Xing, B.S. Adsorption and desorption of oxytetracycline and carbamazepine by multiwalled carbon nanotubes. *Environmental Science and Technology*, 2009. 43(24): p. 9167-9173.

Oleszczuk, P. and Xing, B. Influence of anionic, cationic and nonionic surfactants on adsorption and desorption of oxytetracycline by ultrasonically treated and non-treated multiwalled carbon nanotubes. *Chemosphere*, 2011. 85(8): p. 1312-1317.

Pan, B., Lin, D., Mashayekhi, H. and Xing, B. Adsorption and hysteresis of bisphenol A and 17 α -Ethinyl estradiol on carbon nanomaterials. *Environmental Science and Technology*, 2008. 42: p. 5480-5485.

Pan, B. and Xing, B.S. Adsorption mechanisms of organic chemicals on carbon nanotubes. *Environmental Science and Technology*, 2008. 42(24): p. 9005-9013.

Pan, B., Zhang, D., Li, H., Wu, M., Wang, Z. and Xing, B.S. Increased adsorption of sulfamethoxazole on suspended carbon nanotubes by dissolved humic acid. *Environmental Science and Technology*, 2013. 47(14): p. 7722-7728.

Peigney, A., Laurent, C.H., Flahaut, E., Bacsá, R.R. and Rousset, A. Specific surface area of carbon nanotubes and bundles of carbon nanotubes. *Carbon*, 2001. 39(4): p. 507-514.

Peng, X.J., Li, Y., Luan, Z., Di, Z., Wang, H., Tian, B. and Jia, Z. Adsorption of 1,2-dichlorobenzene from water to carbon nanotubes. *Chemical Physics Letters*, 2003. 376(1-2): p. 154-158.

Peng, X., Jia, J., and Luan, Z. Oxidized carbon nanotubes for simultaneous removal of endrin and Cd(II) from water and their separation from water. *Journal of Chemical Technology and Biotechnology*, 2009. 84(2): p. 275-278.

Peng, H., Pan, B., Wu, M., Liu, Y., Zhang, D. and Xing B.S. Adsorption of ofloxacin and norfloxacin on carbon nanotubes: Hydrophobicity- and structure-controlled process. *Journal of Hazardous Materials*, 2012. 233: p. 89-96.

Petosa, A.R., Jaisi, D.P., Quevedo, I.R., Elimelech, M. and Tujenkji, N. Aggregation and deposition of engineered nanomaterials in aquatic environments: Role of physicochemical interactions. *Environmental Science and Technology*, 2010. 44(17): p. 6532-6549.

Powell, M.C. and Kanarek, M.S. Nanomaterial health effects--part 1: Background and current knowledge. *WMJ: official publication of the State Medical Society of Wisconsin*, 2006. 105(2): p. 16-20.

Pyrzynska, K., Stafiej, A. and Biesaga, M. Sorption behavior of acidic herbicides on carbon nanotubes. *Microchimica Acta*, 2007. 159(3-4): p. 293-298.

Rambabu, N., Guzman, C.A., Soltan, J. and Himabindu, V. Adsorption characteristics of atrazine on granulated activated carbon and carbon nanotubes. *Chemical Engineering and Technology*, 2012. 35(2): p. 272-280.

Rao, G.P., C. Lu, and Su, F. Sorption of divalent metal ions from aqueous solution by carbon nanotubes: A review. *Separation and Purification Technology*, 2007. 58(1): p. 224-231.

Rodriguez, A., Ovejero, G., Sotelo, J.L., Mestanza, M. and Garcia, J. Adsorption of dyes on carbon nanomaterials from aqueous solutions. *Journal of Environmental Science and Health Part a-Toxic/Hazardous Substances and Environmental Engineering*, 2010. 45(12): p. 1642-1653.

Salam, M.A. and Burk, R.C. Thermodynamics of pentachlorophenol adsorption from aqueous solutions by oxidized multi-walled carbon nanotubes. *Applied Surface Science*, 2008. 255(5): p. 1975-1981.

Saleh, N.B., Pfefferle, L.D. and Elimelech, M. Aggregation kinetics of multiwalled carbon nanotubes in aquatic systems: Measurements and environmental implications. *Environmental Science and Technology*, 2008. 42(21): p. 7963-7969.

Schwarzenbach, R.P.G., P.M.; Imboden, D.M., *Environmental organic chemistry*. 2nd ed. 2003, John Wiley & Sons: Hoboken, New Jersey.

Shahryari, Z.G., Goharrizi, A.S. and Azadi, M. Experimental study of methylene blue adsorption from aqueous solutions onto carbon nano tubes. *International Journal of Water Resources and Environmental Engineering*, 2010. 2(2): p. 16-28.

Shen, X.E., Shan, X.Q., Dong, D.M., Hua, X.Y. and Owens, G. Kinetics and thermodynamics of sorption of nitroaromatic compounds to as-grown and oxidized multiwalled carbon nanotubes. *Journal of Colloid and Interface Science*, 2009. 330(1): p. 1-8.

Shi, B.Y., Zhuang, X., Yan, X., Lu, J. and Tang, H. Adsorption of atrazine by natural organic matter and surfactant dispersed carbon nanotubes. *Journal of Environmental Sciences-China*, 2010. 22(8): p. 1195-1202.

Shih, Y.H. and Gschwend, P.M. Evaluating activated carbon-water sorption coefficients of organic compounds using a linear solvation energy relationship approach and sorbate chemical activities. *Environmental Science and Technology*, 2009. 43(3): p. 851-857.

Su, F. and Lu, C. Adsorption kinetics, thermodynamics and desorption of natural dissolved organic matter by multiwalled carbon nanotubes. *Journal of Environmental Science and Health Part a-Toxic/Hazardous Substances and Environmental Engineering*, 2007. 42(11): p. 1543-1552.

Suffet, I.H. and McGuire, M.J. Activated carbon adsorption of organics from aqueous phase. *Abstracts of Papers of the American Chemical Society*, 1978. 176: p. 1-1.

Terrones, M. Science and technology of the twenty-first century: Synthesis, properties and applications of carbon nanotubes. *Annual Review of Materials Research*, 2003. 33: p. 419-501.

Terrones, M. Carbon nanotubes: Synthesis and properties, electronic devices and other emerging applications. *International Materials Reviews*, 2004. 49(6): p. 325-377.

Tibshirani, R. Regression shrinkage and selection via the LASSO. *Journal of Royal Statistical Society: Series B*, 1996. 58: p. 267-288.

Toth, A., Torocsik, A., Tombacz, E. and Laszlo, K. Competitive adsorption of phenol and 3-chlorophenol on purified MWCNTs. *Journal of Colloid and Interface Science*, 2012. 387: p. 244-249.

Upadhyayula, V.K.K., Deng, S., Mitchell, M.C. and Smith, G.B. Application of carbon nanotube technology for removal of contaminants in drinking water: A review. *Science of the Total Environment*, 2009. 408(1): p. 1-13.

US EPA. Carbon adsorption isotherms for toxic organics. 1980, Municipal Environmental Research Laboratory, U.S. Environmental Protection Agency.

Wang, S.G., Liu, X.W., Gong, W.X., Nie, W., Gao, B.Y. and Yue, Q.Y. Adsorption of fulvic acids from aqueous solutions by carbon nanotubes. *Journal of Chemical Technology and Biotechnology*, 2007. 82(8): p. 698-704.

Wang, X., Lu, J. and Xing, B.S. Sorption of organic contaminants by carbon nanotubes: Influence of adsorbed organic matter. *Environmental Science and Technology*, 2008. 42(9): p. 3207-3212.

Wang, X., Tao, S. and Xing, B.S. Sorption and competition of aromatic compounds and humic acid on multiwalled carbon nanotubes. *Environmental Science and Technology*, 2009. 43(16): p. 6214-6219.

Wang, X., Liu, Y., Tao, S. and Xing, B.S. Relative importance of multiple mechanisms in sorption of organic compounds by multiwalled carbon nanotubes. *Carbon*, 2010a. 48(13): p. 3721-3728.

Wang, F., Yao, J., Sun, K. and Xing, B.S. Adsorption of dialkyl phthalate esters on carbon nanotubes. *Environmental Science and Technology*, 2010b. 44(18): p. 6985-6991.

Wu, C.H. Adsorption of reactive dye onto carbon nanotubes: Equilibrium, kinetics and thermodynamics. *Journal of Hazardous Materials*, 2007a. 144(1-2): p. 93-100.

Wu, C.H. Studies of the equilibrium and thermodynamics of the adsorption of Cu^{2+} onto as-produced and modified carbon nanotubes. *Journal of Colloid and Interface Science*, 2007b. 311(2): p. 338-346.

Xia, X.R., Monteiro-Riviere, N.A. and Riviere, J.E. An index for characterization of nanomaterials in biological systems. *Nature Nanotechnology*, 2010a. 5(9): p. 671-675.

Xia, X., Li, Y., Zhou, Z. and Feng, C. Bioavailability of adsorbed phenanthrene by black carbon and multi-walled carbon nanotubes to *Agrobacterium*. *Chemosphere*, 2010b. 78(11): p. 1329-1336.

Yan, X.M., Shi, B.Y., Lu, J.J., Feng, C.H., Wang, D.S. and Tang, H.X. Adsorption and desorption of atrazine on carbon nanotubes. *Journal of Colloid and Interface Science*, 2008. 321(1): p. 30-38.

Yang, K., Wang, X., Zhu, L. and Xing, B.S. Competitive sorption of pyrene, phenanthrene, and naphthalene on multiwalled carbon nanotubes. *Environmental Science and Technology*, 2006a. 40(18): p. 5804-5810.

Yang, K., Zhu, L.Z. and Xing, B.S. Adsorption of polycyclic aromatic hydrocarbons by carbon nanomaterials. *Environmental Science and Technology*, 2006b. 40(6): p. 1855-1861.

Yang, K. and Xing, B.S. Desorption of polycyclic aromatic hydrocarbons from carbon nanomaterials in water. *Environmental Pollution*, 2007. 145(2): p. 529-537.

Yang, K., Wu, W., Jing, Q. and Zhu, L. Aqueous adsorption of aniline, phenol, and their substitutes by multi-walled carbon nanotubes. *Environmental Science and Technology*, 2008. 42(21): p. 7931-7936.

Yang, K. and Xing, B.S., Adsorption of fulvic acid by carbon nanotubes from water. *Environmental Pollution*, 2009. 157(4): p. 1095-1100.

Yang, K., Wu, W., Jing, Q., Jiang, Q. and Xing, B.S. Competitive adsorption of naphthalene with 2,4-dichlorophenol and 4-chloroaniline on multiwalled carbon nanotubes. *Environmental Science and Technology*, 2010. 44(8): p. 3021-3027.

Yang, W., Lu, Y., Zheng, F., Xue, X., Li, N. and Liu, D. Adsorption behavior and mechanisms of norfloxacin onto porous resins and carbon nanotube. *Chemical Engineering Journal*, 2012. 179: p. 112-118.

Yao, J.H. and Strauss, G. Adsorption of cationic surfactants on medical polymers - effects of surfactant and substrate structures. *Langmuir*, 1992. 8(9): p. 2274-2278.

Yao, Y., Feifei, X., Chen, M., Xu, Z. and Zhu, Z. Adsorption of cationic methyl violet and methylene blue dyes onto carbon nanotubes. *Proceedings of the 2010 5th IEEE International Conference on Nano/Micro Engineered and Molecular Systems*, 2010: p. 1083-1087.

Yu, F., Ma, J. and Wu, Y. Adsorption of toluene, ethylbenzene and xylene isomers on multi-walled carbon nanotubes oxidized by different concentration of NaOCl. *Frontiers of Environmental Science and Engineering*, 2012. 6(3): p. 320-329.

Zhang, S., Shao, T., Bekaroglu, S.S.K. and Karanfil, T. The impacts of aggregation and surface chemistry of carbon nanotubes on the adsorption of synthetic

organic compounds. *Environmental Science and Technology*, 2009. 43(15): p. 5719-5725.

Zhang, S., Shao, T., Bekaroglu, S.S.K. and Karanfil, T. Adsorption of synthetic organic chemicals by carbon nanotubes: Effects of background solution chemistry. *Water Research*, 2010a. 44(6): p. 2067-2074.

Zhang, S., Shao, T., Kose, H.S. and Karanfil, T. Adsorption of aromatic compounds by carbonaceous adsorbents: A comparative study on granular activated carbon, activated carbon fiber, and carbon nanotubes. *Environmental Science and Technology*, 2010b. 44(16): p. 6377-6383.

Zhang, D., Pan, B., Zhang, H., Ning, P. and Xing, B.S. Contribution of different sulfamethoxazole species to their overall adsorption on functionalized carbon nanotubes. *Environmental Science and Technology*, 2010c. 44(10): p. 3806-3811.

Zhang, S., Shao, T. and Karanfil, T. The effects of dissolved natural organic matter on the adsorption of synthetic organic chemicals by activated carbons and carbon nanotubes. *Water Research*, 2011. 45(3): p. 1378-1386.